DOE/MC/26029 -- 5685
(DE97005411)

Catalytic Conversion of Light Alkanes-Proof-of-Concept Stage - Phase VI

Final Report
February 1 - October 31, 1994

Work Performed Under Contract No.: DE-FC21-90MC26029

For
U.S. Department of Energy
Office of Fossil Energy
Federal Energy Technology Center
Morgantown Site
P.O. Box 880
Morgantown, West Virginia 26507-0880

By
Sun Company, Inc.
P. O. Box 1135
Marcus Hook, Pennsylvania 19061-0835

Disclaimer

DISCLAIMER

Portions of this document may be illegible electronic image products. Images are produced from the best available original document.

ABSTRACT

During the course of the first three years of the Cooperative Agreement, we uncovered a family of metal perhaloporphyrin complexes which had unprecedented activity for the selective air-oxidation of light alkanes to alcohols. The reactivity of light hydrocarbon substrates with air or oxygen was in the order: isobutane>propane>ethane>methane, in accord with their homolytic bond dissociation energies. Isobutane was so reactive that the proof-of concept stage of a process for producing tert-butyl alcohol from isobutane was begun (Phase V). It was proposed that as more active catalytic systems were developed (Phases IV, VI), propane, then ethane and finally methane oxidations will move into this stage (Phases VII through IX). As of this writing, however, the program has been terminated during the later stages of Phases V and VI so that further work is not anticipated.

Although active, the perhalotetraphenylporphyrin complexes are costly. Generating the perhalophenyl group at the meso position is difficult and it results in a catalyst of high molecular weight. What we learned during the first stage of the Cooperative Agreement is that the important property of a group on the periphery of the porphyrin ring is that it withdraw electrons efficiently. In Phase IV we succeeded in introducing nitro groups into the meso positions of octaethylporphyrin in a simple high-yield prep. Nitro groups are among the most electron withdrawing substituents in organic chemistry and indeed the effect of introducing them is to dramatically increase catalytic activity. Cost of the catalyst is also lower due to the ease of the synthesis and the low molecular weight of the complex.

Although improved porphine synthesis was developed and porphine nitration methods found, nitroporphines were insoluble in organic media and, therefore, impractical for homogeneous catalytic oxidations. For this reason we turned to catalysts having perfluoroalkyl groups on the porphyrin periphery as potentially inexpensive and active light alkane oxidation catalysts.

We made excellent progress during 1994 in generating a class of less costly new materials which have the potential for high catalytic activity. New routes were developed for replacing costly perfluorophenyl groups in the meso-position of metalloporphyrin catalysts with far less expensive and lower molecular weight perfluoromethyl groups. The CF_3 group is more electron-withdrawing than the C_6F_5 group and its effect on catalytic properties was of great interest. We made metalloporphyrin complexes bearing meso-CF_3 groups and indeed they responded electrochemically as predicted. In addition, conceptual economic analysis indicated that these catalysts were far less expensive than our first and second generation materials. However, much like the meso-nitroporphyrins, these materials were extremely insoluble in organic media. We replaced the CF_3 groups with C_3F_7 (perfluoro n-propyl) groups and generated catalysts which had good activity and hydrocarbon solubility. With this catalyst isobutane was converted to TBA rapidly with good selectivity. The C_3F_7 substituent was more costly to introduce than the CF_3 group, however, and we believe that a still less expensive catalyst is required at this time.

Although it is likely that catalysts not too dissimilar from those which convert isobutane to TBA could be used to convert propane to IPA, more robust catalysts will be needed for methane and ethane conversion. During the first three years of the Cooperative Agreement, we found that our first

generation heterogeneous catalyst, operating between 350 and 450°C produced methanol and ethanol from methane and ethane. Selectivities were not high enough for a practical process, however, and detailed kinetic analysis revealed that we need to build the very same characteristics into a vapor phase catalyst as those which we use in liquid phase. Specifically, binuclear sites having high M(III)/M(II) reduction potential in a hydrophobic environment are necessary. We, therefore, began a major program to design synthesize and characterize materials of this type. Considerable synthetic progress has been made and details appear in the body of this report.

TABLE OF CONTENTS

PAGE

TABLE OF CONTENTS
(Cont'd)

PAGE

TABLE OF CONTENTS
(Cont'd)

PAGE

TABLE OF CONTENTS
(Cont'd)

PAGE

1.0 SUMMARY OF PROGRAM INCENTIVES

As petroleum reserves dwindle, all hydrocarbon raw materials which could be converted to usable liquid fuels become more dear. Often the search for oil yields extensive gas reservoirs. Gas availability on a worldwide scale rivals that of crude oil but problems of transportation and differences in end use application often limit its' utility. Most natural gas is found in areas remote to its ultimate use. Currently much of this remote gas is associated with petroleum production. Because it cannot be used at the location where it is produced, it is often flared on a large scale, representing not only a wasted energy resource but also contributing to global warming as a result of carbon dioxide production. Because of its low energy density, methane is relatively costly to transport. Figure 1-1 shows the relative differences between the costs of transporting various liquid and gaseous fuels(1). It is readily seen that the conversion of methane to a liquid fuel such as methanol or a hydrocarbon liquid would both drastically cut the cost of transport of over long distances, and provide an alternative fuel liquid from an abundant, under-utilized resource.

Catalytic alkane conversion science is maturing to the point that one can envision the economically attractive conversion of natural gas to liquid fuels on a commercial scale by the turn of the century. This situation has many international and national implications. Remote accumulations of low value gas such as exist on the North slope of Alaska and various off-shore sites could be exploited. Value could be maximized for domestic gas reserves in high value-added products. The National interests would be well served if the U.S. held the technological lead in gas conversion technology and could influence the course of gas conversion abroad. One of the most costly steps in the current technology for converting natural gas to liquid fuels is the energy-intensive steam reforming step. The products of steam reforming are catalytically converted to methanol which has value as an alternative liquid fuel product or which could be converted to gasoline via existing technology.

We have examined a new catalytic approach to the direct production of a methanol-rich oxidate from natural gas which avoids costly steam reforming completely. Work conducted in Sun laboratories under the joint sponsorship of the Department of Energy (METC), the Gas Research Institute, and the Sun Company, Inc., has produced a family of new catalytic materials which, if successfully developed, will be effective in the conversion of light alkanes to alcohols or other oxygenates. We have found that it is possible to catalytically convert methane, and the C_2-C_4 hydrocarbons that are present in smaller but significant amounts in natural gas, to alcohols by direct reaction with air or oxygen. In particular, we have found that the C_4 component of natural gas can be catalytically converted to fuel oxygenates in excellent yield, and significant progress has been made in converting the C_3 component to an oxygenate product without combusting the hydrocarbon substantially. The C_1 and C_2 components can also be converted to alcohol-rich oxygenates but more progress is still required before a practical catalytic route becomes possible.

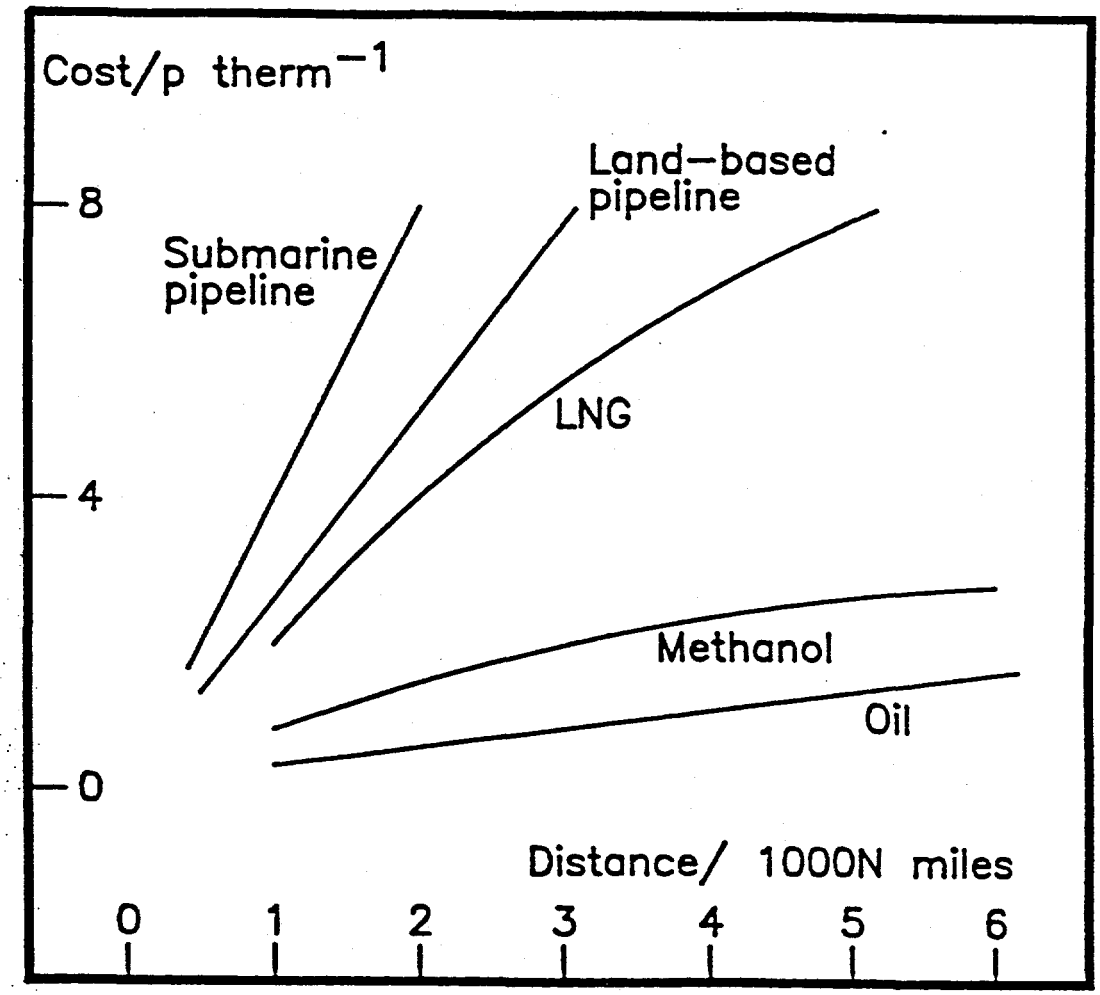

FIGURE 1.1 Relative cost of transport of liquid and gaseous fuels (LNG = liquified natural gas).

At the outset of this work we envisioned converting natural gas to an alcohol-rich oxidate which could subsequently be converted to hydrocarbon gasoline via MTG technology. During the period of this research, however, the benefits of oxygenates as clean-burning, high octane, liquid fuel materials has become apparent. Alcohols and the ethers that can be made from them are the oxygenates that are used to replace aromatics, reduce toxicity and reduce ozone and carbon monoxide in the reformulated gasolines of the 90's. As a result it is more reasonable to consider the direct air-oxidation of light alkanes to produce alcohol-rich oxidates for use as components of reformulated gasoline or as liquid fuel alternatives to gasoline in areas where there is non-attainment of CO or ozone limits set forward by the Clean Air Act. Alcohols of the type that can be formed directly from natural gas components: methanol, ethanol and tert-butyl alcohol, TBA, are not only useful as liquid fuel components themselves but are used in the manufacture of ether oxygenates such as MTBE, TAME, and ETBE as well. Table 1-1 shows some of the fuel-related properties of the C_1-C_4 alcohols and the ethers that can be made from them. It can be seen that these materials have desireable fuel properties in addition to meeting the fuel oxygen-content requirements of the Clean Air Act.

As desireable as it is to convert light alkanes directly to alcohols, doing this in an efficient manner using existing technology is a major problem. The light alkanes: methane, ethane, propane and the butanes, are among the most unreactive of organic substrates. They are also among the most abundant and inexpensive raw materials. They are found not only in natural gas, but in light petroleum fractions, and are being generated in ever-increasing quantities in petroleum refineries due to the increasing severity of catalytic cracking of heavier crudes. There exist few commercial processes for the efficient upgrading of these substrates to high value products and no DIRECT catalytic functionalization of these substrates to produce chemical or fuel alcohols.

During a six-year period in which Sun has invested over six million dollars in research support, coupled with an ongoing program sponsored jointly by Sun, the DOE and GRI, we have formulated and demonstrated a novel catalyst concept which allows the low temperature liquid or vapor phase catalytic conversion of light alkanes, (C_1-C_4), to their respective alcohols or ketones. This concept grew out of an understanding of biomimetic systems, together with new inorganic and catalytic chemistry. It is known that high oxidation state metal oxo (M=O) complexes will react with alkanes to give alcohols under mild conditions. Iron oxo (Fe=O) intermediates are, no doubt, involved in the enzymatic hydroxylation of C-H bonds in vivo (Cytochrome P-450). To date no one has been able to synthesize these Fe=O species under mild conditions using ONLY molecular oxygen as oxidant. Even nature requires the stoichiometric consumption of a co-reductant which donates the electrons and protons needed for closing the catalytic oxidation cycle. Nature's co-reductant is NADH which is converted to NAD while donating electrons and proton. Synthetic biomimetic systems add stoichiometric reagents for providing two protons and two electrons for every hydrocarbon molecule which is oxidized. These reagents are regenerated in*vivo but, in vitro processes require sacrificial consumption of valuable raw materials in the regeneration process. This stoichiometric requirement imposes severe and usually prohibitive economic constraints on commercial applications of such a catalytic process.

TABLE 1-1

PROPERTIES OF ETHERS AND ALCOHOLS

PROPERTY	MTBE	ETBE	GTBA	IPA	ETOH	MeOH
Oxygen, wt %	18.2	15.7	21.6	26.6	34	49.9
Sp. Gravity	0.74	0.74	0.791	0.789	0.79	0.796
Boiling Point, °F	131	163	181	180	172	149
RVP (lbs/in^2)	7.8	2.5	1.8	1.8	2.3	4.6
Blending RVP	9	5	12	14	23	75
RON BV	110–122	117–121	~103	113–119	~122	126
MON BV	98–102	100–105	~91	95–101	~96	104
(R+M)/2 BV	103–110	~110	~97	104–110	~100	115

In our laboratories we have learned how to tune the redox potential of metals in macrocyclic ligand environments to make them active for the selective air-oxidation of alkanes using ONLY molecular oxygen. As we mentioned above, nature uses electrons and protons together with iron to split the oxygen molecule and generate Fe=O. In so doing half of the oxygen molecule is converted to water while the other half is useful in oxidizing a substrate. We have asked the question whether oxygen can be split between two Fe(II) centers to make two Fe=O species using all of the oxygen as effective oxidant. While Cytochrome P-450 and MMO act as monooxygenases, we are making complexes which may act as synthetic dioxygenases. We have incorporated a number of oxidation-active metal centers into our synthetic catalysts in addition to iron and have found that we are able to convert methane, ethane, propane and the butanes either to the corresponding alcohol or carbonyl compound depending on the nature of the metal center in the macrocyclic ligand system. All-inorganic "macrocycles" such as polyoxometallates and framework substituted zeolites have also been investigated for both liquid and vapor phase cataytic oxidations.

The ease of oxidation of the substrates that we have studied are in the order isobutane> butane>propane>ethane>methane, which is also the order of increasing C-H bond dissociation energy,*Figure 1-2. Isobutane is the easiest of the light hydrocarbons to oxidize. As a result we are close to having achieved a practical catalytic process for isobutane oxidation. High rates, yields and selectivities have been observed. For this reason, we proceeded with the proof-of-concept phase for a process that converts isobutane to tert-butyl alcohol. There are many reasons why such a process is of interest. First, sales of field butanes from the gas industry to refiners is down due to the vapor pressure restrictions on automotive transportation fuels. Conversion of C4's to TBA would be a way to put unwanted butanes back into gasoline. TBA is both a commercially tested high octane, clean burning motor fuel component and in addition is the precursor to MTBE, a rapidly growing commodity fuel material which is being used to meet oxygen mandates of the Clean Air Act.

A four year program of work was undertaken to proceed which was planned to involve over 500 man-months of chemist, engineer and technician manpower for a duration of four years at a total cost of approximately 12 MM dollars.

FIGURE 1-2

HYDROCARBON REACTIVITY SERIES

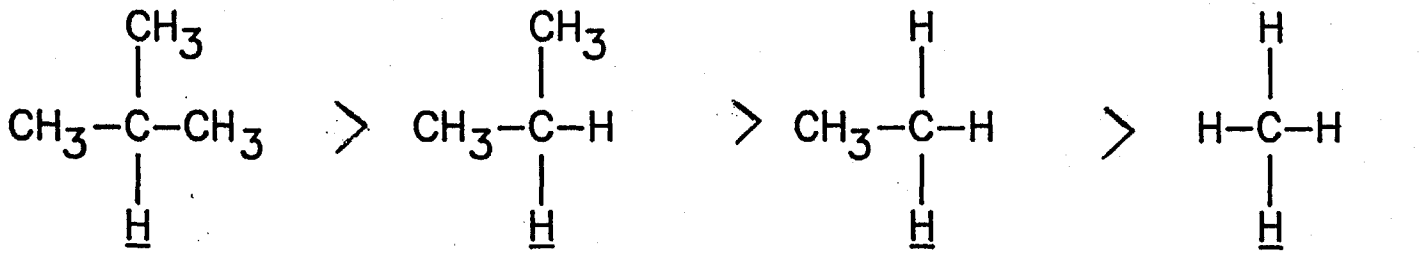

ISOBUTANE (91 Kcal) > PROPANE (94 Kcal) > ETHANE (98 Kcal) > METHANE (104 Kcal)

2.0 INTRODUCTION

2.1 MISSION STATEMENT

The mission of the work presented in this proposal is to generate novel catalytic technology which will permit the development of a simple, efficient and economical process for the direct conversion of natural gas to liquid transportation fuels. This process should be simple enough to liquify natural gas economically even at a remote reservoir site.

The most costly and energy-intensive step in currently applied commercial technology for the conversion of natural gas to liquid fuels is the steam reforming of the light hydrocarbons to produce synthesis gas. The synthesis gas is then converted to methanol which is passed over a catalyst to produce gasoline. If it were possible to catalytically transform natural gas into a methanol rich-oxidate rapidly and efficiently in a single step using air or O_2 as oxidant, the economics of the process would be dramatically improved (1-4). In contrast to the energy-inefficient steam reforming process, a direct "methane-to-methanol" process would be highly exoergic and, if properly carried out, would generate usable energy as steam, electricity or both. For these reasons, we are attempting to develop a process for the direct conversion of natural gas to an environmentally superior, methanol-rich liquid fuel oxygenate.

2.2 TECHNICAL OBJECTIVE

The technical objective of this proposal is to synthesize the first effective, practical molecular catalyst and demonstrate its use for the direct air-oxidation of natural gas to a methanol-rich oxidate which can either be used directly or converted into gasoline via known technology.

The light alkanes found in natural gas - methane, ethane, propane, and butane are among the most unreactive of all organic substrates. No effective catalysts are known for the selective partial oxidation of these relatively refractory materials. The development of an efficient catalyst for the smooth and selective oxidation of these light alkanes to alcohols will not only provide a solution to the problem of liquifying natural gas, but will create new opportunities to utilize the relatively inexpensive and abundant light alkanes for the production of a variety of valuable fuel and chemical products.

Figure 1-2 shows the relative ease of activation of C-H bonds in the kinds of light alkanes that make up natural gas. This trend is reflected in the ease of catalytic air oxidation of the hydrocarbons: isobutane > butane > propane > ethane > methane. The conversion of any major gas component as well as the entire gaseous mixture to an alcohol-rich oxidate has value both to the gas producer and the liquid transportation fuel producer alike. We are currently capable of oxidizing isobutane well and and could be ready for proof-of-concept of a propane to IPA process within two years. Ethane and methane oxidation will require more time than this. Thus it was proposed that the proof-of-concept stage proceed in several discrete stages: isobutane to TBA, propane to IPA, (ethane to ethanol - optional), and finally methane to methanol. Concurrent with the developmental aspects of each of these phases will be research phases geared to enable us to produce catalysts active enough for each succeeding phase.

these phases will be research phases geared to enable us to produce catalysts active enough for each succeeding phase.

3.0 PROGRAM ELEMENTS

Program elements are reviewed in the first Quarterly Report, (January 1-March 31, 1993), of the Cooperative Agreement. Table 3.1 indicates where Phase IV falls in the original, overall plan for the extended Cooperative Agreement.

TABLE 3.1

COMPONENTS OF NEW COOPERATIVE AGREEMENT

TIME	ACTIVITY	APPROX. LEVEL OF EFFORT
2/93 - 2/94	Phase IV C_1-C_4 Research	$1.0 MM
	Phase V TBA Development	$2.0 MM
2/94 - 2/95	Phase V TBA Development	$2.1 MM
	Phase VI C_1-C_3 Research	$0.9 MM

(Research Terminated 10/31/95)

4.0 HALOGENATED METALLOPORPHYRIN COMPLEXES AS CATALYSTS FOR SELECTIVE REACTIONS OF ACYCLIC ALKANES WITH MOLECULAR OXYGEN

James E. Lyons, Paul E. Ellis, Jr., and Harry K. Myers, Jr.

We have shown that halogenation of the porphyrin ring of a metalloporphyrin complex can convert a catalytically inactive material into an exceptionally active catalyst for the selective reaction of an alkane with molecular oxygen. The greater the degree of halogenation of the ring, the greater is the catalytic activity of the metal complex. The product profile, while characteristic of radical reactions, is sensitive to the nature of the metal center. Iron complexes are generally more active than those of cobalt, manganese or chromium. Activity of iron complexes is directly related to the Fe(III)/(II) reduction potential of the porphyrin complex. There is also a similar correlation between the Fe(III)/Fe(II) reduction potential and the rate at which iron haloporphyrin complexes decompose alkyl hydroperoxides. **These iron perhaloporphyrin complexes are not only the most active known liquid phase alkane air-oxidation catalysts, they are also the most active hydroperoxide decomposition catalysts known to date**. The nature of the products formed is dependent on the structure of the aliphatic substrate that is oxidized and can be rationalized by a catalytic pathway that very efficiently generates alkyl and alkoxy radicals at low temperatures. The relationship between the electrochemical properties of these complexes and the rates of alkane oxidation and hydroperoxide decomposition lends insight into possible mechanisms of catalytic activity.

4.1 INTRODUCTION

The selective reaction of an alkane with molecular oxygen to give an alcohol or carbonyl compound without extensive oxidative cleavage or concomitant combustion has considerable potential as an inexpensive means of producing valuable oxygenates. Selective oxidation of an alkane is usually hard to achieve thermally since under conditions necessary to promote facile autoxidation, alkane oxidations are often difficult to stop short of combustion (1). Metalloporphyrin complexes have long been known to catalyze oxidative hydroxylation of alkanes in a biomimetic manner, but these complexes have required either a) stoichiometric oxygen atom donors other than oxygen (2-10), b) sacrificial coreductants (11-20), c) electrochemical reduction (21,22), or d) photolytic assistance (23,24).

Recent work by ourselves (25-34) and others (35-38) has shown that halogenated metalloporphyrins are efficient catalysts for the direct reaction of alkanes with oxygen to give alcohols and/or carbonyl compounds at unprecedented rates under very mild conditions. No coreductants or stoichiometric oxidants are required (25-38). Neither is it necessary to employ photochemical or electrochemical techniques in these oxidations. Because of the potential utility of a direct catalytic reaction of an alkane with molecular oxygen in a selective manner, we report the results of a study on the oxidation of a series of acyclic alkanes under mild conditions catalyzed by halogenated metalloporphyrins.

4.2 RESULTS AND DISCUSSION

4.2.1 Oxidations of Isobutane and Propane

We have found that chromium, manganese and iron complexes of halogenated porphyrinato ligand systems, Figure 1, are active catalysts for the oxidation of unactivated acyclic alkanes having either secondary or tertiary carbon-hydrogen bonds. Primary C-H bonds are quite resistant to oxidative attack in the presence of these catalysts. Table 1 shows the results of oxidations of isobutane at 80*C in benzene solutions of metalloporphyrin complexes using molecular oxygen as the oxidant. tert-Butyl alcohol is the predominant product of the reaction, being formed in yields in the neighborhood of 90%. Several points are evident from the data presented in Table 1. Firstly, halogenation of the phenyl groups of tetraphenylporphyrinatometal complexes causes a large increase in their catalytic activity. Secondly, halogenation of the meso-phenyl groups on the macrocycle has a greater effect on the catalytic activity of iron complexes than on those of manganese and chromium. The effect on catalytic oxidation activity of meso-phenyl halogenation of metallotetraphenylporphyrin complexes is in the order Fe > Mn > Cr. Thus, iron haloporphyrin complexes are the most active of those complexes that we have examined. The catalytic oxidation of isobutane using tetrakispentafluorophenylporphyrinatoiron hydroxo-,azido-,and chloro-complexes is shown in Figure 2. Rates are rapid and no induction periods are apparent. Table 2 shows the effect of the degree of halogenation on the catalytic oxidation activity of porphyrinatoiron chloro, azido oxo and hydroxo complexes. Figure 2 indicates the relative catalytic activities of the hydroxo-, azido-, and chloro forms of $Fe(TPPF_{20})X$. It is interesting to note that any induction period must be very short if it exists at all.

Table 3 shows the results of oxidations of isobutane at 60°C in the presence of perhaloporphyrinatometal azide complexes. At 80°C, Table 1, complexes having axial chloride provide suitable catalysts, whereas for high activity at 60°C or lower it is desirable to use the azido- or hydroxo- forms of the catalyst. Combining the results in Tables 1, 2 and 3, it can be seen that the greater the extent of halogenation of the porphyrin macrocycle, the more active is the metal complex for alkane oxidation. Table 4 shows the results of oxidations of propane at 125°C in the presence of perhaloporphyrinatometal azide complexes. Although higher temperatures are required to oxidize the secondary C-H bond of propane than the tertiary C-H bond of isobutane, the selectivity to a mixture of acetone and isopropyl alcohol is high and only small amounts of carbon oxides are formed.

Table 5 shows the results of oxidations with conventional cobalt oxidation catalysts. Prior to our work on the perhaloporphyrin complexes, the bispyridyliminoisoindoline, BPI, complexes were among the very most active alkane autoxidation catalysts known (39-40). A comparison of the results of Table 5 with those in Tables 1, 2, 3 and 4 indicates that perhaloporphyrin complexes are more active by over an order of magnitude than even the most active cobalt complexes currently available.

4.2.2 Effects of Electron Withdrawal From the Macrocycle

As the number of halogen substituents around the periphery of the porphyrin macrocycle increases, the ease of reducing Fe(III) in the coordination sphere increases (28-34,38). Figure 3 demonstrates a regular relationship between catalytic turnovers for both isobutane and propane

oxidations in a set time period, and the Fe(III)/Fe(II) reduction potential of the catalyst used. Thus, as the degree of halogenation increases, the Fe(III)/Fe(II) reduction potential also increases and the catalytic activity improves. These iron complexes are soluble enough in aliphatic hydrocarbons to allow reactions to proceed in neat alkane solutions, Table 6. When iron haloporphyrin complexes are dissolved in neat isobutane, oxidation to tert-butyl alcohol can be efficiently carried out under very mild conditions of temperature and pressure. These complexes smoothly catalyze isobutane oxidations at temperatures between room temperature and 100°C, and oxygen partial pressures between one and five atmospheres. Reaction rate and catalyst life are unprecedented. We have achieved well over 20,000 turnovers (moles product(s) formed/mole catalyst used) in tert-butyl alcohol, TBA, production. Although catalyst decomposition is a problem at somewhat elevated temperatures (>60°C), well over 10,000 catalytic turnovers have been observed in the room temperature oxidation of neat isobutane catalyzed by tetrakis(pentafluorophenyl -octabromo)iron(III)hydroxide with no noticeable deferration or decay of the catalyst (by UV visible spectroscopy), Table 6.

4.2.3 Mechanism Considerations

As one speculates on how oxidations catalyzed by electron deficient metalloporphyrins might proceed, it is instructive to consider the mechanism by which iron porphyrin systems are thought to catalyze C-H bond oxidations in biological systems, Figure 4,(41-48). In enzymatic pathways electrons and protons are available to the heme system throughout the process. However, in our case, without coreductants (2-20), or photochemical or electrochemical assistance (21-24), monooxygenase activity of the type known to occur in vivo is not possible. Using the electrons of an oxygen-bridging iron catalyst system, Figure 5, one could envision a catalytic dioxygenase pathway. Steps a.,b.,c., and f. in this hypothetical pathway have precedence in the literature (49-51). There remains the question as to whether a hypothetical Fe(IV)oxo intermediate would be effective for C-H bond cleavage, Figure 5,d. Furthermore there is the strong possibility that radicals formed from C-H bond homolysis, if it occurs, Figure 5,d., should be capable of diffusing into the reaction medium and initiating radical chain oxidation processes. Perhaps then, if radical escape is occurring, the pathway shown in Figure 5 ought to be considered as a form of living initiator of alkyl radicals as well as a possible catalytic precursor of alcohol by rebound mechanisms (5,16), Figure 5,e.

The oxidation of organic compounds using metalloporphyrin complexes has been known for some time (52). Catalytic activity was generally poor, catalyst life was short and prior to our work (25-28) no alkane oxidation activity had been observed in unpromoted systems. Why then are the electron-deficient metalloporphyrins such good catalysts? One reason, of course, is the greater oxidative and thermal stability of the catalyst. Replacing hydrogens with halide substituents reduces the number of carbon hydrogen bonds that can undergo oxidative attack. A perhaloporphyrin complex has no carbon hydrogen bonds which might undergo cleavage. In addition, as electron withdrawing halo groups are introduced into the macrocyclic ring of the catalyst, the ligand itself becomes more stable to reduction by the central metal atom. It is well known that the porphyrinato ligand in high oxidation state porphyrinatoiron oxo complexes exists as the radical cation due to electron transfer from the ligand to the iron center(35,53). Thus, there may be a greater tencency for the active catalyst to behave as an oxo centered radical, (P)Fe-O*, than a ferryl species, (P^{+*})Fe=O, with increased electron withdrawal from the macrocycle (35).

Our work has shown that not only are electron-deficient metalloporphyrin complexes more robust, but initial rates of oxidation are far faster than observed when non-halogenated porphyrin complexes are used as catalysts. In fact, using halogenated metalloporphyrin catalysts, oxidations occur at temperatures so low that most metalloporphyrin complexes are completely inactive, Tables 1-4. Increased reaction rate can be rationalized as a result of increased Fe(III)/Fe(II) reduction potential due to electron withdrawal from the metal center by the electron deficient ligand system. Thus, in most metalloporphyrin-catalyzed oxidations, the pool of iron exists largely or exclusively as iron(III). Initial formation of Fe(II) is disfavored, and the process represented in Figure 5,e does not occur readily. Most of the iron is rapidly converted to the μ-oxo dimer, Figure 5,f, which is usually inactive (54,55). We have shown that μ-oxo dimers are active catalysts in the perhaloporphyrin series, Tables 1,2 and that both iron(III) μ-oxo dimer and Fe(II) species co-exist under reaction conditions (30). Therefore, although we by no means have established the existance of the scheme depicted in Figure 5, electron deficient porphyrins might indeed possess the necessary properties to behave in this manner, while more electron-rich porphyrin complexes do not.

4.2.4 Radical Routes and Hydroperoxide Intermediates

The homolysis of C-H bonds in biological systems occurs in a cage which encourages rebound to produce alcohols. Radicals do not readily escape into an aqueous medium in vivo as they might be expected to do cf. Figure 5,d, when an electron-deficient metalloporphyrin catalyst is used in organic media. If a substantial amount of the reaction proceeds through a radical pathway, then a free radical inhibitor should quench the reaction. We have shown that as little as one mole of di-tert-butyl-p-cresol per mole of catalyst can substantially quench the oxidation reaction. Furthermore, if radical pathways are important, then peroxidic and hydroperoxidic intermediates formed by reactions of alkyl radicals with dioxygen should be involved, eq. 1,2(56-58).

$$R^{\bullet} + O_2 \longrightarrow RO_2^{\bullet} \qquad (1)$$

$$RO_2^{\bullet} + RH \longrightarrow RO_2H + R^{\bullet} \qquad (2)$$

It was interesting, therefore, to find (59) that halogenated porphyrins are highly active catalysts for the decomposition of alkyl hydroperoxides to form alcohols in a selective manner, eq. 3, Table 7, Fig 6. In addition, the more highly halogenated the porphryin macrocycle, the greater the activity of

$$RO_2H \longrightarrow ROH + O_2 \qquad (3)$$

the metalloporphyrin catalyst for this reaction. Thus, as shown in Figure 3 and Table 8, the greater the Fe(III)/Fe(II) reduction potential, the greater the rate of alkane oxidation and the greater the rate of hydroperoxide decomposition. We have proposed (59) that a modified Haber-Weiss cycle, Figure 7, creates the alkoxy and alkylperoxy radicals that lead to the stable products of decomposition: ROH and oxygen. A kinetic analysis of this data (60) by Labinger has shown that such a pathway, with the slow step being reduction of Fe(III) to Fe(II) by alkyl hydroperoxide could account for rapid TBA formation during autoxidation when electron deficient porphyrins with high Fe(III)/Fe(II) reduction potentials are used as catalysts. In fact, Labinger's analysis suggests that the majority of the isobutane

oxidation reaction may proceed through a metalloporphyrin-assisted radical chain rather than a purely catalytic reaction mechanism.

4.2.5 Alkane Structure and Product Profile

The high selectivity observed for the oxidations of isobutane and propane shown above is not characteristic of radical reactions. The reason for this may be the low temperatures at which it is possible to conduct reactions using the highly active metallohaloporphyrin catalysts. A structural feature of these two substrates that enhances selectivity is that all carbon-carbon bonds are carbon-methyl bonds. This results in a low likelihood of C-C bond cleavage (β-scission)(61) from a possible alkoxy radical intermediate since β-scission requires formation of an unstable methyl radical (eq. 4). Thus, few carbon-carbon bond cleavage or combustion products are formed in the mild oxidations of isobutane and propane. If, on the other hand, one conducts reactions of n-butane with

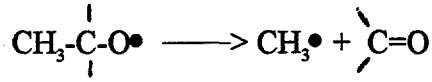

$$CH_3\text{-}\overset{|}{\underset{|}{C}}\text{-}O\bullet \longrightarrow CH_3\bullet + \diagdown\!\!\!\!\diagup C{=}O \qquad (4)$$

oxygen in the presence of perhaloporphyrin complexes, significant oxidative cleavage results, forming by-products such as acetic acid and acetaldehyde, Table 9. It is of interest to note that selectivity to 2-butanone is enhanced by chromium complexes over those of iron. The azido form of the chromium complex is most effective for generating ketones via alkane oxidations. Oxidations carried out in the presence of this catalyst are very rapid and exhibit the characteristic sigmoid kinetic curve of autoxidations including the presence of a substantial induction period, Figure 8.

Table 10 details the product profiles for the oxidations of a series of branched alkanes with 3°C-H bonds and Figure 9 summarizes the dependence of product profile on substrate structure for oxidations catalyzed by tetrakis(pentafluorophenyl β-octabromo)porphyrinatoiron(III)hydroxide. Those hydrocarbons having tertiary C-H bonds react at temperatures of 60°C or less while those having secondary but no tertiary C-H bonds require more elevated temperatures and primary C-H bonds have very low reactivity at any of the temperatures used. The relative C-H bond reactivity pattern: 3°> 2°> 1° is consistent with that of radical initiated oxidation pathways (1b,49, 50, 62).

The ratio of selective oxidation to cleavage products in the case of propane or isobutane oxidations is ~9/1. On the other hand, the ratio of four or five-carbon oxidation products to cleavage products is less than 2/1 in oxidations of n-butane and 2-methylbutane respectively, and when 3-methylpentane is oxidized, the oxygenation/cleavage ratio drops below 1. It is interesting in this regard that decomposition of tert-amyl hydroperoxide, TAHP, leads to a far greater extent of carbon-carbon bond cleavage than decomposition of tert-butyl hydroperoxide, Table 11. Furthermore, the ratio of tert-amyl alcohol to acetone produced during catalyzed TAHP decomposition in benzene at room temperature is very similar to the ratio of these products formed via 2-methyl butane oxidation, Table 10. This observation is consistent with the common intermediacy of the 2-methyl-but-2-oxy radical in both cases, eq.5.

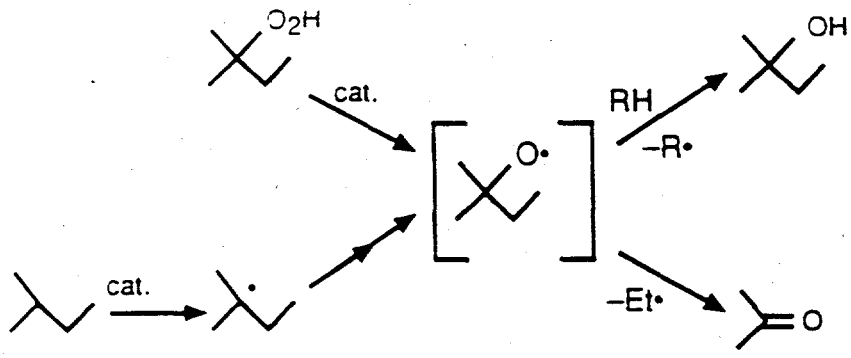

(5)

When the symmetrical hydrocarbon, 2,3-dimethylbutane is used, a substrate having two easily abstractable 3° C-H bonds and an isopropyl group adjacent to either internal carbon atoms, cleavage predominates over six-carbon oxidation products by a wide margin.

Thus, by varying the structure of the alkane substrate we are able to move from selective oxygenations that retain the intact carbon skeleton and give only 10% carbon-carbon bond cleavage or less, to greater than 90% C-C bond cleavage reactions in these alkane oxidations. The direction of the effect of alkane structure on carbon-carbon bond scission is consistant with the intermediacy of alkoxy radicals as significant reaction intermediates (61, 62).

Iron haloporphyrin catalyzed oxidation of 2,2,3-trimethylbutane, eq.6,7 gives rise to equimolar amounts of acetone and products of the very stable tert-butyl radical. The hypothetical alkoxy radical in this case would cleave nearly exclusively giving very little C_7 oxygenate.

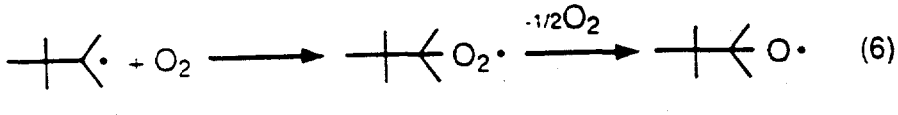

(6)

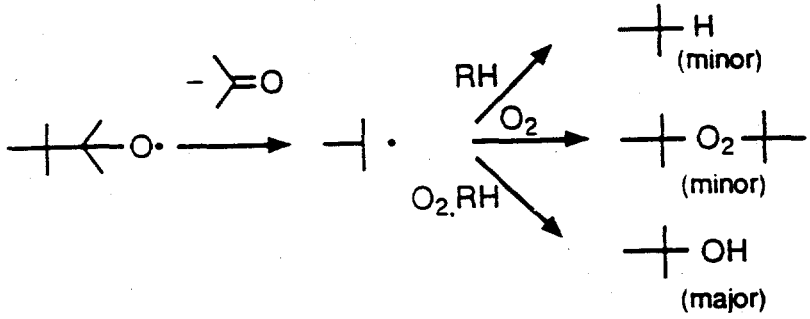

(7)

Greene and coworkers (62) have demonstrated that the ratio of rates of alkyl cleavage from alkoxy radicals vs. H abstraction from cyclohexane at 40°C increases dramatically from methyl to ethyl to isopropyl. In Table 12 we compare the % cleavage products formed during catalytic oxidations at 60 and 80°C with this ratio and find qualitative similarities. Differences arise since H-abstraction in the oxidation cases would be largely from 3° C-H rather than from 2° C-H bonds. Nonetheless, there is clear directional similarity between the extent of intramolecular C-C bond cleavage reactions from alkoxy radicals and the selectivity of metalloporphyrin catalyzed oxidations that we have conducted.

4.3 CONCLUSIONS

Halogenated metalloporphyrin complexes are extremely active catalysts for the selective oxidation of alkanes and the decomposition of alkylhydroperoxides to alcohols. Perhalotetraphenylporphyrinatoiron complexes are the most active catalysts known for both of these reactions giving rates an order of magnitude greater than any previously reported. The low temperatures at which these oxidations can be conducted result in some unique and useful selectivities.

Although biomimetic chemistry may be involved in initiation of radical chains, Figure 5d, and indeed in a degree of dioxygenase-like catalysis, Figure 5e, decomposition of peroxidic intermediates by iron perhaloporphyrin catalysts is also of great importance. The bulk of the available evidence indicates that radical chain processes are occurring. Figure 10 indicates a possible scheme in which the metal complexes initiate formation of radicals, 1, that generate hydroperoxides, 2, which are catalytically converted to radicals, 3, that produce stable oxidation products, 4. If this is so, then the majority of the alcohol produced in the oxidation of isobutane, for example, would arise by hydrogen abstraction, 5, rather than by biomimetic rebound fig 4,e. It seems likely that all of these processes are proceeding in these oxidations and further work will sort out the relative importance of each.

4.4 EXPERIMENTAL SECTION

4.4.1 **General**. ^{1}HNMR (300MHz Bruker MSL), ^{19}FNMR (300 MHz Nicolet NT-300), IR spectra (Mattson R/S FTIR), absorption spectra (HP 8452A) and ion cycloctron resonance mass spectra (Nicolet FTMS) were collected routinely. Fast atom bombardment mass spectra were collected by M-Scan, Inc. (West Chester, PA.) Laser desorption mass spectra were collected at the University of Delaware on a Nicolet LD-FTMS 2000 instrument.

4.4.2 **Solvents**. All solvents used were HPLC grade from Aldrich and were used as purchased unless further purification is noted. $CHCl_3$ used contained 0.75% ethanol unless it is noted that ethanol-free $CHCl_3$ was used.

4.4.3 **Reagents**. All non-porphyrin reagents were purchased from Aldrich unless noted and were certified ACS reagent grade or better. FeTPPCl, MnTPP(OAc), and $(FeTPP)_2O$ were purchased from Strem Chemicals. $FeTPPF_{20}Cl$ and H_2TPPF_{20} were purchased from Aldrich. $Fe(TPPCl_8\text{-}Br_4)Cl$ was purchased from Midcentury Chemicals. CrTPPCl(63), $MnTPPN_3$ and $CrTPPN_3$ (64), $FeTPPN_3$ (65), $[Fe(TPP\text{-}Br_4)]_2O$ (66), $Fe(TPP\text{-}Br_4)Cl$ (67), $Fe(TPPCl_8)Cl$ and

$Fe(TPPCl_8)OH$ (68), $Fe(TPPF_{20})OH$ and $(FeTPPF_{20})_2O$ (69), $Cr(TPPF_{20})Cl$ (70), $Mn(TPPF_{20})OAc$ (71), Co(BPI)OAc (72), and $Co(BPI)(O_2Bu^t)$ (40) were made by the referenced methods.

4.4.4 **Oxidation Methods**. Oxidations were carried out either in 60 cc Fisher-Porter aerosol tubes or in 300-500 ml batch autoclaves as indicated in the Tables. Reactions run in Fisher-Porter tubes equipped with a baffled magnetic stirrer, were carried out at 100 psig total pressure at the temperatures indicated in the Tables. The catalyst was dissolved in either the neat alkane or in a benzene solution to which the alkane was added. The Fisher-Porter tube was attached to a manifold for adding and releasing gases. Oxygen was admitted to the tube and the tube was then submerged in a constant temperature bath at reaction temperature. The reaction mixture was magnetically stirred for the amount of time indicated in the Table. Gas uptake was measured by a pressure gauge and oxygen was replenished as it was consumed. At the time indicated in the Table, the tube was removed from the bath, cooled to 0°C and the gas slowly vented. The liquid product was weighed and analyzed by standardized glpc. Caution: Many of the reactions conducted in this work were done within the explosion range. Reactions were performed in a properly barricaded laboratory area for safety.

Propane oxidations were routinely performed in a glass-lined 300 ml stainless steel autoclave fitted with thermocouple and magnedrive stirrer. All internals: cooling coils, thermocouple, and stirrer blades and shaft were coated with Teflon. A solution of the catalyst in benzene was added to the glass liner, the autoclave secured and liquid propane was pumped into the reactor. Air was added to a total pressure of 1500 psig and the reactor heated to reaction temperature. After the reaction time indicated in the Tables, the reactor was cooled to room temperature, gases slowly vented into a gas bag for glpc analysis, and liquid product was analyzed by standardized glpc.

4.4.5 **Hydroperoxide decompositions**. A solution of the catalyst in p-xylene (internal standard) was quickly added to a rapidly stirring solution of tert-butyl hydroperoxide in benzene at room temperature. Oxygen evolution was measured manometrically and liquid products were analyzed periodically by standardized gas chromatography. [CAUTION - Reactions should be run in dilute solutions of catalyst and/or hydroperoxide to avoid exotherms and dangerously fast gas evolution.]

Benzene, (99.99%, Aldrich), tert-butyl alcohol, (99.6%, Aldrich), and p-xylene, (99 + %, Aldrich) were used as purchased. tert-Butyl hydroperoxide (90%, 5% water, 5% tert-butyl alcohol) was used as purchased from Aldrich.

4.4.6 **Metalloporphyrin Synthesis $Mn(TPPF_{20})N_3$**. 0.4 g of Mn $(TPPF_{20})OAc$ is dissolved in 40 ml of $CHCl_3$. 10 ml of saturated aqueous NaN_3 solution is stirred vigorously with the $CHCl_3$ solution overnight. The water layer is separated and 10 ml of fresh NaN_3 solution is added and stirred again overnight. The water layer is removed and the $CHCl_3$ is washed 3 times with 20 ml of H_2O. The $CHCl_3$ solution is dried over Na_2SO_4 then filtered and rotovapped to dryness. This material is washed with copious amounts of H_2O then dried overnight in a vacuum over P_2O_5 at 60*. Yield 0.36 g. IR shows a N-N stretch at 2030 cm^{-1}.

$Cr(TPPF_{20})N_3$. 400 mg of $Cr(TPPF_{20})Cl$ is dissolved in 100 ml of acetone. 4.0 g of NaN_3 is added and the mixture is stirred for 48 hrs. at room temperature. After the solvent is removed and the solid product is washed with H_2O and dried, a yield of 350 mg of $Cr(TPPF_{20})N_3$ is obtained. IR(KBr) shows a N-N stretch at 2053 cm^{-1}.

$Fe(TPPF_{20})N_3$. 0.5 g of $Fe(TPPF_{20})Cl$ is dissolved in 100 ml of acetone. To this is added 5.0 g of NaN_3. Most of the NaN_3 and all of the $Fe(TPPF_{20})Cl$ is dissolved. This mixture is stirred at room temperature for 24 hrs. then filtered and rotovapped to dryness. The material is washed with large amounts of H_2O then vacuum dried overnight at 60°. Yield 0.4 g. IR shows (N-N) stretch of azide at 2053 cm^{-1}. Large crystals were grown by recrystallization in 5% hexane in chloroform.

$Fe(TPPF_{20}$ β-$Br_8)Cl$. Under N_2, 0.500g of $Fe(TPPF_{20})Cl$ is dissolved in 300 ml of degassed CCl_4 which was freshly distilled (over P_2O_5). 100 ml of $6MBr_2/CCl_4$ is added quickly to this solution while at reflux. After 18 hours the Soret absorption has moved from 418 nm to 429 nm. 50 ml more of $6MBr_2$ in CCl_4 is added at this point. After several more hours of reflux the Soret absorption remains at 429 nm. The solution is cooled, filtered and washed three times with H_2O then evaporated to dryness. The greenish-brown material is chromatographed on neutral alumina eluting with $CHCl_3$. The first green band is collected, treated with dilute HCl and evaporated to dryness. After drying in vacuo at 110°C, 590mg of the $Fe(TPPF_{20}β\text{-}Br_8)Cl$ is obtained. FAB/MS:M^+-Cl 1659.

$Fe(TPPF_{20}β\text{-}Br_8)N_3$. 300 mg of $Fe(TPPF_{20}β\text{-}Br_8)Cl$ is dissolved in 300 ml of methanol and 200 ml of acetone. To this solution is added 3.5 g of NaN_3 then 10 drops of glacial acetic acid. The solution is stirred for 72 hr. then filtered and the solvent is removed by rotary evaporation. The dry material is washed with water and dried <u>in vacuo</u> at room temperature. Yield is quantitative. IR(KBr): $_{N\text{-}N}$ 2049 cm^{-1}.

$Cr(TPPF_{20}β\text{-}Br_8)Cl$. Under N_2, 0.700 g. of $Cr(TPPF_{20})Cl$ is dissolved in 600 ml. of freshly distilled (over P_2O_5) CCl_4. The solution is heated to 40°C and 150 ml. of Br_2 is added dropwise with stirring. The Soret absorption of the unreacted chromium porphyrin at 436 nm shifts to 481 nm after 22 hrs. reaction time. At this point, the solution is cooled, filtered and washed three times with water, then evaporated to dryness. The green material is redissolved in a minimum of $CHCl_3$ and chromatographed on neutral alumina. The solution is washed with 1N HCl then evaporated to dryness. Yield 350 mg. UV/VIS (toluene), 400, 483, 599 nm.

$Cr(TPPF_{20}β\text{-}Br_8)N_3$. 300 mg of $Cr(TPPF_{20}β\text{-}Br_8)Cl$ is dissolved in 300 ml of methanol and 200 ml of acetone. To this solution is added 3.5g of NaN_3 then stirred for 48 hr. After filtering, the solvent is removed by rotary evaporator and the solids washed with water and dried <u>in vacuo</u> at room temperature. Yield: 260 mg. IR(KBr): $_{N\text{-}N}$ 2050 cm^{-1}.

$Mn(TPPF_{20}β\text{-}Br_8)Cl$. $Mn(TPPF_{20})Cl$, .0.400g., is dissolved in 300 ml of freshly distilled (over P_2O_5) CCl_4 under N_2. The solution is warmed and 125 ml of Br_2 is added dropwise with stirring. The reaction is continued until a sample shows a Soret of greater than 450 nm. After washing three times with water the solvent is evaporated. The material is dissolved in a minimum of $CHCl_3$ and chromatographed on neutral alumina. The $CHCl_3$ solution is washed with 1N HCl then evaporated to dryness. Yield 320 mg. UV/VIS (Toluene): 399, 452, 495, 603.

$Mn(TPPF_{20}\beta\text{-}Br_8)N_3$. 150 mg of $Mn(TPPF_{20}\beta\text{-}Br_8)Cl$ is dissolved in 150 ml of methanol and 100 ml of acetone. 1.5 g of NaN_3 is added and the mixture stirred for 48 hours. After filtration and removal of the solvent, the solids are washed with water. 130 mg of product is recovered IR(KBr): $\nu_{N\text{-}N}$ $2037cm^{-1}$.

$H_2TPPF_{20}\beta\text{-}Cl_8$. The preparation of this porphyrin is accomplished by the chlorination of $ZnTPPF_{20}$ with Cl_2 and in-situ removal of Zn with HCl.

A three-necked flash fitted with reflux condenser and N_2 inlet port is charged with 1.0 g (0.96 mmol) of $Zn(TPPF_{20})$ and 500 ml CCl_4 degassed previously with N_2. The N_2 flow is terminated and Cl_2 is bubbled through the solution slowly for 4 min. while the solution is refluxed. After 4 min. the Cl_2 flow is stopped and N_2 is used above the condenser to blanket the apparatus. Ater 1 hr. of reflux an aliquot is removed and the Soret absorption is checked. The reaction is complete when the Soret reaches 448 nm. If the reaction is incomplete then a second 4 min. Cl_2 addition is performed with subsequent 1 hr. of additional reflux period. The solution is allowed to cool to 60° then HCl gas is bubbled through the hot solution for 2 min. and stirred for 15 min. more. TLC (silica gel, CH_2Cl_2) is used to check that the Zn removal is complete. The green solution is cooled then washed with 200 ml of 5% $NaHCO_3$ then the solvent is removed by rotary evaporation. Chromatography on neutral alumina eluting with $CHCl_3$ gave 1.28 g (71% yield). LDMS: M^+=1250. ^{19}FNMR ($CDCl_3$, 282.307 MHz referenced to C_6D_5F):- 136.88 (m, 8F, o-ArF), -148.34 (t, 4F, p-ArF), -160.50 (m, 8F, m-ArF).

$Fe(TPPF_{20}\beta\text{-}Cl_8)Cl$. In a 250 ml flask is charged 750 mg of $H_2TPPF_{20}\beta\text{-}Cl_8$, 200 ml of DMF and 10 ml of acetic acid. After heating to 160° under N_2, 240 mg of powdered $FeCl_2.4H_2O$ is added with stirring. After 10-15 min. the solution is cooled and poured into 200 ml of H_2O. After standing overnight the mixture is filtered and the solids dissolved in $CHCl_3$ and chromatographed on alumina eluting with $CHCl_3$ giving 580 mg (72% yield) after treatment with Na_2SO_4 and drying. ^{19}FNMR ($CDCl_3$ referenced to C_6D_5F):δ-114.4, -119.2 (broad resonances, 8F, o-ArF), -148.4 (4F, p-ArF), 157.1 (8F, m-ArF). LDMS:M-Cl^+ 1304,M^+ 1339.

$Fe(TPPF_{20}\beta\text{-}Cl_8)N_3$. This azide complex was prepared by reacting 100 mg of $Fe(TPPF_{20}\beta\text{-}Cl_8)Cl$ with 1.0 g of NaN_3 in 200 ml of acetone with vigorous stirring for 24 hours. The product mixture was filtered. The filtrate was evaporated to dryness and the remaining solid washed with water. The solid product was then dried in vacuo at 70°C. The infrared spectrum shows a sharp $\nu_{N\text{-}N}$ stretch at 2037 cm^{-1}.

$Cr(TPPF_{20}\beta\text{-}Cl_8)Cl$. A 250 ml flask containing a solution of H_2 $TPPF_{20}\beta\text{-}Cl_8$ (750 mg, 0.60 mmol) in 200 ml DMF under a nitrogen atmosphere was placed in an oil bath preheated to 160°C. After the solution had started refluxing, $Cr(CO)_6$ (132 mg, 0.60 mmol) was added every 30 min. until the chromium insertion was judged to be complete by TLC. The reaction mixture was cooled to room temperature under a N_2 atmosphere. At this point the solution was poured into 200 ml of cold saturated NaCl solution and stirred for 10 min. The brown flocculate was isolated from the aqueous solution by vacuum filtration. The resulting brown paste was dissolved in 20 ml $CHCl_3$ and chromatographed on Al_2O_3 with $CHCl_3$ steadily enriched with methanol. The product was the second

porphyrin component which came off the column and eluted as a broad red-brown band and was treated in the normal fashion with 1NHCl. The solvent was removed by rotary-evaporation to give $Cr(TPPF_{20}\beta\text{-}Cl_8)Cl$ in 30% yield. LDMS: M^+ -Cl 1299, M^+ 1336. UV/VIS ($CHCl_3$):432 nm.

$Cr(TPPF_{20}\beta\text{-}Cl_8N_3$. The complex, $Cr(TPPF_{20}\beta\text{-}Cl_8)Cl$, 96 mg, and sodium azide, 1.0 g. were stirred in 200 ml of acetone at room temperature for 72 hours under nitrogen. After this time the solution was filtered. The filtrate was evaporated to dryness giving a solid product which was washed thoroughly with water and dried in vacuo. The purple azide complex ($_{N\text{-}N}$ 2055 cm^{-1}) was recovered in quantitative yield. UV/VIS ($CHCl_3$):418,440 nm.

$Mn(TPPF_{20}\beta\text{-}Cl_8)Cl$. The free base, $H_2TPPF_{20}\beta\text{-}Cl_8$, 300 mg, was dissolved in 33 ml of DMF. The solution was stirred at reflux under nitrogen for 15 minutes. At this point $Mn(OAc)_2\bullet 4H_2O$, 200 mg, was added and the mixture was stirred at reflux under nitrogen for an additional 30 minutes. An additional 50 mg of $Mn(OAc)_2\bullet 4H_2O$ was added and the mixture refluxed an additional 30 minutes. At this point an aliquot was taken, evaporated to dryness, and the solid taken up in $CHCl_3$. A TLC check of this solution revealed no starting porphyrin. The DMF solution of manganese complex was then allowed to cool to room temperature and added to 50 ml of a 30 weight % solution of sodium chloride in water. The mixture was refrigerated overnight during which time the product precipitated from solution. The solid product was washed with water (5x20 ml), filtered, air dried for a hour then dissolved in a minimum of $CHCl_3$. The $CHCl_3$ solution was chromatographed on alumina then the product was taken to dryness in a rotary evaporator. The solid product was dried at 80°C in a vacuum oven. Recovered was 240 mg of product having a Soret at 450 nm.

$Mn(TPPF_{20}\beta\text{-}Cl_8)N_3$. To a round-bottom flask under N_2 is charged 100 mg of $Mn(TPPF_{20}\beta\text{-}Cl_8)Cl$, 300 ml of acetone, 50 ml of methanol, and 1.0 g of NaN_3. This mixture is stirred vigorously at room temperature for 12 hrs., filtered and the solvent removed by rotary evaporation. The solids are dissolved in 50 ml of CH_2Cl_2 and washed twice with 25 ml of H_2O after which the organic layer is dried over Na_2SO_4. The solvent is removed by rotary evaporation and the purple solids dried in vacuo overnight at room temperature. The yield is quantitative. IR(KBr):$_{N\text{-}N}$ = 2031 cm^{-1} with a shoulder at 2066 cm^{-1}.

$Co(TPPF_{20}\beta\text{-}Cl_8)$. A stirred solution of 200 mg of $Co(OAc)_2\bullet 4H_2O$ in 50 ml of DMF is heated to 140° in an oil bath then 250 mg of the free base, $H_2TPPF_{20}\text{-}Cl_8$ is added as a powder all at once. After 15 min. an aliquot is taken, evaporated to dryness and a TLC check is made on alumina eluting with $CHCl_3$. No free base is seen by TLC. The total reaction time is limited to 30 min. The contents of the flask are cooled quickly to room temperature and added to an equal volume of saturated NaCl solution. The resulting precipitate was filtered giving a reddish-brown paste which is redissolved in $CHCl_3$ and chromatographed on neutral alumina eluting with $CHCl_3$. After evaporation of the solvent and drying in vacuo at 110°, 210 mg of the product is obtained. UV/VIS($CHCl_3$):427,552,578 nm. LDMS:M^+ 1307.

$Co(BPI)N_3$. In an erlenmeyer flask under N_2 is stirred 0.5 g of Co(BPI)(OAc) in 200 ml of methanol. At reflux 0.6 g of NaN_3 is added and reflux is continued for 1 hr. After cooling and filtering, the volume is reduced to 100 ml then an equal volume of ether is added to precipitate the

product which is washed with water, then ether and then dried in vacuo overnight at room temperature. Yield is quantitative. IR(KBr): $_{N-N}$ = 2015 cm^{-1}.

Fe(TPPβ-Br_4)N_3. In a round-bottomed flask under N_2 is charged 100 mg of Fe(TPPβ-Br_4)Cl and 100 ml of $CHCl_3$. With stirring 1.0g of NaN_3 in 50 ml of H_2O and 5 drops of H_2SO_4 is added. After stirring for 12 hr. the $CHCl_3$ is separated, filtered and washed twice with water. The $CHCl_3$ layer is reduced in volume by rotary evaporation until a precipitate forms. The material is filtered and washed with H_2O then dried in vacuo. Yield is 90 mg. UV/Vis ($CHCl_3$):433, 523, 602. IR(KBr): $_{N-N}$ = 2030 cm^{-1}.

Fe(TPPCl_8)N_3. In an erlenmeyer flask under N_2 is dissolved 200 mg of Fe(TPPCl_8)Cl in 100 ml of $CHCl_3$. To this is added 2g of NaN_3 dissolved in 40 ml of H_2O and 5 drops of H_2SO_4. This two phase mixture is stirred vigorously for 24 hr. then the $CHCl_3$ layer is separated, dried over Na_2SO_4 and evaporated to dryness. The purple solids are washed with water and dried in vacuo. The yield is 150 mg. IR(KBr): $_{N-N}$ = 2055 cm^{-1}.

Fe(TPPCl_8β-Br_4)N_3. A quantity of 100 mg of Fe(TPPCl_8β-Br_4)Cl is dissolved in 100 ml of $CHCl_3$ and 1.0 of NaN_3 dissolved in 20 ml of H_2O with a few drops of H_2SO_4 is added. This two phase mixture is stirred vigorously for 24 hrs, then the organic layer is separated, washed twice with H_2O and dried over Na_2SO_4. After removal of the solvent the solids were washed with H_2O and dried in vacuo at room temperature. The yield is 80 mg of purple powder. IR(KBr): $_{N-N}$ = 2050 cm^{-1}.

ABBREVIATIONS

TPP	*meso*-tetraphenylporphyrin dianion
TPPβ-Br_4	meso-tetraphenylβ-tetrabromoporphyrin dianion
TPPCl_8	*meso*-tetrakis(2,6-dichlorophenyl)porphyrin dianion
TPPCl_8β-Br_4	*meso*-tetrakis(2,6-dichlorophenyl)β-tetrabromo porphyrin dianion
TPPF_{20}	*meso*-tetrakis(pentafluorophenyl)porphyrin dianion
TPPF_{20}β-Cl_8	*meso*-tetrakis(pentafluorophenyl)-β-octachloroporphyrin dianion
TPPF_{20}β-Br_8	*meso*-tetrakis(pentafluorophenyl)-β-octabromoporphyrin dianion

4.5 REFERENCES

1a. Lyons, J. E., "Surface Organometallic Chemistry:Molecular Approaches to Surface Catalysis", J. M. Basset, ed., Kluwer Academic Publishers, 97 (1988).

b. Lyons, J. E., "Applied Industrial Catalysis", B. E. Leach, ed., Ch. 6, Vol. 3, Academic Press, New York, 131 (1984)

c. Lyons, J. E., *Hydrocarbon Processing,* 107 (1980).

2. Groves, J. T., Nemo, T. E., and Myers, R. S., *J. Am. Chem. Soc.* , **98**,859 (1976).

3. Groves, J. T., Nemo, T. E., and Myers, R. S., *J. Am. Chem. Soc.* , **101,**1032 (1979).

4. Groves, J. T. and Kruper, W. J., Jr., *J. Am. Chem. Soc.*, **101**, 7613 (1979).

5. Meunier, B., *Chem. Rev.*, **92**, 1411 (1992).

6. Mansuy, D., Bartoli, J. F., Chottard, J. C. and Lange, M., *Agnew. Chem. Int. Ed. Eng.*, **19**, 909 (1980).

7. Hill, C. L. and Schardt, B.C., *J. Am. Chem. Soc.*, **102**, 6374 (1980).

8. Chang, C. K. and Ebina, F., *J. Chem. Soc. Chem Comm.*, 778 (1981).

9. Groves, T. and Nemo, T. E., *J. Am. Chem. Soc.*,**105**, 6243 (1983).

10. DePorter, B., Ricci, M., Bortolino, O., and Meunier, B., J. *Mol. Cat.*, **31**, 221 (1985).

11. Tabushi, I. and Yazaki, A., *J. Am. Chem. Soc.*, **103**, 7371 (1981).

12. Tabushi, I. and Koga, N., *J. Am. Chem. Soc.*, **101**, 6456 (1979).

13. Tabushi, I., *Coord. Chem.Rev.* **86**, 1 (1988).

14. Mansuy, D., Fontecave, M., and Bartoli, J. F., J. *Chem. Soc. Chem. Comm.*, 253 (1983).

15. Fontecave, M. and Mansuy, D., *Tetrahedron*, **40**, 4297 (1984).

16. Ji, L., Liu, M., Hsieh, A. K., and Hor, T. S. A., *J. Mol. Cat.*, **70**, 247 (1991).

17. Iwanejko, R., Mlodnicka, T., and Poltowicz, J., "New Developments in Selective Oxidation," (G. Centi and F. Trifiro, eds.), Elsevier, Amsterdam, 195 (1990).

18. Battioni, P., Bartoli, J. F., Leduc, P., Fontecave, M., and Mansuy, D., *J. Chem. Soc. Chem.Comm.*, 791 (1987).

19. Karasevich, E. I., Khenkin, A. M.,and Shilov, A.E., *J. Chem. Soc. Chem* Comm., 73 (1987).

20. Shulpin., G. B. and Druzhinina, A. N., *Izv. Akad. Nauk SSSR, Ser. Khim.*, 2739 (1991).

21. Leduc, P., Battioni, P., Bartoli, J.F. and Mansuy, D., *Tett. Lett.*, **29**, 205 (1988).

22. Bedioui, F., Granados, S. G., and Devynck, J., *New J. Chem.*, **15**, 939 (1991).

23. Hendrickson, D. N., Kinnaird, M. G., and Suslick, K. S., *J. Am. Chem. Soc.*, **109**, 1243 (1987)

24. Maldotti, A., Bartocci, C., Amadelli, R., Polo, E., Battioni, P., and Mansuy, D., *J. Chem. Soc. Chem.* Comm., 1487 (1991).

25. Ellis, P. E., Jr. and Lyons, J. E., *J. Chem. Soc. Chem. Commun.*, 1188 (1989).

26. Ellis, P. E., Jr. and Lyons, J. E., *J. Chem. Soc., Chem. Commun.*, 1190 (1989).

27. Ellis, P. E., Jr. and Lyons, J. E., *J. Chem. Soc., Chem. Commun.*,1316 (1989).

28. Ellis, P. E., Jr. and Lyons, J. E., *Catal. Lett.*, **3**, 389 (1989).

29. Lyons, J. E., and Ellis, P. E., Jr., *Catal. Lett.*, **8**, 45 (1991).

30. Ellis, P. E., Jr. and Lyons, J. E., *Coord. Chem. Rev.*,**105**, 181 (1990).

31. Lyons, J. E., Ellis P. E., Jr., and Durante, V.A., "Studies in Surface Science and Catalysis," **67**, R. Grasselli, ed., Elsevier, New York, 99 (1991).

32. Ellis, P. E., Jr. and Lyons, J. E., *Preprints Petr. Div.*, **35**, 174 (1990).

33. Lyons, J. E., Ellis, P. E., Jr., Wagner, R. W., Thompson, P. B., Gray, H. B., Hughes, M. E., and Hodge, J. A., *Preprints Petr. Div.*, **37**, 307 (1992).

34. Lyons, J. E., and Ellis, P. E., Jr., "Metalloporphyrins in Catalytic Oxidations," R. A. Sheldon, ed., Marcel Dekker, New York, 291-324 (1994).

35. Bartoli, J. F., Brigoud, O., Battioni P., and Mansuy, D., J. *Chem. Soc., Chem. Commun.*, 440 (1991).

36. Bartoli, J. F., Battioni, P., DeFoor, W. R., and Mansuy, D., *J. Chem. Soc. Chem. Commun.*, 23 (1994).

37. Mansuy, D., "The Activation of Dioxygen and Homogeneous Catalytic Oxidation," D. H. R. Barton et. al., ed., Plenum Press, New York, 347-358 (1993).

38. Grinstaff, M. W., Hill, M. G., Labinger, J., and Gray, H.B., *Science*, **264**, 1311 (1994).

39. Tolman, C. A., Druliner, J. P., Krusic, P. J., Nappa, M. J., Seidel, W.C., Williams, I. D., and Ittel, S.D., *J. Mol. Catal.*, **48**, 129 (1988).

40. Saussine, L., Brazi, E., Robine, A., Mimoun, H., Fischer J., and Weiss, R., *J. Am. Chem. Soc.*, **107**, 3534 (1985).

41. Groves, J. T., *Adv. Inorg. Biochem.*, **1**, 119 (1979).

42. White, R. E., and Coon, M. J., *Ann. Rev. Biochem.*, **49**, 315 (1980).

43. Guengerich F. P., and MacDonald, T., *Acc. Chem. Res.*, **17**, 9 (1984).

44. Hamilton, G. A., in "Molecular Mechanisms of Oxygen Activation", O. Hayaishi, ed, Academic Press, New York 405 (1974).

45. Ortiz de Montellano P. R., in "Cytochrome P-450," P. R. Ortiz de Montellano, ed.), Plenum Press, New York, 235-239 (1986).

46. McKenna E. J., and Coon, M. J., *J. Biol. Chem.*, **245**, 3882 (1970).

47. Colby J. and Dalton, H., *Biochem. J.*, **157**, 495 (1976).

48. Woodland, M. P., and Dalton, H. J., *J. Biol. Chem.*, **259**, 53 (1984).

49. Balch, A. L., Chen, Y. W., Cheng, R. J., LaMar, G. N., Latos-Grazynski, L., and Renner, M. W., *J. Am. Chem. Soc.*, **106**, 7779 (1984).

50. Reviewed in Momenteau, M. and Reed C. A., Chem. Rev., **94**, 659 (1994).

51. Ozawa, S., Watanabe, Y., Nakashima, S., Kitigawa T., and Morishima, I., *J. Am. Chem. Soc*, **116**, 634 (1994).

52. Paulson, D.R., Ulllman, R., and Sloane, R. B, *J. Chem. Soc. Chem. Comm.*, 186 (1974).

53. Dolphin, D. and Felton, R. H., *Acc. Chem. Res.*, 7, 26 (1973).

54. Traylor, P. S., Dolphin, D., and Traylor, T. G., *J. Chem. Soc. Chem. Comm.*, 279 (1984).

55. Chin, D., Balch, A.L., and LaMar, G. N., *J. Am. Chem. Soc.*, **102**, 1446 (1980).

56. Al-Malaika, D., "Atmospheric Oxidation and Antioxidants", G. Scott, ed., Elsevier, New York, 45-82 (1993).

57. Howard, J., "Free Radicals vol. II", J. Kochi,ed., Wiley, New York, 3 (1970).

58. Howard, J., Chenier J., and Holden, D., *Can. J. Chem.*, **56**, 170 (1978).

59. Lyons, J. E., Ellis, P. E., Jr., Myers, H. K., and Wagner, R. W., *J. Catal.*, **141**, 311 (1993).

60. Labinger, J. A., *Catal, Lett.*, **26**, 95 (1994).

61. Kochi, J. K., "Free Radicals, Vol. II," Wiley, New York, 683-686 (1973).

62. Greene, F. D., Savitz, M.L., Osterholtz, F. D., Lau, H. H., Smith W. N., and Zanet, P.M., *J. Org. Chem.*, **28**, 55 (1963).

63. Summerville, D.A., Jones, R.D., Hoffman, B.M. and Basolo, F., *J. Am. Chem. Soc.*, **99**, 8195 (1977).

64. Buchler, J. W. and Dreher, C., *Z. Naturforsch*, **396**, 222 (1984).

65. Summerville, D.A. and Cohen, I. A., *J. Am. Chem. Soc.*, **98**, 1747 (1976).

66. Ledon, H., *C. R. Acad. Sci.* (Paris), **288**, C29 (1979).

67. Donohoe, R.J., Atamian, M., and Bocian, D.F., *J. Am. Chem. Soc.*, **109**, 5593 (1987).

68. Traylor, P.S., Dolphin, D., and Traylor, T. G., *J. Chem. Soc. Chem. Comm.*, 279 (1984).

69. Jayaraj, K., Gold, A., Toney, G. E., Helms, J. H. and Hatfield, W. E., *Inorg. Chem.*, **25**, 3516 (1986).

70. Liston, D. J. and West, B.O., *Inorg. Chem.*, **24**, 1568 (1985).

71. Banfi, S., Montanari, F., and Quici, S., *J. Org. Chem.*, **53**, 2863 (1988).

72. Siegl, W. O., *J. Org. Chem.*, **42**, 1872 (1977).

Table 1 Effect of Fluorination of The meso-Phenyl Groups on The Activity of Tetraphenyporphyrinato Metal Complexes for Reactions of Isobutane with Oxygen[a]

Catalyst	mmoles Catalyst	Catalyst Turnovers[b]	Selectivity to tert-Butyl Alcohol, [c]%
Fe(TPP)Cl	0.025	0	-
$Fe(TPPF_{20})Cl$	0.016	2040	90
$Fe(TPP)N_3$	0.013	130	93
$Fe(TPPF_{20})N_3$	0.016	2060	89
$Mn(TPP)N_3$	0.013	180	88
$Mn(TPPF_{20})N_3$	0.016	750	87
$Cr(TPP)N_3$	0.025	280	89
$Cr(TPPF_{20})N_3$	0.016	450	97
$[Fe(TPP)]_2O$	0.013	0	-
$[Fe(TPPF_{20})]_2O$	0.007	1730	92

[a]Isobutane, 7g, was oxidized (6 hrs.) in 25 ml benzene containing the designated catalyst at 80°C under 100 psig oxygen. [b]Moles of oxygen consumed/mole catalyst used. [c][moles tert-butyl alcohol/moles liquid product] x 100.

Table 2 Effect of Ring Halogenation on The Isobutane Oxidation Activity of Porphyrinatoiron(III) Complexes[a]

Catalyst	mmoles	O_2 Uptake mmoles	T.O.[b]	Selectivity to TBA,%
Fe(TPP)Cl	0.025	0.0	0	-
Fe(TPPβ-Br_4)Cl	0.013	2.0	155	-
Fe(TPPCl_8)Cl	0.019	5.0	263	89
Fe(TPPCl_8β–Br_4)Cl	0.020	17.3	865	83
Fe(TPPF_{20})Cl	0.016	32.6	2,040	90
Fe(TPPF_{20}β–Br_8)Cl	0.013	40.2	3,090	89
Fe(TPP)N_3	0.013	1.7	130	89
Fe(TPPβ–Br_4)N_3	0.013	2.3	177	-
Fe(TPPCl_8)N_3	0.023	15.0	653	80
Fe(TPPCl_8β–Br_4)N_3	0.023	21.5	934	82
Fe(TPPF_{20})N_3	0.016	33.0	2,060	89
[Fe(TPP)]$_2$O	0.019	0.0	0	-
[Fe(TPPβ–Br_4)]$_2$O	0.013	0.0	0	-
Fe(TPPCl_8)OH	0.013	9.2	711	83
[Fe(TPPF_{20})]$_2$O	0.013	24.0	1,846	84
Fe(TPPF_{20})OH	0.013	29.2	2,245	82

[a] A solution of the catalyst in 25 ml benzene containing 7 grams of isobutane was stirred at 80°C under 100 psig of O_2 for 6 hours. [b]Moles O_2 consumed/mole catalyst used.

Table 3 Isobutane Oxidations Catalyzed by Perhaloporphyrin Complexes[a]

Catalyst	T, °C	T.O.[b]	Sel., %
$Fe(TPPF_{20}\beta\text{–}Br_8)N_3$	60	1550	87
	40	670	89
	27	620	na
$Fe(TPPF_{20}\beta\text{–}Cl_8)N_3$	60	1800	90
	40	760	92
$Cr(TPPF_{20}\beta\text{-}Br_8)N_3$	60	110	92
$Cr(TPPF_{20}\beta\text{-}Cl_8)N_3$	80	450	88
$Mn(TPPF_{20}\beta\text{-}Br_8)N_3$	60	270	87
$Mn(TPPF_{20}\beta\text{-}Cl_8)Cl+NaN_3$[c]	80	1289	86
$Mn(TPPF_2\beta\text{–}Cl_8)Cl+NaN_3$[c]	60	156	88
$Co(TPPF_{20}\beta\text{-}Cl_8)$	60	355	91

[a]Isobutane (7g) was oxidized (6 hrs.) in 25 ml benzene at the designated temperature under 100 psig oxygen using 0.013 mmole of the designated catalyst. [b] Moles of oxygen consumed/mole catalyst used. [c] After warming the reaction mixture for 6 hr. as indicated in footnote a, the reaction mixture was cooled to room temperature, 10 mg of NaN_3 added and the procedure repeated according to footnote a. The T.O. are calculated based on the second 6 hr. period.

Table 4 Propane Oxidations Using First Row Metal Complexes of $TPPF_{20}\beta$-Br_8 as Catalysts[a]

Catalyst	time, hours	T, °C	T.O.[b]	IPA/Acetone[c]
$Fe(TPPF_{20})N_3$	3	125	330	0.8
$Fe(TPPF_{20}\beta\text{–}Br_8)N_3$	4.5	125	541	0.9
$Cr(TPPF_{20})N_3$	4.5	125	41	<0.1
$Cr(TPPF_{20}\beta\text{–}Br_8)N_3$	4.5	125	87	0.6
$Mn(TPPF_{20})N_3$	3	125	0	-
$Mn(TPPF_{20}\beta\text{–}Br_8)N_3$	4.5	125	87	1.0

[a]Propane (1.36 mol) was added to benzene (48 ml) containing the catalyst (0.013 mmol) . The solution was stirred for 3 hours at 125°C under 1000 psig of air in a glass lined autoclave . [b]Moles of acetone plus isopropyl alcohol formed per mole of catalyst used. [c]Molar ratio isopropyl alcohol to acetone formed.

Table 5 Alkane Oxidations Catalyzed by Cobalt Complexes

Comple	mmoles Complex	Substrate	Reaction T,°C	Total P,psig	Reaction t, hrs	Catalyst Turnovers	Product, Selectivity, % TBA-HP[c]	Acetone	IPA
$Co(acac)_2$	0.100	i-C_4H_{10}[a]	80	100	6	52	89	10	-
$Co(acac)_3$	0.100					15	88	10	-
Co(BPI)(OAc)	0.025					24	88	12	-
$Co(BPI)N_3$	0.025					200	87	13	-
$Co(BPI)(O_2Bu^t)$	0.025					260	89	11	-
$Co(acac)_2$	0.023	C_3H_8[b]	125	1,000	3	21	-	62	35
$Co(acac)_2$	0.023				18	122	-	62	35
$Co(acac)_3$ (+t-C_4H_9OOH)	0.023 (0.23)				3	27	-	64	33
$Co(BPI)(O_2Bu^t)$	0.023				3	20	-	>90	<10

[a] Isobutane, 7g, was oxidized as in Table 1. [b] Propane, 60g, was oxidized as in Table 4. [c] mole percent (TBA + TBHP).

Table 6 Iron Haloporphyrin Catalyzed Isobutane Oxidation[a]

						Reaction Products, (mmoles)			Conversion	Sel.%	
Catalyst	T°C	t,Hrs.	i-C_4H_{10}(mmols)	O_2(psi)	t-BuOH	Acetone	CO	CO_2	-C_4H_{10}(%)	t-BuOH[b]	T.O.[c]
Fe(TPPF$_{20}$)OH	80	3	1869	53	310	46	7	18	17	87	11,330
	24	143	1871	53	382	17	0	18	19	95	11,600
Fe(TPPF$_{20}$β-Cl$_8$)Cl	80	3	1865	142	334	38	6	29	20	88	12,400
	21	120	1865	63	366	16	tr	na	20.5	95	12,730
Fe(TPPF$_{20}$β-Br$_8$)Cl	80	3	1862	148	414	81	6	28	27	84	16,500
	80	3	1870	53	277	43	8	23	17	87	10,060
	24	71	1862	53	372	35	tr	27	22	92	12,150

[a]Isobutane containing 0.03 mmole of dissolved catalyst was oxidized by an oxygen-containing gas mixture (75 atm. diluent - N_2) in the liquid phase (180 ml) for 3 hours. Oxygen added as consumed. [b](moles t-BuOH/moles liquid product) x 100. [c]Moles (t-BuOH and acetone) produced/mole catalyst used.

Table 7 Conversion of tert-Butyl Hydroperoxide to tert-Butyl Alcohol

Catalyst	time hrs.	t-BuO_2H Conv., %	Product, Molar Sel., % t-BuOH	$(t\text{-}BuO)_2$	$(CH_3)_2CO$
$Fe(acac)_3$	2.3	<5	67	tr	32
Fe(TPP)Cl	1.9	27	82	7	11
$Fe(TPPF_{20})Cl$	3.3	72	87	10	3
$Fe(TPPF_{20}\beta\text{-}Br_8)Cl$	1.9	95	90	8	2
$Fe(TPPF_{20}\beta\text{-}Cl_8)Cl$	3.3	100	90	8	2

[a]The catalyst, 2×10^{-4} mmoles, in 2.4 ml p-xylene was rapidly added to a stirred solution of 10 ml t-BuO_2H (90%) in 48 mls benzene. O_2 evolved was measured manometrically and liquid samples taken periodically and analyzed by standardized gc.

Table 8 Relationship Between Catalyst Reduction Potential and Hydroperoxide Decomposition Activity

Catalyst	Fe(III)/(II)[a] $E_{1/2}$(V)	TBA yield[b] % at 0.5 Hr
Fe(TPP)Cl	-0.221	4.8
Fe(TPPF_{20})Cl	+0.07	16.0
Fe(TPPF_{20}β-Br_8)Cl	+0.19	51.2
Fe(TPPF_{20}β-Cl_8)Cl	+0.28	67.2

[a]Cyclic voltammetry in CH_2Cl_2 vs. SCE, TBAC-supporting electrolyte, glassy carbon electrode.
[b]Room temperature decomposition of TBHP in Benzene.

Table 9 n-Butane Oxidations Catalyzed By $TPPF_{20}\beta\text{-}Cl_8$ Complexes of Iron and Chromium[a]

Catalyst	Solvent	React. Time,Hr.	TO	Oxidation Product Molar Selectivity, % SBA ($2\text{-}C_4H_9OH$)	MEK ($2\text{-}C_4H_8O$)	Acetal-dehyde (CH_3CHO)	Acetic acid (CH_3CO_2H)
$Fe(TPPF_{20}\beta\text{-}Cl_8)Cl$	Benzene	4.5	243	28	56	(tr)	15
$Cr(TPPF_{20}\beta\text{-}Cl_8)Cl$	Benzene	5.5	9	40	60	-	-
	Benzene	23.0	711	10	60	3	27
	Acetonitrile	23.0	1518	7	48	5	40
$Cr(TPPF_{20}\beta\text{-}Cl_8)N_3$	Benzene	2.2	659	7	64	4	25
	Acetonitrile	3.5	1508	12	51	3	34

[a]Butane, 60g in 48 ml of the solvent containing 0.023 mmole catalyst was oxidized at 125°C under 1500 psig of air.

Table 10 Alkane Oxidations Catalyzed by Iron Halotetraphenylporphyrins[a]

Alkane	Catalyst	T,°C	TO[b]	Products, mmole/100g reaction mix[c]					Ox./ Clvg[d]
				>=O					
2-Methylbutane	$Fe(TPPF_{20})OH$	40	105	2 9	0 4	1.1	5 8	0 3	2.2
	$Fe(TPPF_{20}\beta\text{-}Br_8)Cl$	40	195	3 0	0.5	1.9	8 9	0 3	3.2
	$Fe(TPPF_{20})OH$	60	670	12 8	1 0	3.3	13.2	0 8	1.3
	$Fe(TPPF_{20}\beta\text{-}Br_8)Cl$	60	980	21 6	2.7	6.3	25.4	1 2	1.4
	$Fe(TPPF_{20})Cl$	80	2110	55 3	3 5	11.3	32.5	2 0	0 8
	$Fe(TPPF_{20}\beta\text{-}Br_8)Cl$	80	3200	61 3	4 0	14.8	41.4	2 3	0.9

				Products, mmole/100g reaction mix[c]					
				AA[e]					
3-Methylpentane	$Fe(TPPF_{20}\beta\text{-}Br_8)Cl$	80	1556	na	28.9	11 5	14 1	2 0	na
	$Fe(TPPF_{20}\beta\text{-}Br_8)Cl$	80	1556	19.0	28 1	11.2	13.4	1 9	0 56

				Products, mmole/100g reaction mix[c]				
								
2,3-Dimethylbutane	$Fe(TPPF_{20}\beta\text{-}Br_8)Cl$	60	2245	120.4	10.3	22.3		0 17
	$Fe(TPPF_{20}\beta\text{-}Br_8)Cl$	80	5650	329 0	22.0	40 0		0 11

				Products, mmole/100g reaction mix[c]				
						$C_7H_{15}OH$		
2,2,3-Trimethylbutane	$Fe(TPPF_{20})OH$	60	1310	30 1	26	2 8		0 09
	$Fe(TPPF_{20}\beta Cl_8)OH$	60	1490	23.3	20.1	1.9		0.08

[a]Oxidations carried out by reacting oxygen with the neat alkane, 30 ml, containing 0.013 mmoles of the catalyst at T,°C at a total pressure of 100 psig for 6 hours. Product analysis by standardized GLPC. [b]Moles O_2 consumed/mole catalyst used. [c]mmoles product/100 grams of recovered product mixture, by GLPC. [d] Ratio of moles C-C bond cleavage products/moles oxidation products with carbon skeleton intact. [e]AA=acetic acid.

Table 11 Comparison of the Product Profile of 2-Methylpentane Oxidation[a] with that of tert-Amyl Hydroperoxide Decomposition Catalyzed by Perhaloporphyrinato Iron Complexes

Substrate	Reaction	T.O.	Products, mmole/100g reaction mix					MB-2ol/ Acetone[c]
					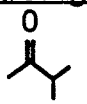	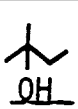	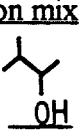	
	Oxidation[a]	195	3.0	0.5	1.9	8.9	0.3	3
	Decomposition[b]	$3.3x10^5$	33.4	4.5	-	116.8	-	3.5

[a]Oxygen is reacted with the neat alkane, 30ml, containing 0.013 mmole of $Fe(TPPF_{20}\beta-Br_8)OH$ at 40°C at a total pressure of 100 psig for 6 hours. Product analysis by standardized GLPC.
[b]tert-Amyl hydroperoxide, 10ml (82%), is added to a solution of $Fe(TPPF_{20}\beta Cl_8)Cl$, 4×10^{-6}M, in benzene. Oxygen evolution is followed manometrically and products are analyzed periodically by standarized GLPC. The analysis reported in Table II was peformed after 1.9 hours.
[c]2-MB-2ol/Acetone=the ratio of 2-methylbutane-2-ol to acetone formed in the decomposition reaction.

Table 12 Product Profile as a Function of R in Oxidation of $R_1R_2R_3CH$ Catalyzed by $Fe(TPPF_{20}\beta\text{-}Br8)Cl$[a]

Alkane	R_1	R_2	R_3	Predominant Hypothetical Alkoxy Radical	Predominant Cleaved Alkyl Radical	k_{t-} / k_{H-} [d]	% Cleavage Products Formed in Oxidation[b]
 [c]	CH_3	CH_3	CH_3	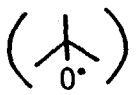	$CH_3\cdot$	0.021	10
	CH_3	CH_3	C_2H_5	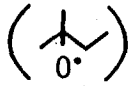	$C_2H_5\cdot$	2.09	53
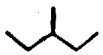	CH_3	C_2H_5	C_2H_5	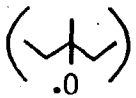	$(2)C_2H_5\cdot$		64
	CH_3	CH_3	$i\text{-}C_3H_7$	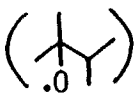	$(CH_3)_2CH\cdot$	76.4	90

a) Oxidations carried out by reacting oxygen with the neat alkane, 30 ml, containing 0.013 mmoles of $Fe(TPPF_{20}\beta\text{-}Br_8)Cl$ at 80°C at a total pressure of 100 psig for 6 hours. Product analysis by Standardized GLPC b)(Moles alkane converted to C-C bond cleavage products/moles alkane oxidized) x 100 . c)A 25 weight % solution of isobutane in benzene was oxidized in this experiment.
d) Ratio of Rates of Alkyl Cleavage and H-Abstraction from cyclohexane (61) in the reaction

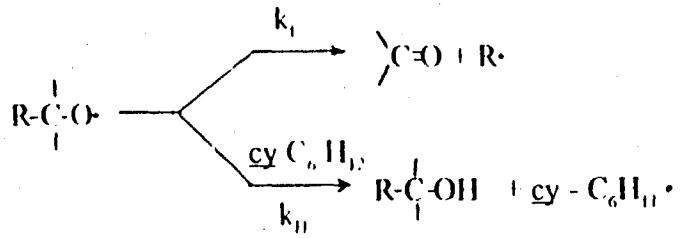

FIGURE 1 The Substituted Porphyrinato Ligand; Y=β-Cl,Br,orH;Z=C_6H_5(TPP), o-$C_6H_4Cl_2$($TPPCl_8$) or C_6F_5($TPPF_{20}$).

FIGURE 2 Oxidation of Isobutane in Benzene at 80°C using Fe($TPPF_{20}$)X; X=Cl, □ N_3, • , and OH, ○ as axial ligands.

FIGURE 3 Catalyst Turnovers as a function of Fe(III)/Fe(II) Oxidation Potential. -o- Isobutane Oxidations at 60°C; -o- Propane Oxidations at 125°C. See Tables 3, 4 for experimental procedures. 1, Fe(TPP)OH; 2Fe($TPPCl_8$β-Br_4)OH; 3, Fe($TPPF_{20}$)OH; 4, Fe($TPPF_{20}$β-Br_8)OH; 5, Fe($TPPF_{20}$β-Cl_8)OH.

FIGURE 4 Schematic representation of biological and biomimetic alkane oxidation (40-47)

FIGURE 5 Conceptual scheme for a hypothetical catalytic cycle for conversion of an alkane to an alcohol using an electron deficient iron porphyrin complex (porphyrin ring omitted).

FIGURE 6 Formation of tert-butyl alcohol, TBA, from tert-butyl hydroperoxide (10 ml) in benzene (48 ml)-p-xylene (2.4 ml) using 2 x 10-4 mmoles of catalyst: O Fe($TPPF_{20}$β-Cl_8)Cl, □ Fe($TPPF_{20}$)Cl, • O Fe(TPP)Cl, ■ Fe(acac)3.

FIGURE 7 Haber-Weiss decomposition of hydroperoxides using metalloporphyrins as catalysts (porphyrin ring omitted).

FIGURE 8 Oxidation of n-butane in acetonitrile at 125°C catalyzed by Cr($TPPF_{20}$β-Cl_8)N_3. Details given in Table 10.

FIGURE 9 Dependence of product profile on substrate structure for alkane oxidations catalyzed by Fe($TPPF_{20}$β-Br_8)OH.

FIGURE 10 Possible pathways occuring during selective oxidation of alkanes catalyzed by iron perhaloporphyrin complexes. a) hypothetical alkoxy radical.

FIGURE 1

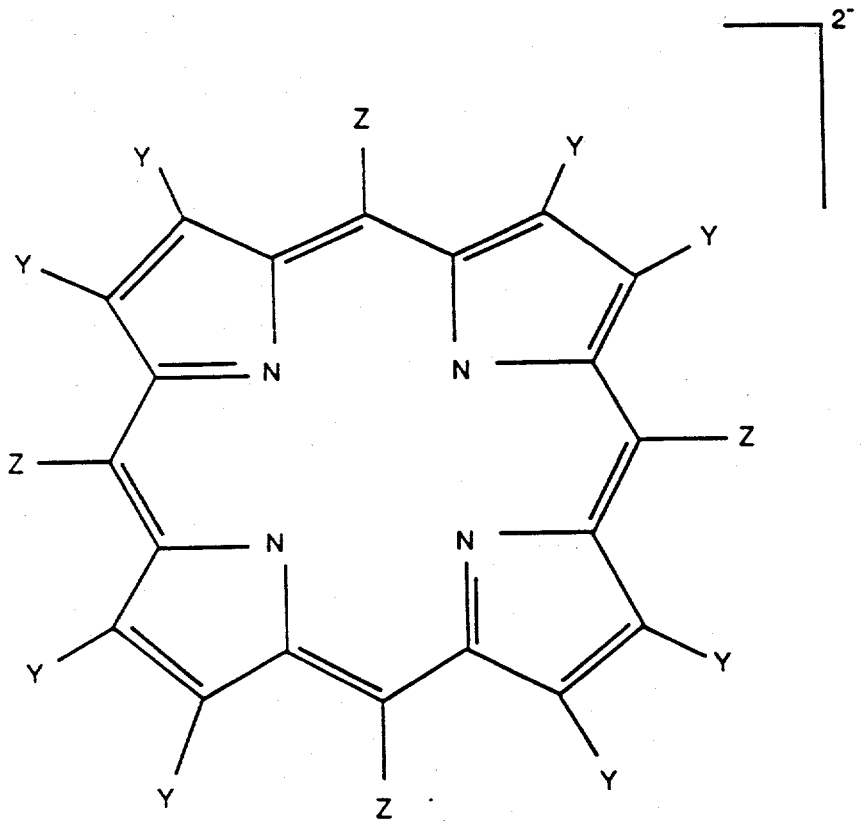

FIGURE 2

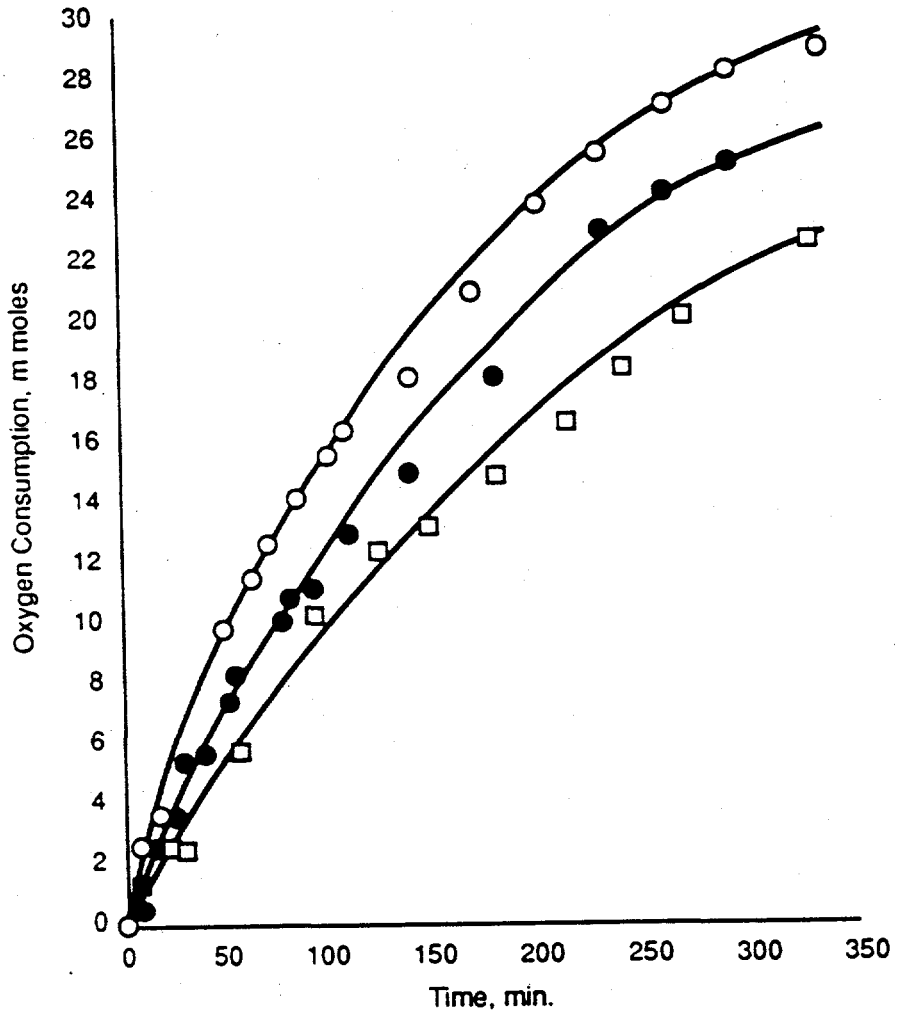
Oxygen Consumption, m moles
30
28
26
24
22
20
18
16
14
12
10
8
6
4
2
0
0
50
100
150
200
250
300
350
Time, min.

FIGURE 3

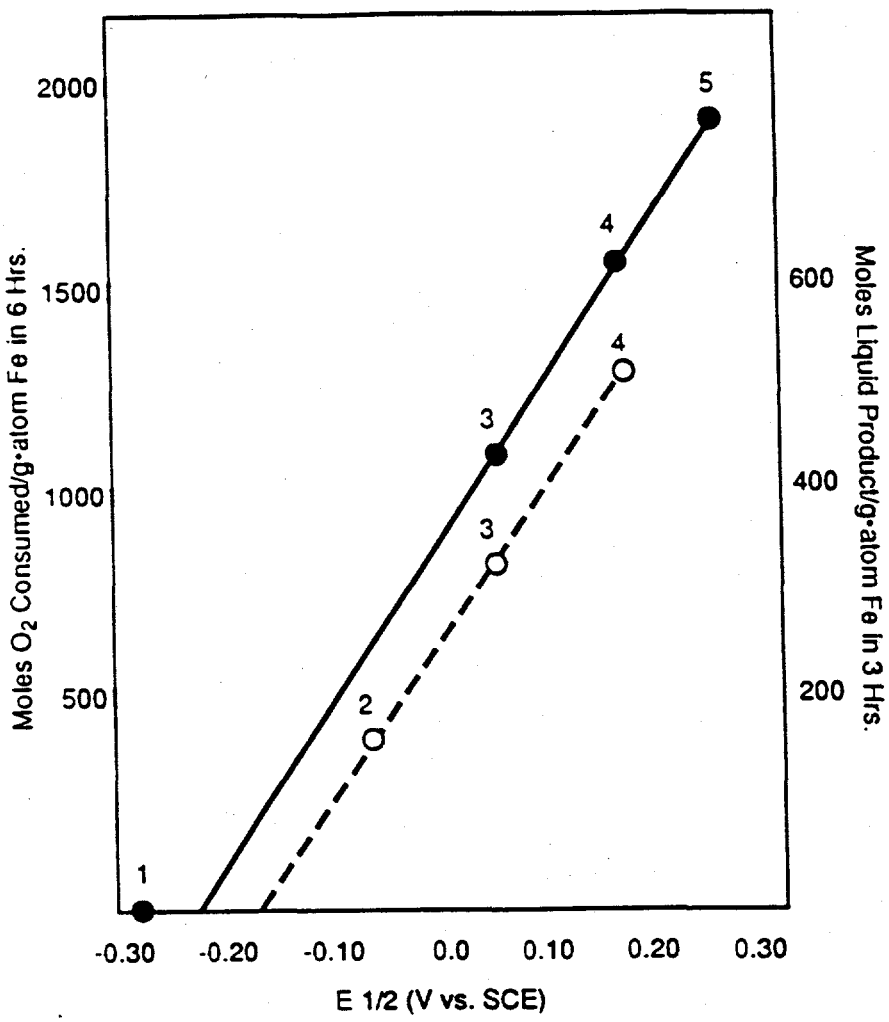
2000
1500
1000
500
Moles O_2 Consumed/g·atom Fe in 6 Hrs.
600
400
200
Moles Liquid Product/g·atom Fe In 3 Hrs.
1
2
3
4
5
3
4
-0.30
-0.20
-0.10
0.0
0.10
0.20
0.30
E 1/2 (V vs. SCE)

FIGURE 4

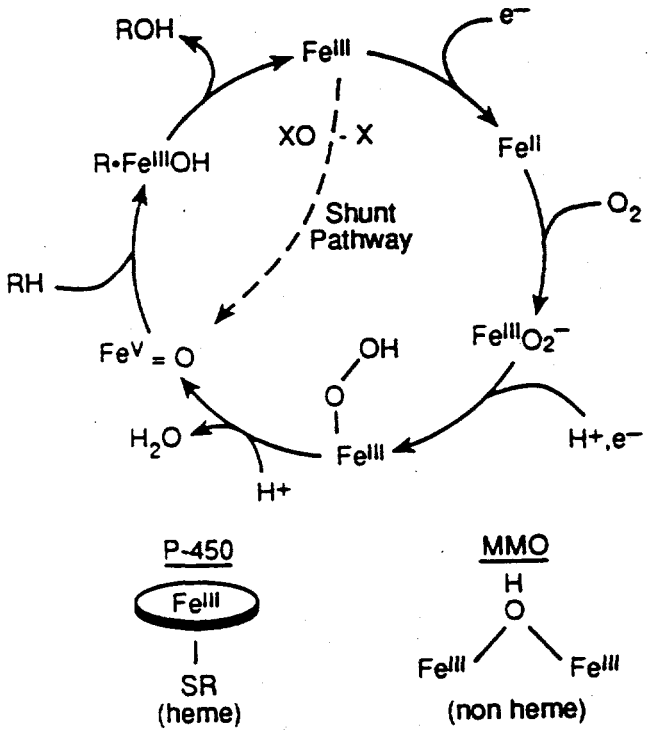
ROH
Fe^{III}
e$^-$
XO
- X
R•Fe^{III}OH
Fe^{II}
Shunt
Pathway
O$_2$
RH
Fe^{III}O$_2^-$
Fe^{V} = O
OH
O
H$_2$O
Fe^{III}
H+,e$^-$
H+
P-450
Fe^{III}
SR
(heme)
MMO
H
O
Fe^{III}
Fe^{III}
(non heme)

FIGURE 5

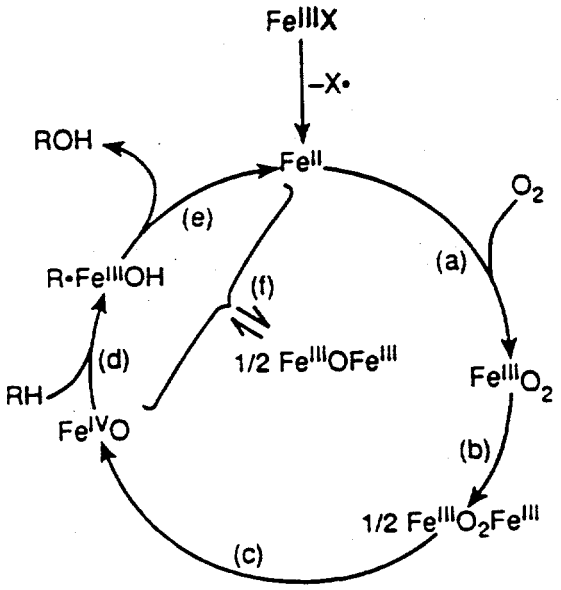
Fe^{III}X
–X•
Fe^{II}
ROH
(e)
R•Fe^{III}OH
(f)
1/2 Fe^{III}OFe^{III}
(d)
RH
Fe^{IV}O
(a)
O$_2$
Fe^{III}O$_2$
(b)
1/2 Fe^{III}O$_2$Fe^{III}
(c)

FIGURE 6

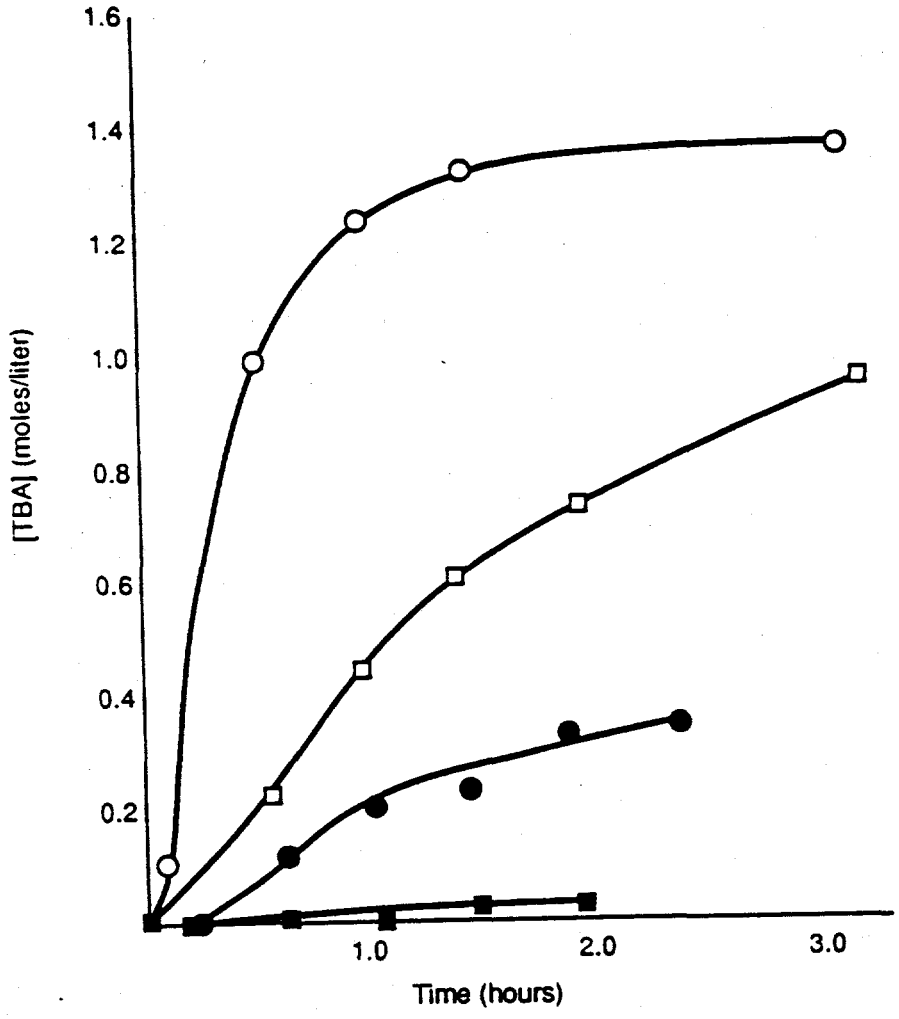

FIGURE 7

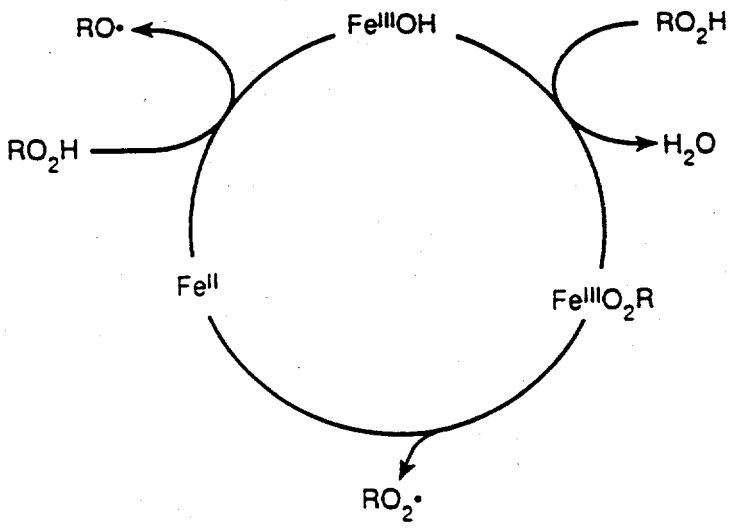

$$2RO_2H \longrightarrow RO_2\bullet + RO\bullet + H_2O$$

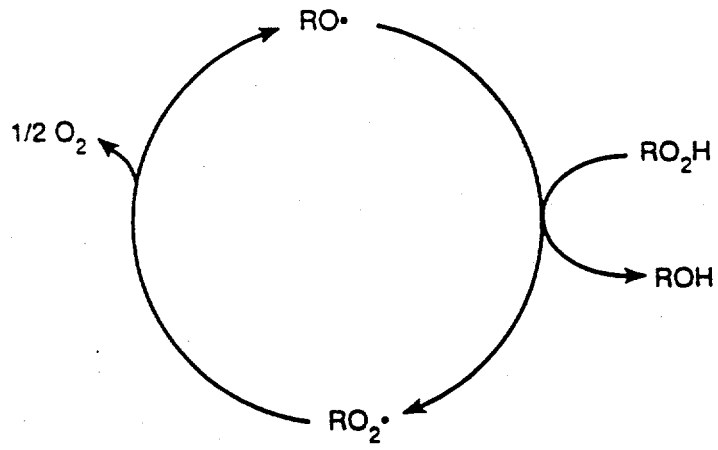

FIGURE 8

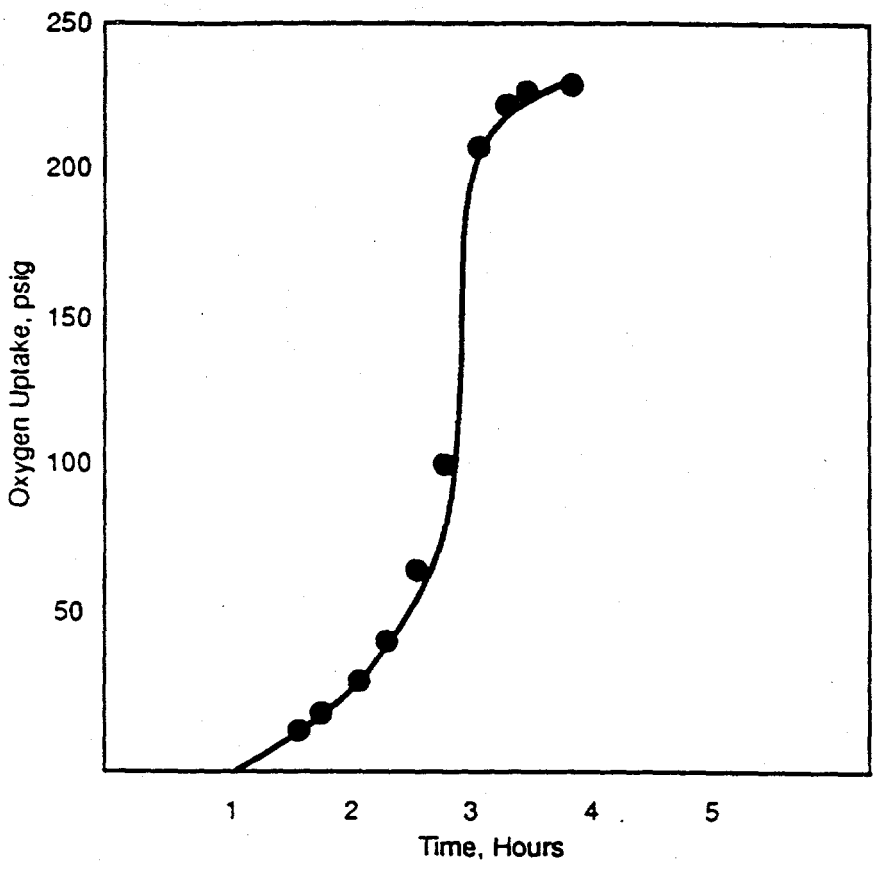

FIGURE 9

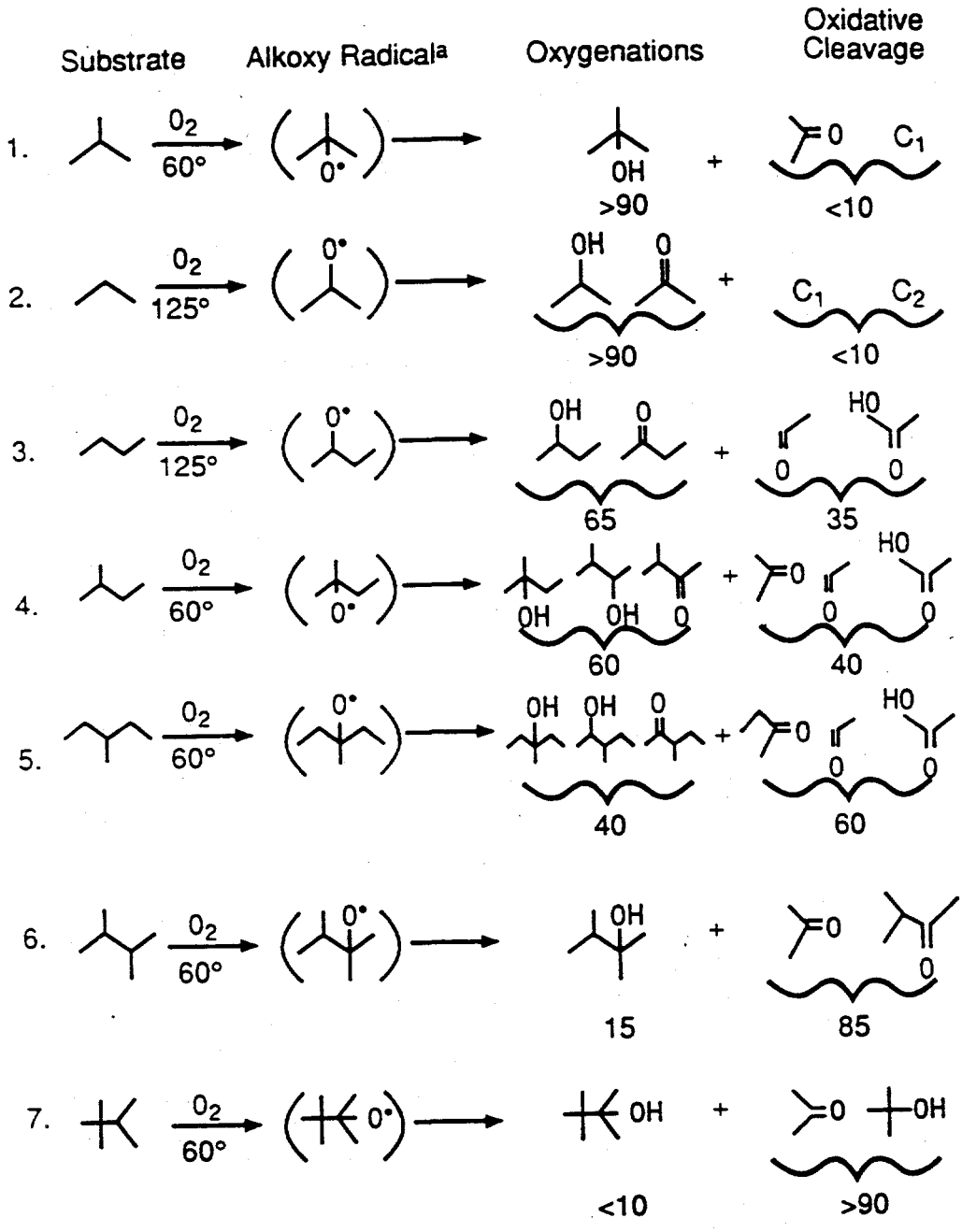
Substrate
Alkoxy Radical[a]
Oxygenations
Oxidative Cleavage
1.
O_2
60°
0•
OH
>90
0
C_1
<10
2.
O_2
125°
0•
OH
0
>90
C_1
C_2
<10
3.
O_2
125°
0•
OH
0
65
HO
0
0
35
4.
O_2
60°
0•
OH
OH
0
60
HO
0
0
40
5.
O_2
60°
0•
OH
OH
0
40
HO
0
0
60
6.
O_2
60°
0•
OH
15
0
0
85
7.
O_2
60°
0•
OH
<10
0
OH
>90

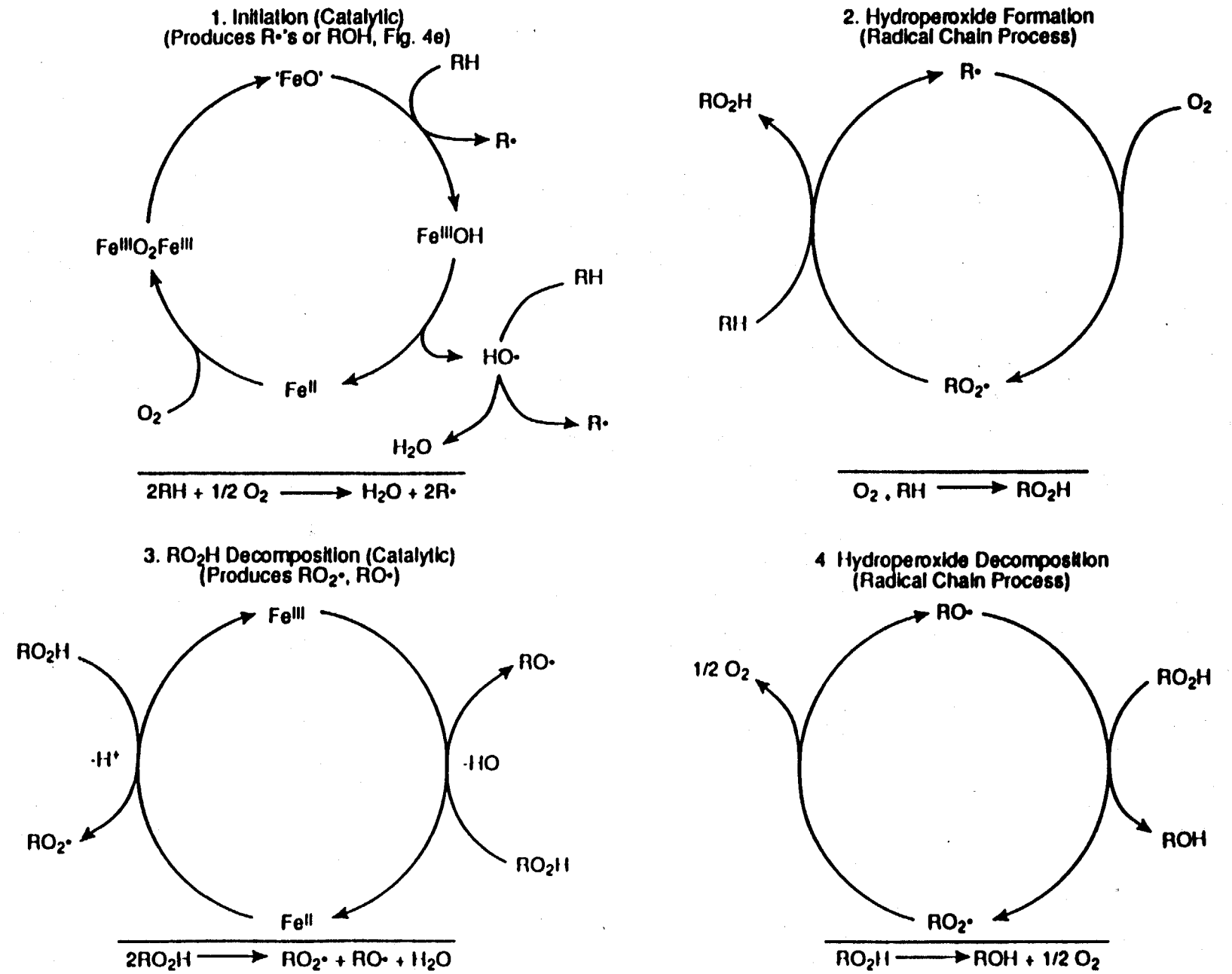
1. Initiation (Catalytic)
(Produces R•'s or ROH, Fig. 4e)
'FeO'
RH
R•
Fe^{III}OH
Fe^{III}O$_2$Fe^{III}
RH
HO•
Fe^{II}
O$_2$
H$_2$O
R•
2RH + 1/2 O$_2$ ⟶ H$_2$O + 2R•
2. Hydroperoxide Formation
(Radical Chain Process)
R•
RO$_2$H
O$_2$
RH
RO$_2$•
O$_2$, RH ⟶ RO$_2$H
3. RO$_2$H Decomposition (Catalytic)
(Produces RO$_2$•, RO•)
Fe^{III}
RO$_2$H
RO•
-H'
-HO
RO$_2$•
RO$_2$H
Fe^{II}
2RO$_2$H ⟶ RO$_2$• + RO• + H$_2$O
4 Hydroperoxide Decomposition
(Radical Chain Process)
RO•
1/2 O$_2$
RO$_2$H
ROH
RO$_2$•
RO$_2$H ⟶ ROH + 1/2 O$_2$

FIGURE 10

5.0 GENERATION OF A POTENTIALLY LESS EXPENSIVE PERHALOPORPHYRIN CATALYST

T. P. Wijesekera, J. E. Lyons, and M. V. Bhinde

The most active catalysts known for isobutane oxidation are the iron perhaloporphyrin complexes which we have developed on the Cooperative Agreement and which are discussed in detail the previous section. These catalysts all have the perfluorophenyl group in the meso-position on the porphyrin ring. The perfluorophenyl group is introduced in porphyrin synthesis by way of perfluorobenzaldehyde. Perfluorobenzaldehyde can be made only by a very costly multi-step process which makes the final catalyst prohibitively expensive. A perhaloalkyl group, such as CF_3, could however be introduced **via** a far less expensive precursor, as discussed in past reports. We synthesized analogous iron porphyrin tetrakis(trifluoromethyl)porphyrinato complexes, (F_{12}PFeX), having the meso-CF_3 group in place of the meso-C_6F_5 group but found that these complexes were insoluble in the hydrocarbon media in which we carry out the reaction. In order to both create solubility, ehance stability and increase activity, we brominated the beta-positions of the tetrakis(trifluoromethyl)porphyrinato system. To date the only successful bromination procedure we have found, leaves a pyridine residue on the resulting perhaloporphyrin complex which appears to poison its catalytic activity.

Another approach to solving this problem was to use a bulkier perfluoroalkyl group in the meso-position-C_3H_7, in place of CF_3. For this reason, we prepared a tetrakis(heptafluoropropyl) porphyrinato iron complex and tested it for isobutane oxidation and tert-butylhydroperoxide decomposition. It was quite active for both reactions.

5.1 RESULTS

5.1.1 New Porphyrin Catalysts with meso-CF_3 groups

5.1.1.1 Catalytic Activity of Novel Iron "F_{16}" Porphyrins

We have shown how to make a series of β-substituted porphyrins which have C_6F_5 groups in two meso-positions and CF_3 groups in the other two meso-positions. Since these porphyrins have 16 F's they are called 'F16' porphyrins. These complexes were a logical transition between porphyrin catalysts having four costly meso-C_6F_5 groups and four inexpensive meso-CF_3 groups. Table IA shows that as one puts increasing numbers of electron-withdrawing Br-groups in the β-position of FeF_{16} complexes, activity for one-step oxidation of isobutane to TBA, eq. 1, increases. Figure 1A shows that as the number of β-Br groups increases activity for the second step of a two step route from isobutane to TBA, eq. 3, increases as well.

$$(CH_3)_3CH + 1/2O_2 \xrightarrow{\text{CAT.}} (CH_3)_3COH \quad (1)$$

$$(CH_3)_3CH + O_2 \xrightarrow{\text{NO-CAT.}} (CH_3)_3CO_2H \quad (2)$$

$$(CH_3)_3CO_2H \xrightarrow{\text{CAT.}} (CH_3)_3COH \quad (3)$$

In the next section of this report, we show how to synthesize complexes having CF_3 groups in all four meso position - the potentially inexpensive 'F12' porphyrins.

5.1.1.2 Novel 'F12' Porphyrin Complexes

5.1.1.2.1 Objectives

A. Prepare sufficient quantities of bis(pyrrol-2-yl)-trifluoromethylmethane, the key dipyrromethane intermediate for the 2+2 synthesis of meso-trifluoromethyl porphyrins.

B. Use the above dipyrromethane to prepare 5,10,15,20-tetrakis(trifluomethyl)porphyrin [$F_{12}PH_2$] and insert iron to give $F_{12}PFeCl$

C. Attempt to improve the catalytic activity by:

   a. appropriately modifying the axial ligand
   b. substitution of the peripheral β-positions with electron-withdrawing groups

5.1.1.2.2 Highlights

A. Approximately 50g of the dipyrromethane were prepared using a procedure that gives >80% GC yields and 65% isolated yields

B. The dipyrromethane intermediate was used to prepare approximately 500mg of $F_{12}PH2$ of which 300mg were converted to the hemin $F_{12}PFeCl$

C. Two samples of the azide [$F_{12}PFeN_3$] were prepared and submitted for screening. In addition, β-bromination was carried out on $F_{12}PFeCl$ and the preliminary analytical data suggest that the reaction has produced the octabrominated derivative $Br_8F_{12}PFeCl$.

TABLE 1A

EFFECT OF β-BROMINATION OF Fe(F16P) COMPLEXES ON CATALYTIC ACTIVITY[a] FOR ISOBUTANE OXIDATION

DATE	RUN NO.	CATALYST - NO.	T,°C	O_2 T.O.[b]	TBA PROD. mmole/100g	S, %
2/16/93	1011123A	$Fe(Br_7F_{16}P)$-1011573	60	1334	58.2	88
2/16/93	1011123B	$Fe(Br_6F_{16}P)$-1011568	60	1045	52.7	88
2/6/93	1011124A	$Fe(Br_4F_{16}P)$-1011546B	60	956	56.5(?)	89
2/16/93	1011124B	$Fe(Br_2F_{16}P)$-1011549C	60	600	36.2	88
9/21/93	1011105B	$[Fe(F_{16}P)]O$-1010124	60	400	20.9	90

a) Approximately 7 grams isobutane was bubbled into a chilled solution of ~0.013 mmoles of catalyst in 25 ml benzene in a Fisher-Porter Aerosol tube. The tube was fitted to a gas manifold, flushed with O_2 and then filled with pure O_2. The tube was plunged into a constant temperature bath at 60°C ±2°C and filled with O_2 to 100 psig. The solution was stirred magnetically at 60°C for 6 hours between 90 and 100 psig total gas pressure. As O_2 was consumed, it was replenished from a reservoir. After 6 hours the reaction mixture was cooled, returned to atmospheric pressure and the liquid analyzed by standardized glpc.

b) Moles O_2 consumed/mole catalyst used in 6 hours.

c) gc analysis TBA - m mols/100 g reaction mix

d) Selectivity to TBA, mole %. (acetone-major by product.)

FIGURE 1A

OXYGEN ABSORPITON VS TIME

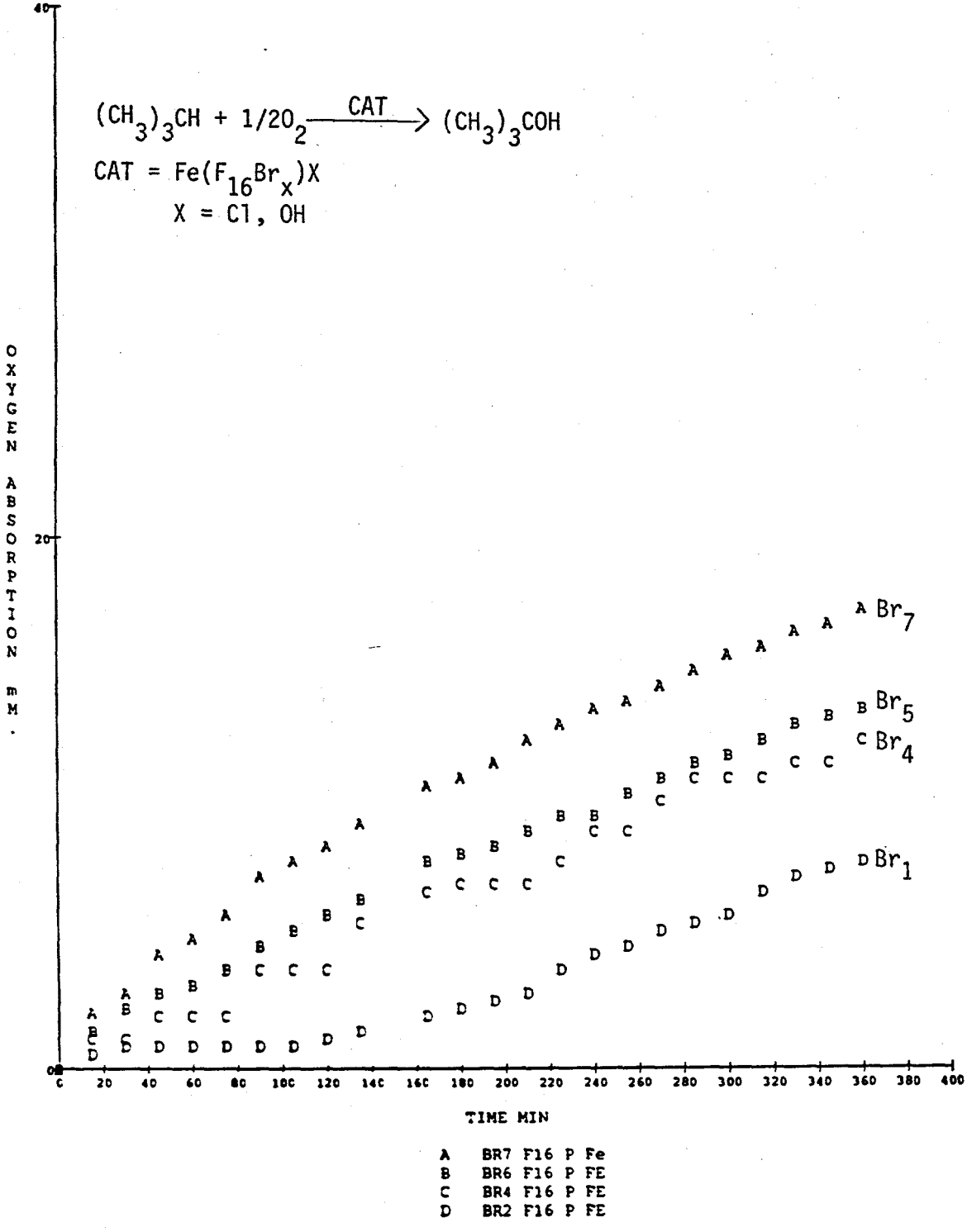

5.1.1.2.3 Results And Discussion

The synthetic studies related to meso-trifluoromethylporphyrinatoiron complexes were continued with the primary objective being the development of a less expensive but more active catalyst by substituting the C_6F_5 groups of $(C_6F_5)_4PFeX$ with CF_3 groups. A cost evaluation study led to the conclusion that the two basic raw materials for this synthesis, i.e. pyrrole and trifluoroactaldehyde should be available for <$20/lb and <$10/lb respectively.

The emphasis has been to prepare sufficient quantities of $(CF_3)_4PFeCl$ [abbreviated as $F_{12}PFeCl$] and attempt to fine tune its catalytic activity by both axial ligand modifications and -halogenation.

Axial Ligand Modification

A. Treatment with Azide

In an attempt to improve the catalytic activity, $F_{12}PFeCl$ (80mg) was converted to its azide derivative by stirring an acetone solution (15mL) with solid NaN_3 for 20h under an inert atmosphere. The excess NaN_3 was removed by filtration and the solvent was evaporated to isolate the product. In an attempt to remove any remaining NaN_3, the residue was taken up in CH_2Cl_2 for subsequent filtration. However, the product was only partially soluble in this solvent and it appeared to slowly decompose into the μ-oxo dimer as indicated by the color change from a red-violet to greenish, with some green material depositing on the flask as an insoluble film. The solvent was immediately removed, dried and the material (1011591) isolated.

The uv spectrum (Figure 1) exhibited the Soret at 378nm with a shoulder at 418nm and a peak at 570nm. The IR spectrum (Figure 2) showed a strong bound-azide stretch at 2054 cm^{-1} with another band at 2137cm^{-1}, the latter corresponding to the free-azide stretch. The laser desorption mass spectrum (Figure 3) exhibited the parent peak for $F_{12}PFeN_3$ at 678amu, with a base peak at 636amu ($M^+ - N_3$) and a weak peak at 1289amu corresponding to the μ-oxo dimer.

In order to check the reproducibility, a 65mg batch of $F_{12}PFeCl$ was converted to the azide (1011598) as before but was not treated with CH_2Cl_2 at any stage of the work-up. Both samples were submitted for screening.

B. Treatment with Hydroxide

i) Treatment of a $CHCl_3$ solution of F12PFeCl with 1M NaOH (immiscible) resulted in a immediate change in color of the organic layer from purple to green with some green solid separating out (possibly μ-oxo dimer aggregates). The solid is soluble in acetone and exhibits a UV spectrum (Figure 4): 382 (broad Soret), 420 (sh), 570 (sh) and 602 (wk) nm.

ii) Treatment of an acetone solution of F12PFeCl with 1M NaOH (miscible) resulted in a green solution with a UV (Figure 5): 426 (broad Soret), 456 (sh), 564 (sh), 598 (wk) and 722 (wk) nm. The blue shift of the Soret [cf. (i) above] as well as the general appearance of the spectrum indicate that this material is different fron that formed in (i) above.

iii) A 60mg sample of F12PFeCl in acetone (20mL) was stirred with 1M NaOH (1mL) under argon for 1h. Two strong Soret bands were observed (378 and 420nm) with weak peaks at 574 and 604nm, suggesting that this is probably a mixture of (i) and (ii) above. Some green solid that formed was filtered and the solvent removed by freeze-drying. The residue was redissolved in acetone, filtered and the product isolated by evaporation of the filtrate. The uv spectrum had now changed to a broad Soret at 384nm, with the peak at 420nm being a shoulder similar to (i) above. This material (1011596) was submitted for screening.

β-Bromination of $F_{12}PFeCl$

A study was undertaken to determine the ideal conditions for bromination of the β-positions of meso-trifluoromethyl porphyrins. In that study, 5,15-bis(pentafluorophenyl)-10,20- (trifluoromethyl) porphyrinatoiron(III) [$F_{16}PFeCl$] was used since this porphyrin can be synthesized in higher yields and hence larger quantities of material were in hand. The information obtained was used during this quarter to to carry out β-brominations on the meso-tetrakis(trifluoromethyl)porphyrin system. Once again, in order to keep the costs down, bromination was attempted on the iron complex $F_{12}PFeCl$. However, the starting material exhibited very poor solubility in CCl_4 (unlike $F_{16}PFeCl$), hence the use of $CHCl_3$ instead.

i) $F_{12}PFeCl$ (15mg) in CCl_4 (8mL) was heated at reflux with N-bromosuccinimide (NBS) and Br_2 (0.2mL). Even after 24h reflux, the Soret band exhibited only a 4-6nm red shift although some broadening of the peak was observed. The uv spectrum of the material isolated after work up and treatment with hydroxide, exhibited a Soret at 400nm with a shoulder at 432nm and a weak absorption at 610nm. The results indicate partial bromination.

ii) $F_{12}PFeCl$ (35mg) in $CHCl_3$ (15mL) and pyridine (1mL), was heated at reflux with Br_2 (0.4mL) for 3h. Within the first hour, the uv spectrum changed from the split Soret at 348/404nm of the starting material, to a broad symmetrical Soret band at 466nm and a weak band at 670nm. No change was observed during the next 2h. The reaction mixture was allowed to stir overnight at room temperature. The supernatant $CHCl_3$ solution was

isolated, washed with 6M HCl to remove any excess pyridine, treated with aqueous NaOH and chromatographed on neutral alumina. The product isolated exhibited a strong Soret at 460nm and an absorption at 680nm (Figure 6). The laser desorption mass spectrum (Figure 7) exhibited peaks at 1225, 1262 and 1304 corresponding to $Br_7F_{12}PFeCl$, $Br_8F_{12}PFe$ and $Br_8F_{12}PFeCl$ respectively, indicating that bromination has been successful.

Bromination of $F_{12}PFeCl$ appeared to proceed faster and to completion when compared with the bromination of $F_{16}PFeCl$. This may well be due to the change in the reaction solvent from CCl_4 (for $F_{16}PFeCl$) to $CHCl_3$ (for $F_{12}PFeCl$). It was rather surprising to observe mass spectral peaks corresponding to the hemins (axial Cl ligated) since the material had been thoroughly treated with aqueous NaOH before isolation. Assignment of peaks above 1304 (the parent mass of $Br_8F_{12}PFeCl$) is currently being attempted to identify contaminating by products.

In order to confirm the hypothesis ,that efficient bromination of $F_{16}PFeCl$ by Br_2/pyridine may, at least in part, be due to the formation of pyridinium hydrobromide perbromide in situ, bromination was attempted using the commercially available reagent. It is interesting to note that no uv spectral shift was observed even after 6h reflux with pyridinium hydrobromide perbromide in $CHCl_3$, in the absence of added Br_2 and pyridine. Addition of Br_2 appears to assist the reaction but the red shift of the Soret is not significant. This suggests that axial ligation of pyridine at the iron center may be an important factor in the extent of bromination.

A larger batch of $F_{12}PFeCl$ (120mg) was brominated under the conditions described in (ii) above.

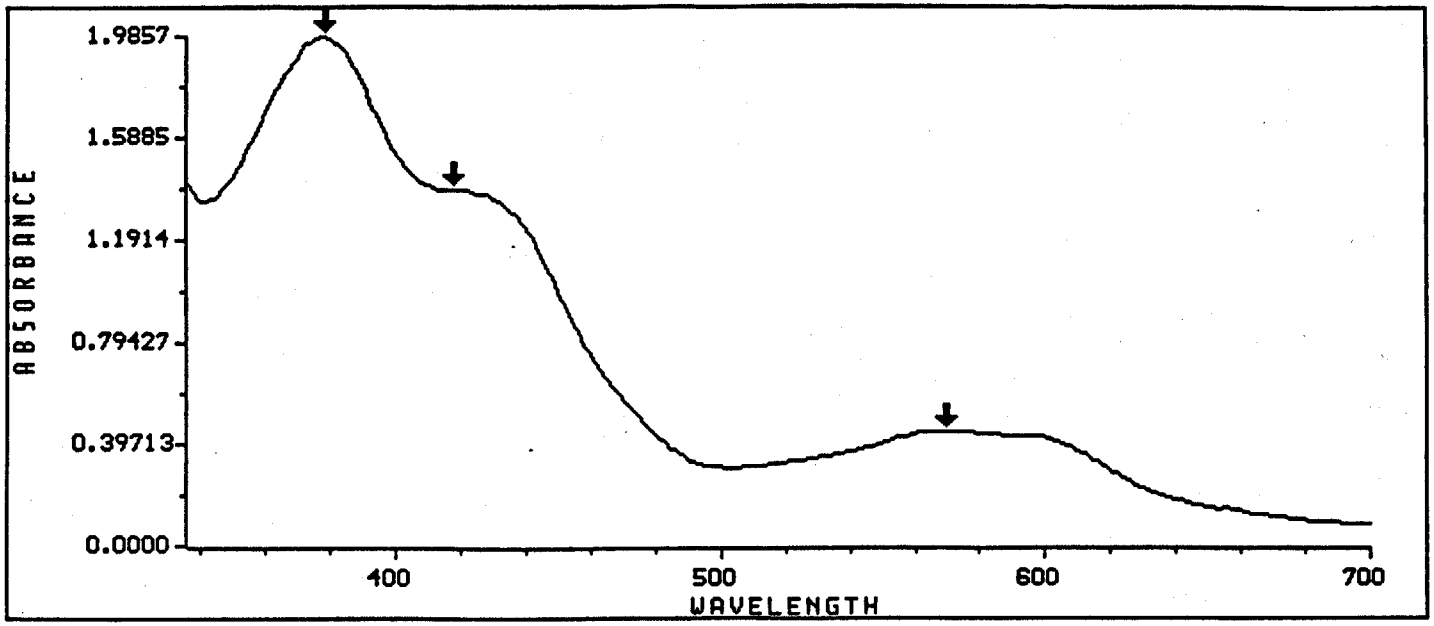

Annotated Wavelengths:

1 :	Wavelength =	378	Result =	1.985672
2 :	Wavelength =	418	Result =	1.390106
3 :	Wavelength =	570	Result =	0.448624

FIGURE 1. UV SPECTRUM OF $F_{12}PFeN_3$ IN ACETONE

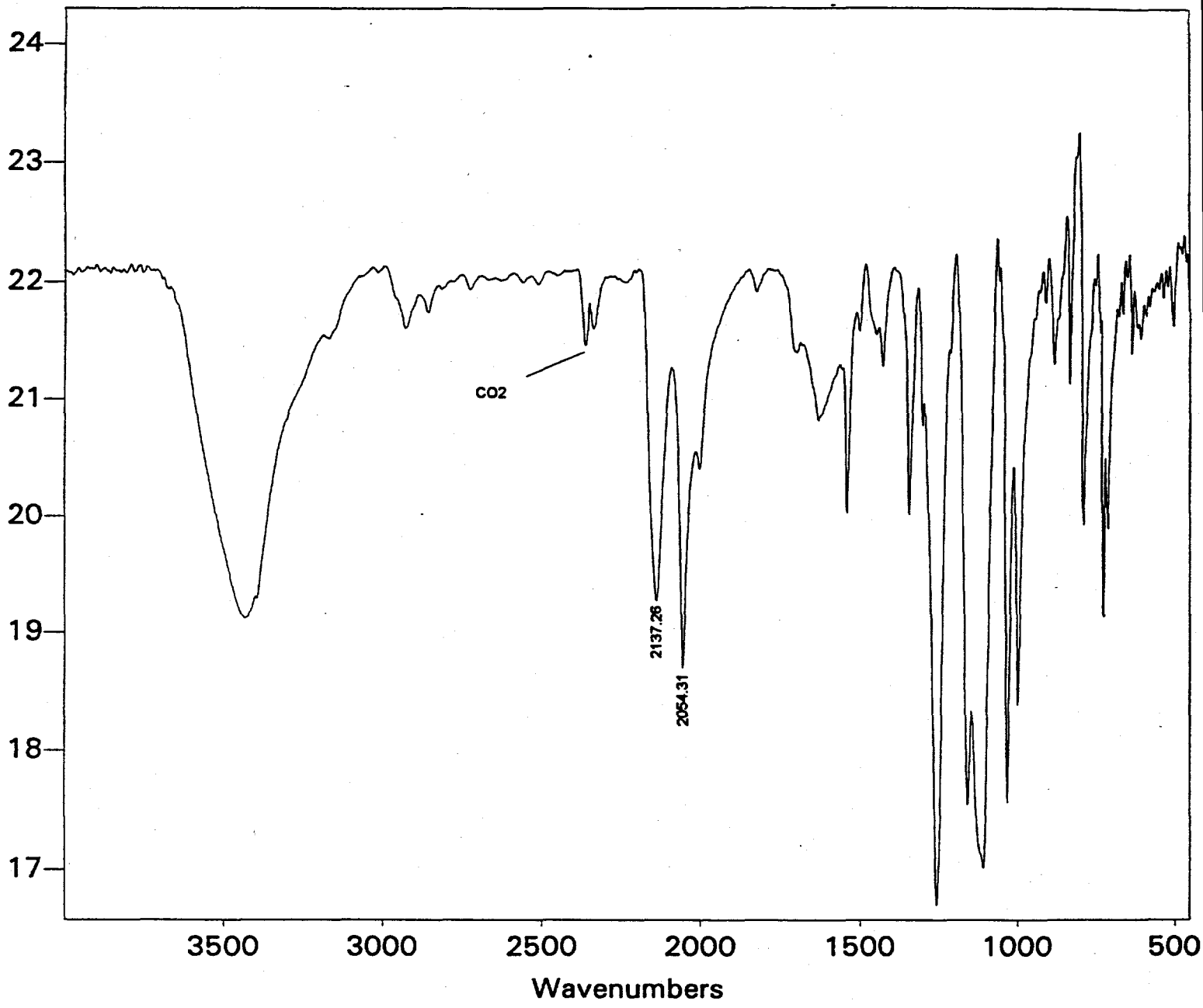

FIGURE 2. INFRARED SPECTRUM OF $F_{12}PFeN_3$

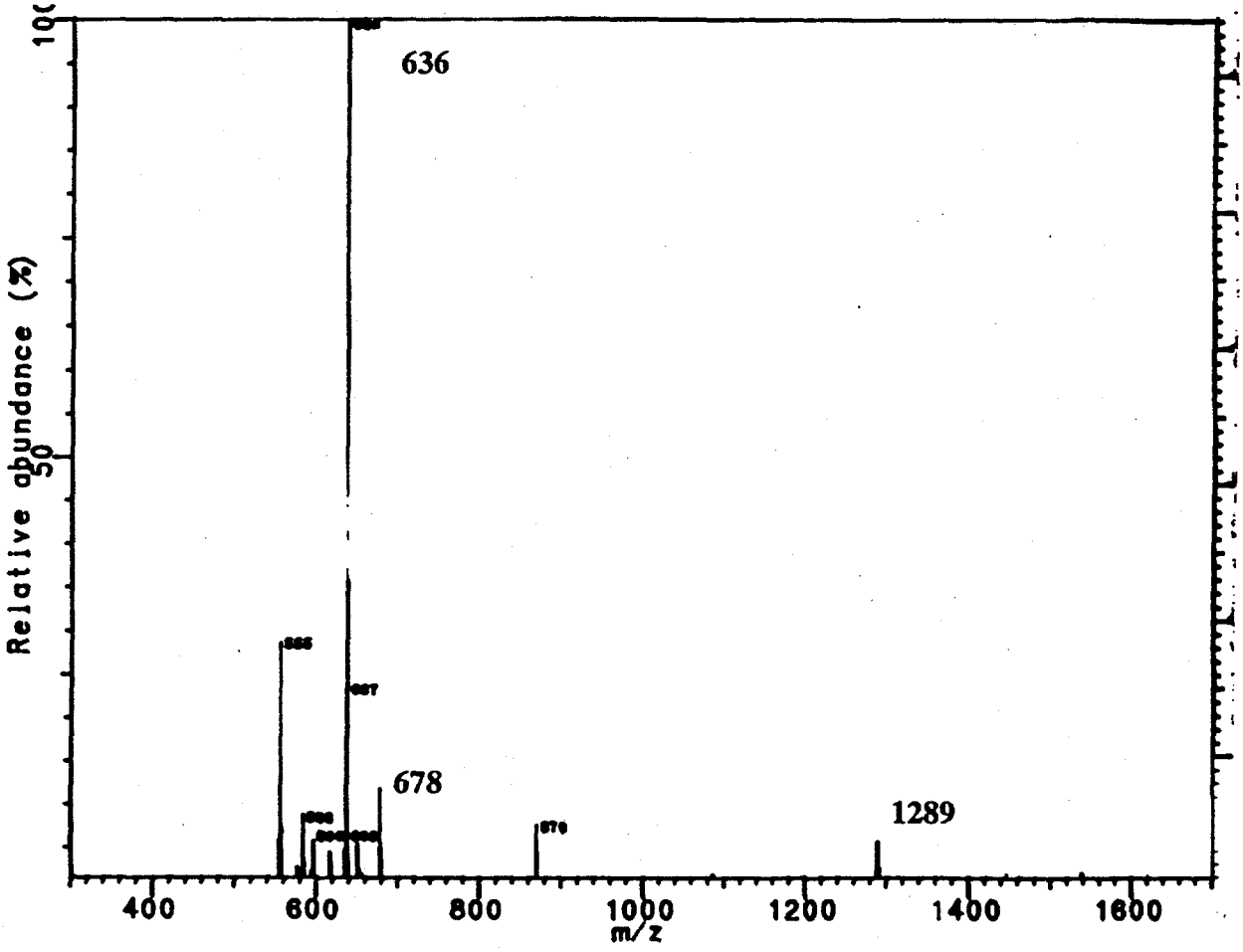

FIGURE 3: MASS SPECTRUM OF $F_{12}PFeN_3$

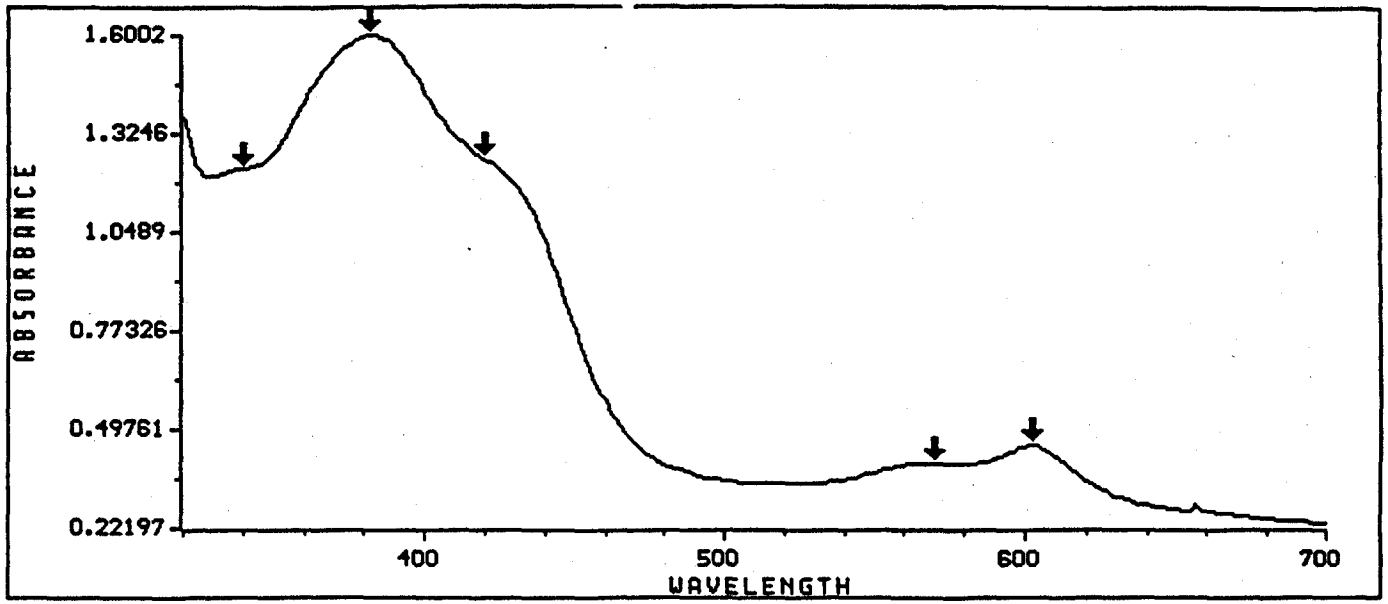

Annotated Wavelengths:

1	: Wavelength =	340	Result =	1.226456
2	: Wavelength =	382	Result =	1.600204
3	: Wavelength =	420	Result =	1.253937
4	: Wavelength =	570	Result =	0.401611
5	: Wavelength =	602	Result =	0.448669

FIGURE 4: UV SPECTRUM OF NaOH TREATED $F_{12}PFeCl$ in $CHCl_3$

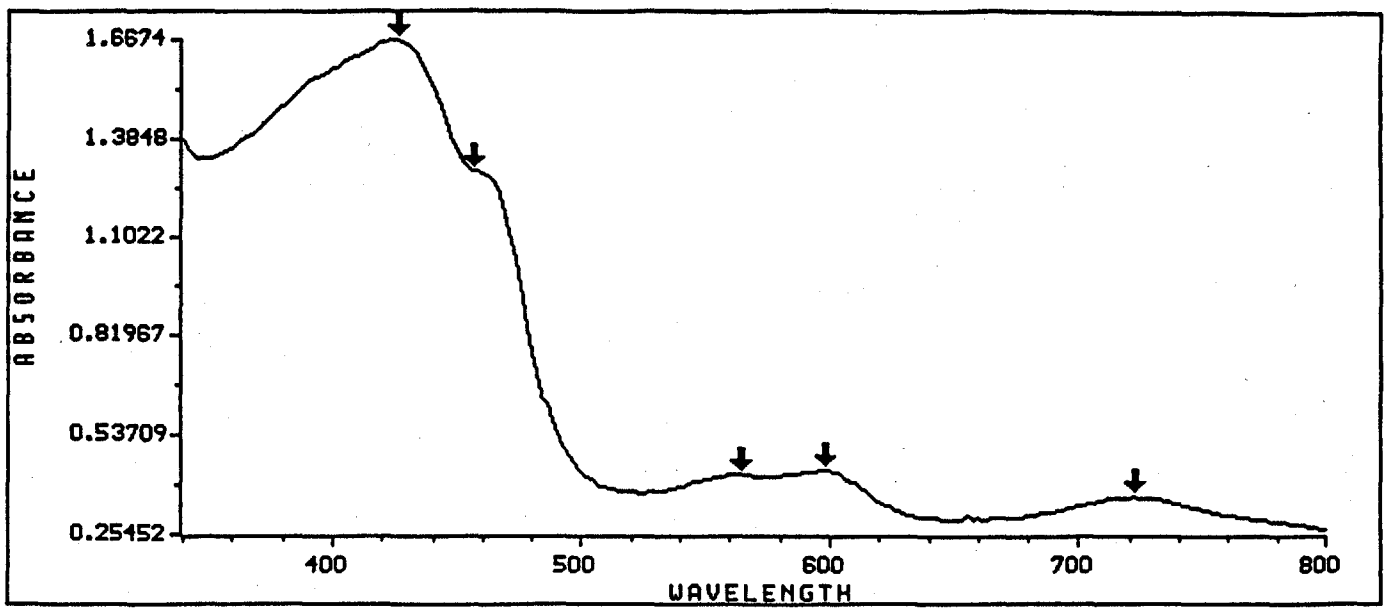

Annotated Wavelengths:

1	: Wavelength =	426	Result =	1.667389
2	: Wavelength =	456	Result =	1.299423
3	: Wavelength =	564	Result =	0.421249
4	: Wavelength =	598	Result =	0.434357
5	: Wavelength =	722	Result =	0.358917

FIGURE 5: UV SPECTRUM OF NaOH TREATED $F_{12}PFeCl$ in ACETONE

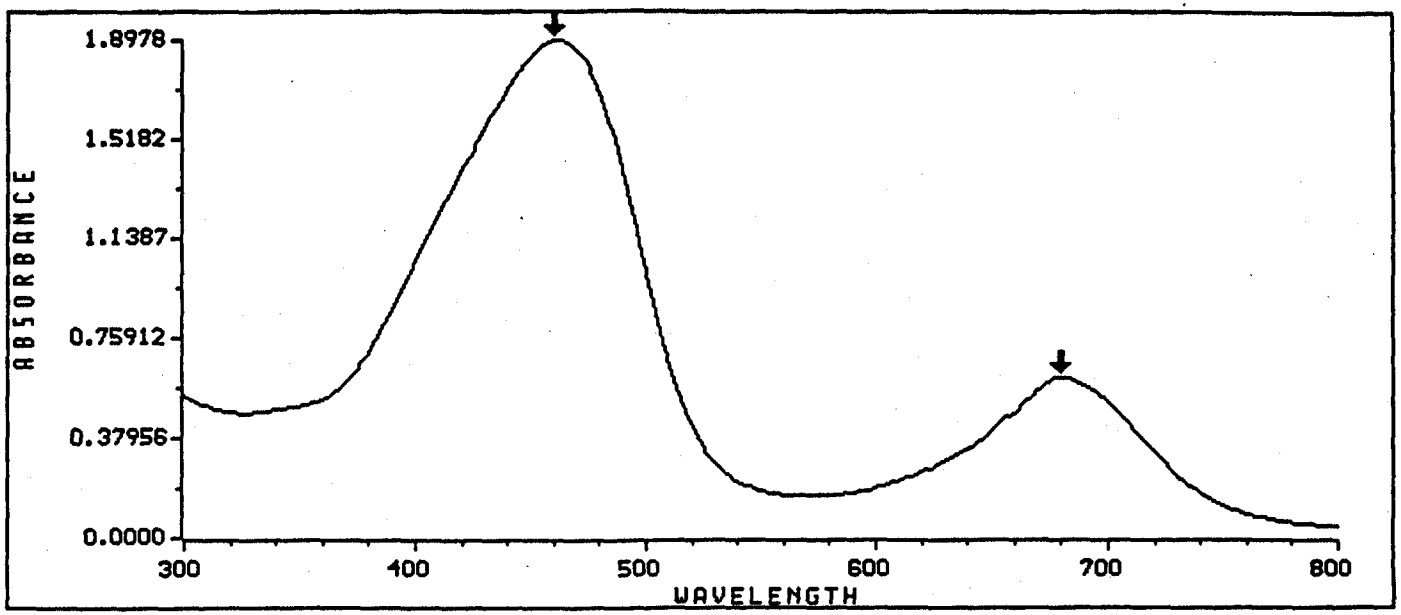

Annotated Wavelengths:
1 : Wavelength = 460 Result = 1.897812
2 : Wavelength = 680 Result = 0.604263

FIGURE 6: UV SPECTRUM OF BROMINATED F_{12}PFeX

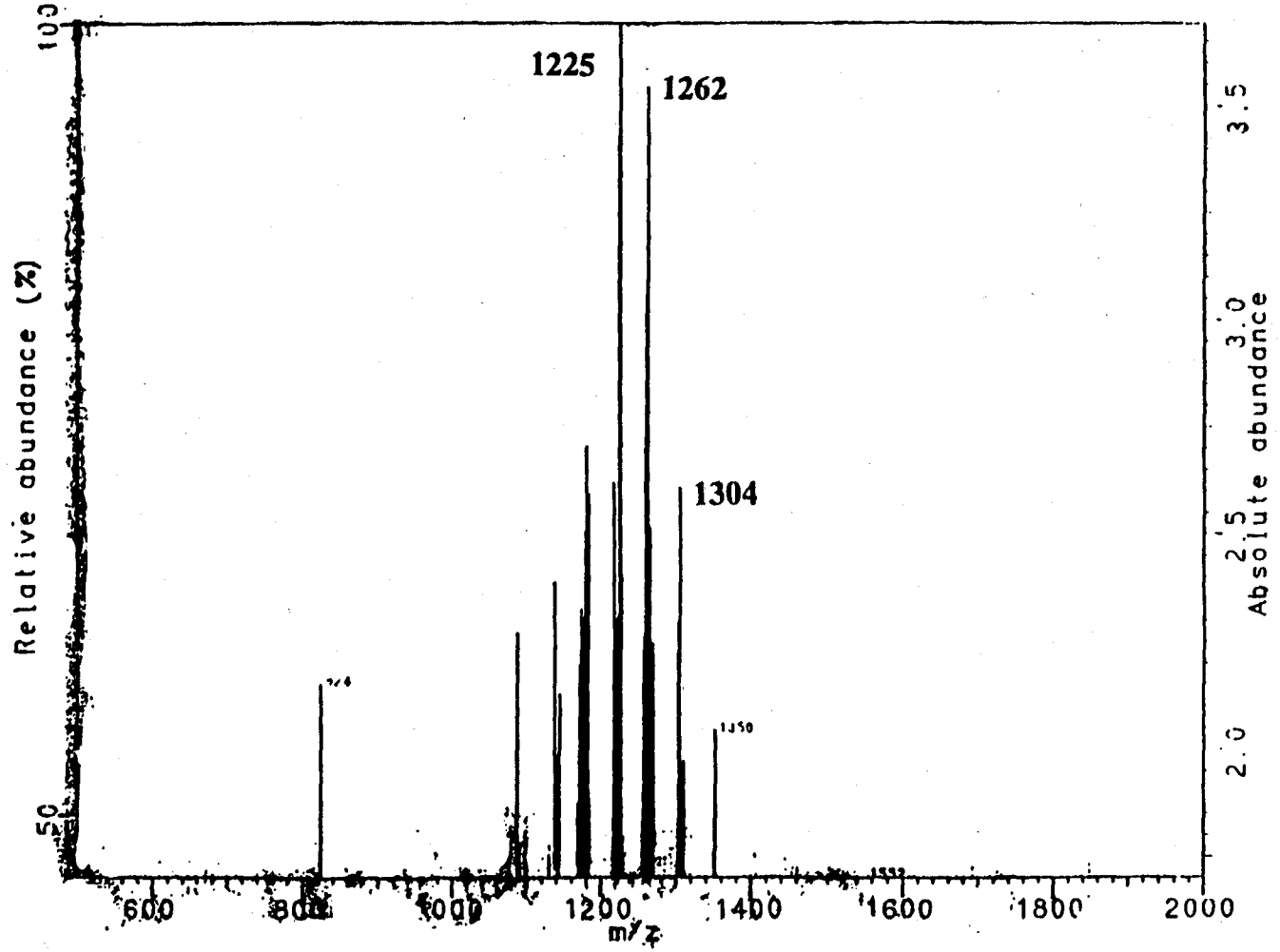

FIGURE 7: MASS SPECTRUM OF BROMINATED F_{12}PFeX

5.2 NEW PORPHYRIN CATALYSTS WITH MESO-CF_3 GROUPS

T.P Wijesekera

We have shown that substituting the highly electron-withdrawing perfluorophenyl (C_6F_5-) and nitro (NO_2) groups for the meso-hydrogen atoms in the porphine nucleus results in exceptionally active catalysts for the oxidation of light alkanes. These groups withdraw electrons from the porphyrin nucleus in two ways: by inductive and by mesomeric effects. Another powerful electron withdrawing group, the perfluoromethyl group (CF_3) has now been substituted for the meso-hydrogen of the porphine nucleus. In past reports we have discussed porphyrin complexes having two CF_3 groups and two C_6F_5 groups in the meso position and the catalytic activity of this complex. We have now prepared complexes having CF_3 groups in all four meso positions to produce a porphine which we call "$F_{12}P$" and have further produced iron complexes which bear bromines in each of the eight β-pyrrolic positions. This perhaloporphyrin complex has been given the short-hand designation: Fe($F_{12}P$-Br_8). We have made Fe(III) complexes of this type with a variety of axial ligands. To date catalytic activity of these materials has been hampered by an axial pyridine ligand which arises during the synthesis and which blocks substrate binding. An interesting feature of the $F_{12}P$ series is that the CF_3 group has only one mode of electron withdrawal. Although a powerful electron withdrawing group it can act only inductively and will not exhibit mesomeric effects with the delocallized porphyrin system. The following sections detail synthetic activities in both F_{12} and F_{16} systems.

5.2.1 Objectives

Attempt to substitute the β-positions of meso-(trifluoromethyl)porphyrinatoiron complexes [F_{12}PFeX and F_{16}PFeX] in order to improve catalytic activity.

Prepare sufficient quantities of bis(pyrrol-2-yl)-trifluoromethylmethane intermediate and convert to the porphyrins $F_{12}PH_2$ and $F_{16}PH_2$ as well as their iron complexes F_{12}PFeX and F_{16}PFeX respectively.

5.2.2 Highlights

A procedure was developed to β-brominate F_{12}PFeCl reproducibly to give hepta/octa-brominated material. However, analytical data suggest that some residual pyridine (reaction solvent) may be coordinated to the iron center, thus affecting catalytic activity.

β-Nitration of $F_{16}PH_2$ using a published procedure produced >80% of mono-nitrated porphyrin as two positional isomers.

5.2.3 Results and Discussion:

β-Bromination of
5,10,15,20-Tetrakis-(Trifluoromethyl)porphyrinatoiron (III) chloride
$F_{12}PFeCl$

As reported in the first quarter (1994) report, a procedure had been developed for the efficient peripheral bromination of $F_{12}PFeCl$ (reflux for 1h with Br_2 in $CHCl_3$/pyridine), which produced a material whose LDMS exhibited peaks corresponding to $Br_7F_{12}PFeCl$, $Br_8F_{12}PFe$ and $Br_8F_{12}PFeCl$. Since the reaction product had been subjected to a final base (NaOH) wash followed by chromatography on deactivated alumina before isolation, the existence of hemins (iron chloride) in the sample was rather surprising. Although this material could be prepared reproducibly, it showed very low activity for isobutane oxidation. This required a closer examination of its molecular structure.

The ^1H NMR spectrum of the sample 1011612 (Figure 1) did not exhibit any resonances above d = 8 ppm (paramagnetic range was also examined) indicating near complete β-bromination. However, three resonances were observed at d = 3.49, 5.60 and 6.46 ppm (relative intensity 2:2:1) which may result from ligated pyridine. Pyridine is used as a co-solvent/promoter in the bromination reaction and is removed by acid-wash (6M HCl) during work up. It is possible that strong ligation exists between pyridine and the iron center which may be the reason for the poor catalytic activity. In order to confirm pyridine ligation, the bromination was carried out using perdeuterated pyridine (pyr-d5). The material isolated, 1013816, did not exhibit any resonances between d = 3.0 and 6.5 ppm in its ^1H NMR spectrum, but the ^2H (deuterium) NMR spectrum essentially mirrored the ^1H NMR spectrum of 1011612 thus confirming pyridine-ligation. Several samples (1013840, 50mg; 1013805, 60mg; 1013862, 90mg and 1013869, 310mg) have been prepared using this bromination procedure and all exhibit essentially the same mass spectrum (Laser Desorption). Attempts will be made to remove the ligated pyridine and increase the activity at the metal center.

A sample of $F_{16}PFeCl$ was also brominated with Br_2 in $CHCl_3$/pyridine and the reaction was found to proceed to completion faster than when CCl_4 was used as the solvent. The Soret band shifted up to λ= 446nm within 1h with no change thereafter (in CCl_4, the red-shift was up to λ = 436 in 1h; no change thereafter). In two separate preparations, the work-up involving an acid wash (to remove excess pyridine), a base wash (to convert to a hydroxo/oxo-dimer form) followed by chromatography (neutral alumina - 15% H_2O added), led to products that were spectroscopically different. One sample (1013852-1) exhibited a Soret at λ= 436nm with a short wavelengh shoulder and a featureless visible region (Figure 2a) while the other sample (1013880) had a 2-band spectrum (Figure 2b; Soret λ= 444nm) similar to that of the material prepared in CCl_4 (1011573; Soret λ= 418nm) except that it is red-shifted. It is interesting to note that both these samples (1013852-1 and 1013880) were not as active as 1011573 and required certain promoters to increase their activity.

β-Nitration of 5,15-Bis(Pentafluorophenyl)-10,20-Bis(Trifluoromethyl)porphyrin $F_{16}PH_2$

Introduction of nitro groups on the porphyrin periphery is known to increase the electron-deficiency of the macrocycle and hence the catalytic activity (towards oxygen activation) of the iron complex. Mansuy and co-workers (J.Chem.Soc. Chem. Commum., 1994, p23) have recently shown that nitration of meso-tetrakis-(pentafluorophenyl)porphyrin [$F_{20}TPPH_2$] with 100 equivalents of red-fuming HNO_3 at room temperature over 8h, produce a mixture of regioisomers of the β-tetranitro derivative. Due to the relative ease of synthesis of $F_{16}PH_2$ (cf. $F_{12}PH_2$), the study of β-nitration of meso-trifluoromethylated porphyrins was undertaken initially on this porphyrin.

A 5mM solution of $F_{16}PH_2$ in $CHCl_3$ (30mL) was treated with 100 equivalents of red fuming HNO3, added over a 3h period. This was followed by a further 60 equivalents of acid and the reaction mixture stirred at room temperature for a total of 72h. Within 40h, the Soret absorption had shifted from λ=406nm to 420nm and remained unchanged.

After neutralizing the acid, the crude material was chromatographed on a 2mm preparative silica-gel layer using CH_2Cl_2/n-hexane (2:1) as the eluting solvent. Six bands were observed; in the order of increasing polarity: a reddish-purple band (1; major), a greenish blue band (2; major), a pale green band (3), a yellow band (4) and two purple bands (5 and 6) very close to the origin. Bands 3 and 4 were very minor and were discarded while bands 1, 2, 5 and 6 were isolated. When bands 5 and 6 were rechromatographed on neutral alumina, they were found to be identical to band 1 and were therefore combined (on silica gel, this compound probably protonated and adsorbed strongly at the origin).

The only two major reaction products were band 1 (1013823 and band 2 (1013833). Absorption spectra of both 1013823 (Figure 3a) and 1013833 (Figure 4a) exhibited Soret bands at λ = 418nm indicating the structural similarity (electron-deficiency and macrocyclic deformation) of the two materials, but the visible region was distinctly different. Laser desorption mass spectra exhibited parent ions at m/z = 824/825 for both 1013823 (Figure 3b) and 1013833 (Figure 4b) suggesting that they are positional isomers of mononitrated $F_{16}PH_2$. They will be further characterized by ^1H NMR spectroscopy. It was possible to reproduce this reaction and isolate the same two major components without the use of preparative layer chromatography.

An attempt was made to force the reaction to lead to further nitration at the β-positions. A reaction mixture similar to that above was heated at reflux and monitored by uv-visible spectroscopy. Within 4h, the Soret band moved to λ = 426nm but further red-shift was not observed even after 20h. Work-up of the reaction mixture indicated that extensive decomposition had occurred with <10% of porphyrinic material remaining.

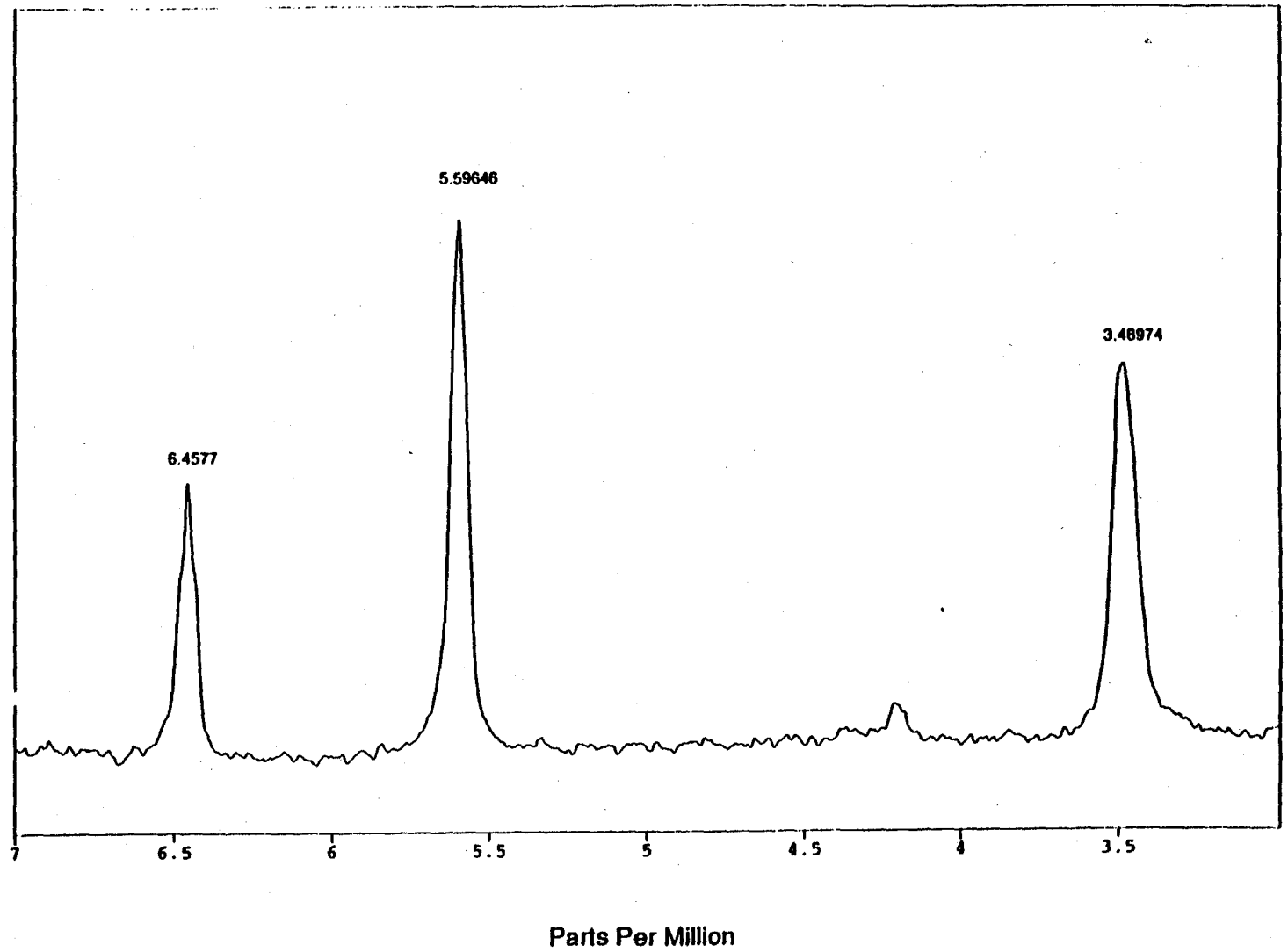

Figure 1: **^{1}H NMR Spectrum of 1011612 [$Br_nF_{12}PFeX$; n= 7-8]**

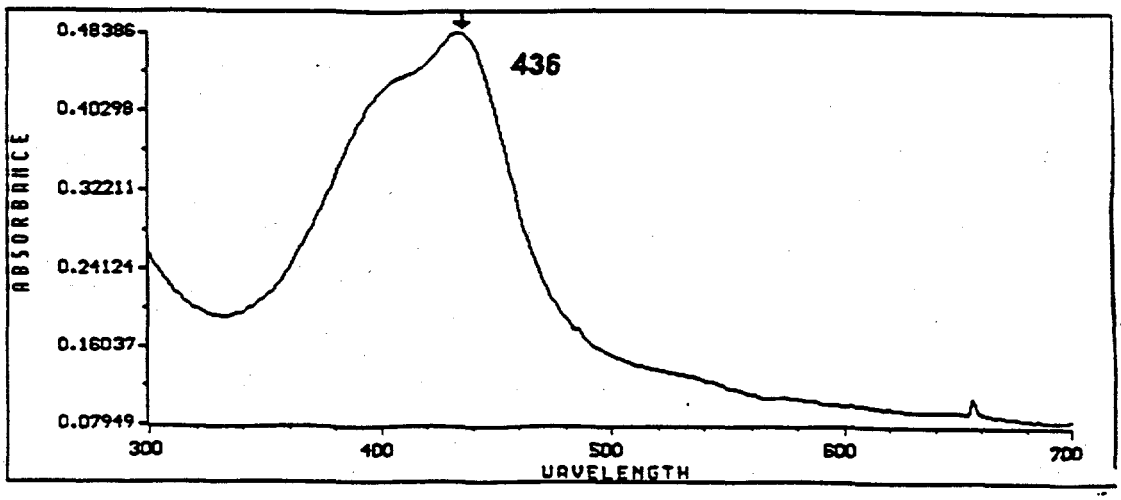

Figure 2a: Absorption Spectrum of 1013852-1
[$Br_nF_{16}PFeX$; n = 7-8]

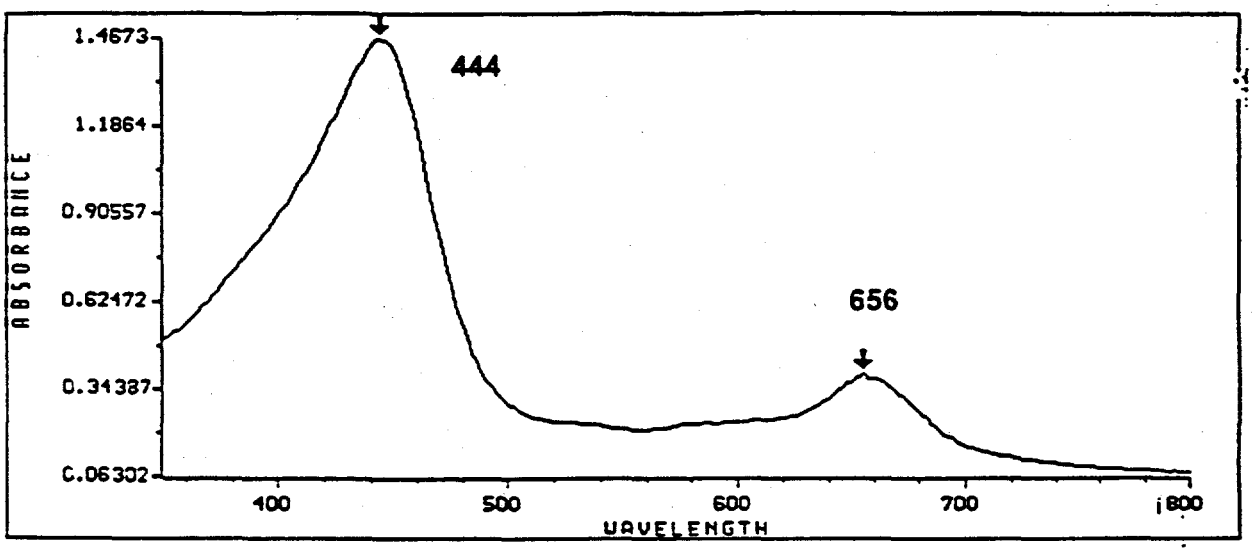

Figure 2b: Absorption Spectrum of 1013880
[$Br_nF_{16}PFeX$; n = 7-8]

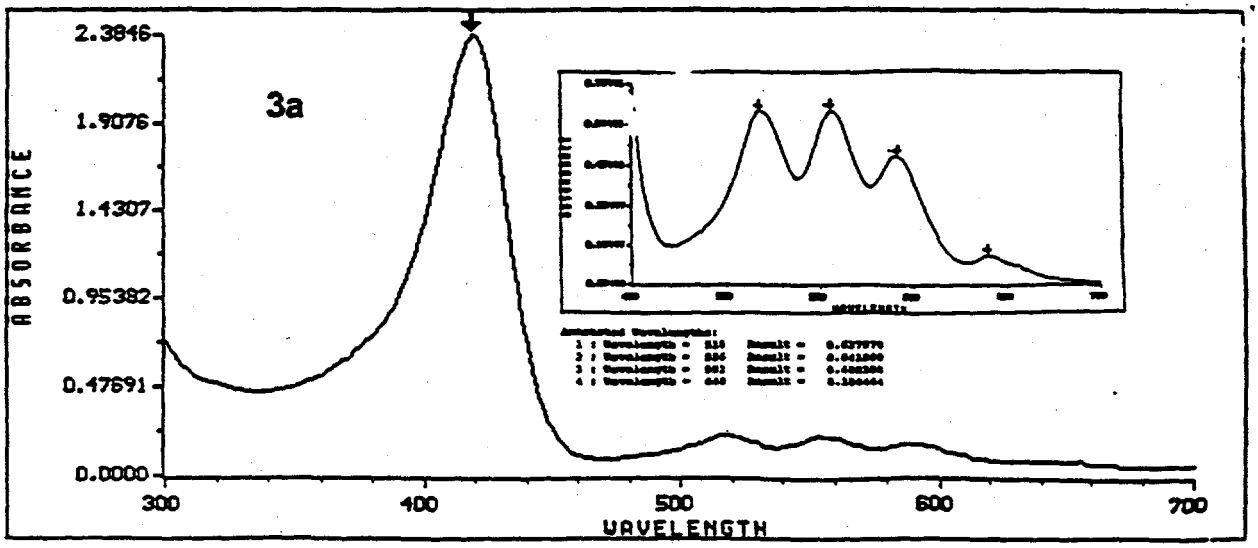

Annotated Wavelengths:
1 : Wavelength = 418 Result = 2.384552

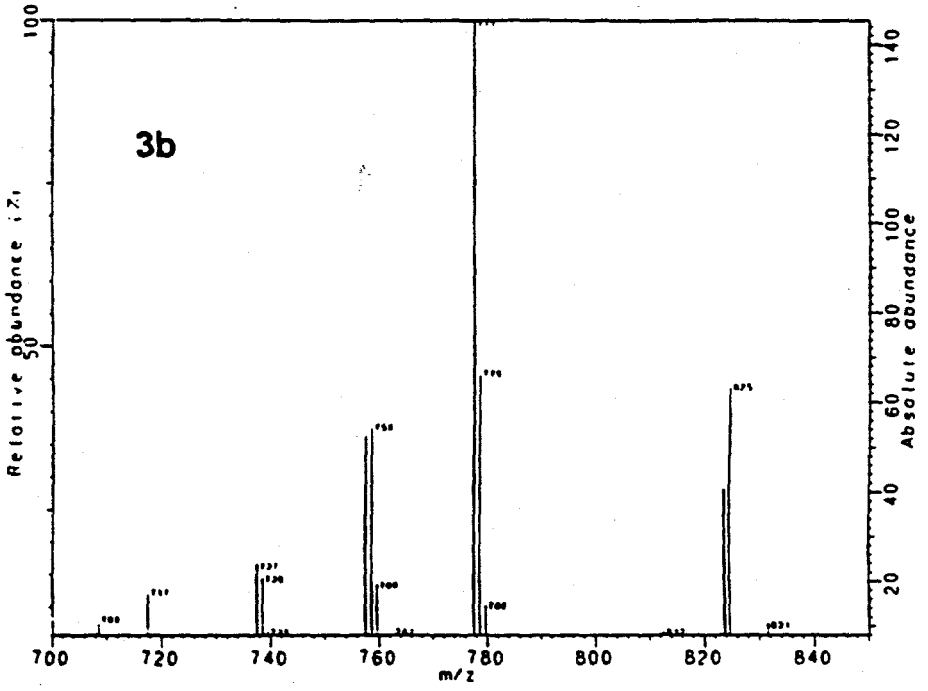

Figure 3: Absorption (3a) and LDMS (3b) Spectra of 1013823 [$(NO_2)F_{16}PH_2$]

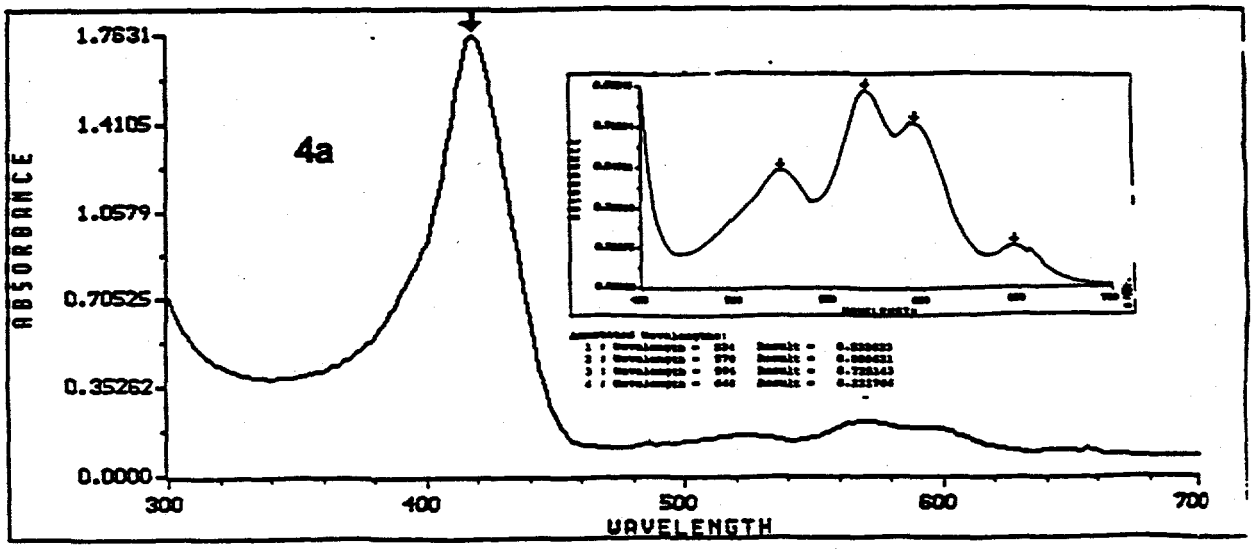

Annotated Wavelengths:
1 : Wavelength = 418 Result = 1.763123

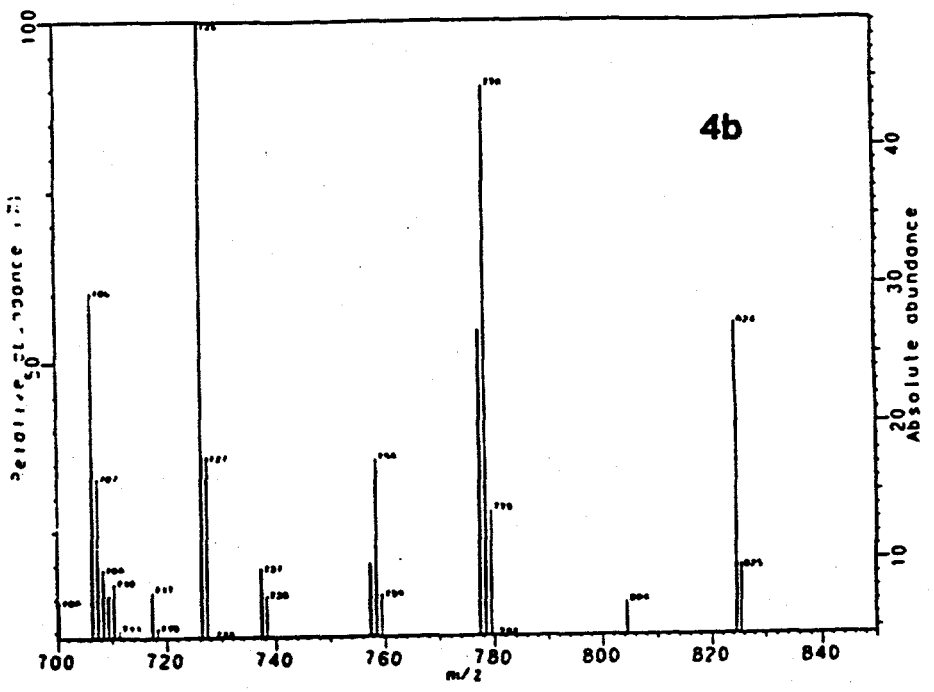

Figure 4: Absorption (4a) and LDMS (4b) Spectra of 1013833 [$(NO_2)F_{16}PH_2$]

5.3 CREATING A SOLUBLE PERHALOALKYL PORPHYRIN

5.3.1 Objectives

Synthesis of a perfluoroalkyl analogue of *meso*-tetrakis(trifluoromethyporphyrinato) iron(III) [F_{12}PFeX], which in its catalytically active hydroxo [X=OH] or oxo-bridged dimer [X= -O(PF_{12})] form exhibits reasonable solubility in hydrocarbon solvents for screening for isobutane oxidation activity.

Attempt improve the activity of the β–perbrominated F_{12}PFeX by removing the undesirable axial ligands associated with the complex.

5.3.2 Highlights

Pyrrole and heptafluorobutyraldehyde were successfully coupled to prepare the *meso*-heptafluoropropyldipyrromethane, which was condensed independantly with heptafluorobutyraldehyde and pentafluorobenzaldehyde to give 5,10,15,20-tetrakis- (heptafluoro propyl)porphyrin [$F_{28}PH_2$] and 5,15-bis(heptafluoropropyl)-10,20-bis- (pentafluorophenyl)porphyrin [$F_{24}PH_2$] respectively. Preliminary iron insertion studies indicated that both F_{28}PFeX and F_{24}PFeX have high solubility in hydrocarbon solvents.

Attempts to remove undesirable axial ligands from βBr_8F_{12}PFeX catalysts led to significant decomposition of the metalloporphyrin.

5.3.3 Results and Discussion

Synthesis of Other Perfluoroalkyl analogues of *meso*-tetrakis(trifluoromethyl)porphyrinatoiron(III) [F_{12}PFeX]

The rationale for the synthesis of *meso*-tetrakis(trifluoromethyl)porphyrinatoiron(III) [F_{12}PFeX] as a catalyst for isobutane oxidation was, that introducing a lower mass but equally (or more) powerful electron-withdrawing CF_3 group should generate a more economical catalyst than the C_6F_5 analogue, F_{20}TPPFeX. Although a new route was successfully developed for the synthesis of *meso*-trifluoromethylporphyrins, a rather disappointing observation with the F_{12}PFeX catalyst system was, that in its active hydroxo/oxo-dimer form, it exhibits an unusually low solubility. This observation can be explained by the enhanced self-aggregation of the catalyst (a common phenomenon for porphyrin systems) due to the removal of steric bulk from the *meso*-position (in replacing C_6F_5 with CF_3) eventually leading to the observed low-solubility. However, this made it impossible to obtain

satisfactory oxidation data for F_{12}PFeX in order to make a direct comparison of its catalytic behaviour with that of the F_{20}TPPFeX system.

Although theoretical calculations as well as physical studies have previously shown that the CF_3 group can be an excellent electron-withdrawing group particularly in the *meso*-position [**Gassman et. al.,** *J. Am. Chem. Soc.,* **114**, 9990 (1992)], how this translates into improved catalytic activity of a metalloporphyrin system could not be evaluated due to the solubility reasons described above. This therefore left the most important question "Should the electron-withdrawal at the *meso*-position of a metalloporphyrin be of a mesomeric rather than an inductive nature for it to be effective in the improvement of catalytic activity?", unanswered. This is particularly so, because all of the previously tested active catalysts had a mesomerically active electron-withdrawing group at the *meso*-position (e.g. perfluorophenyl, nitro). In order to answer the above question, it was therefore essential that a different metalloporphyrin analogue with perhaloalkyl groups in the *meso*- positions be synthesized, and its activity tested. Heptafluoropropyl group was selected to replace the trifluoromethyl groups in F_{12}PFeX since the analogous complex *meso*-tetrakis(heptafluoropropyl)- porphyrinatoiron(III) [F_{28}PFeX] was predicted to have good solubility in organic solvents (due to significantly lower aggregation) while still maintaining a similar electron-deficiency in the catalytic system.

The two step procedure previously developed for the synthesis of F_{12}PFeX and F_{16}PFeX catalysts is undoubtably the most promising approach for the synthesis of any *meso*-perfluoroalkyl porphyrins. In the first step, pyrrole is coupled with a perfluoroalkyl aldehyde (or its synthetic equivalent) under experimental conditions that would maximize the yield of the *meso*-substituted dipyrromethane (**Scheme 1**), which is isolated and condensed with the appropriate aldehyde in the second step (**Scheme 2**) to give the desired porphyrin. In the heptafluoropropyl series, the products (**3b** and **5d**) and their yields corresponded in many ways to those in the trifluoromethyl series, thus further establishing the generality of the previously developed synthetic scheme. The porphyrin with two pentafluorophenyl groups at opposite *meso*-positions and two heptafluoropropyl groups at the other *meso*-positions (**5c**) was also synthesized for comparison purposes.

Synthesis of the Dipyrromethane:

5-Heptafluoropropyldipyrromethane (**3b**) was prepared in modest yields (50%) by reacting pyrrole and heptafluorobutyraldehyde hydrate in a 2:1 molar ratio. The reaction conditions (not optimized for this synthesis) involved, refluxing the reagent mixture in tetrahydrofuran (THF) and concentrated hydrochloric acid (40:1) for 2-3h under an inert atmosphere. During isolation, a prepurification of the reaction mixture (prior to chromatography) via extraction into petroleum ether (successful with the CF_3 analogue) was not possible due to the high solubility of polymeric by-products in this solvent. This resulted in product purities not greater than 90% after one filtration through activity I neutral alumina. Further purification by chromatography led to loss of material since the high mass impurities always moved fast and ahead of the desired product even in 1:1 CH_2Cl_2-hexane eluting solvent. The dipyrromethane was fully characterized by mass (GC) spectroscopy (**Figure 1**), ^{1}H NMR (**Figure 2**) and ^{19}F NMR spectroscopy (**Figure 3**).

5.3.4 Synthesis of the Porphyrins

5,15-bis(heptafluoropropyl)-10,20-bis(pentafluorophenyl)porphyrin [$F_{24}PH_2$; **5c**]

5,10,15,20-tetrakis(heptafluoropropyl)porphyrin [$F_{28}PH_2$; **5d**]

The dipyrromethane **3b** was condensed with pentafluorobenzaldehyde (**4a**) and heptafluorobutyraldehyde (**4c**) to give 5,15-bis(heptafluoropropyl)-10,20-bis(pentafluorophenyl) porphyrin [$F_{24}PH_2$; **5c**] and 5,10,15,20-tetrakis(heptafluoropropyl) porphyrin [$F_{28}PH_2$; **5d**] respectively (**Scheme 2**). The reactions were carried out in refluxing chloroform using activated Montmorillonite K10 as the catalyst. As with the trifluoromethyl analogues $F_{16}PH_2$ (**5a**) and $F_{12}PH_2$ (**5b**), longer reaction times were required to maximize the yields of $F_{28}PH_2$ (**5d**; 20-30h) compared with $F_{24}PH_2$ (**5c**; 8-10h), although the final yields were consistently lower (6-10% for **5d** vs 15-20% for **5c**). This of course can be explained by the powerful destabilizing effect that a perfluoroalkyl group has on the formation of a carbenium ion adjacent to it [**Allen et. al.**, *Can. J. Chem.*, **68**, 1709, (1990) and references cited therein]. Although the isolated yields of $F_{28}PH_2$ (**5d**) were somewhat higher than those obtained for the trifluoromethyl analogue $F_{12}PH_2$ (**5b**), its purity was lower. A dark colored impurity appeared to move almost together with the porphyrin **5d** in several eluting solvent systems thus making it rather difficult to separate. Recrystallization from CH_2Cl_2-CH_3OH appeared to be the most useful purification technique although the visible region of the absorption spectrum (**Figure 5**) as well as the ^1H NMR spectrum (**Figure 9**) indicated the incomplete removal of the impurity (cf. absorption spectrum of **5c**; **Figure 4**). However, this impurity did not interfere with the subsequent iron insertion reaction (details in the final report) and was easily separated from the iron complex. Mass spectroscopy (**Figure 6**; M+1 = 979 for **5c** and **Figure 7**; M+2 = 984 for **5d**) as well as ^1H and ^{19}F NMR spectroscopy (**Figures 8, 9, 10, 11**) confirm the structures of the two porphyrins **5c** and **5d.**

Insertion of Iron:

Iron insertions to **5c** and **5d** were carried out on small scale and no problems were observed. Synthetic details, purification procedures as well as spectral and analytical data will be included in the final report.

5.3.5 β-Brominated 5,10,15,20-Tetrakis(Trifluoromethyl)porphyrinatoiron(III) $\beta Br_8F_{12}PFeX$

Two previous quarterly reports (1/94 and 2/94) revealed that a synthetic method was developed to prepare $\beta Br_8F_{12}PFeX$ in good yield but the catalyst exhibited very low isobutane oxidation activity. Extensive structure analysis by ^1H and ^2H NMR spectroscopy suggested that this unusual behaviour could very well be due to pyridine ligated to the metal center. Attempts to remove pyridine by heating the solid material under high vacuum were not successful.

In an attempt to remove pyridine by complexation, a 100mg sample of $\beta Br_8F_{12}PFeX$ was retreated with Br_2 in the absence of any pyridine. Since pyridine is known to form pyridinium hydrobromide perbromide on reaction with bromine, it was believed that refluxing with Br_2 may remove any bound pyridine. After refluxing a $CHCl_3$ solution with Br_2 for 1h, the excess reagent was removed, the solution washed with 2M NaOH, H_2O and the crude product chromatographed on neutral alumina. However, only 30-40% of porphyrinic material could be recovered indicating significant loss by decomposition. FABMS analysis suggested that some loss of bromine had occurred.

Bromination of $F_{12}PFeCl$ was repeated with significantly smaller quantities of pyridine but even after 20h at reflux, very little reaction had taken place and the unreacted starting material could be recovered.

Perbromination of $F_{12}PFeCl$ to produce a catalytically active $\beta Br_8F_{12}PFeX$ sample remains to be a problem.

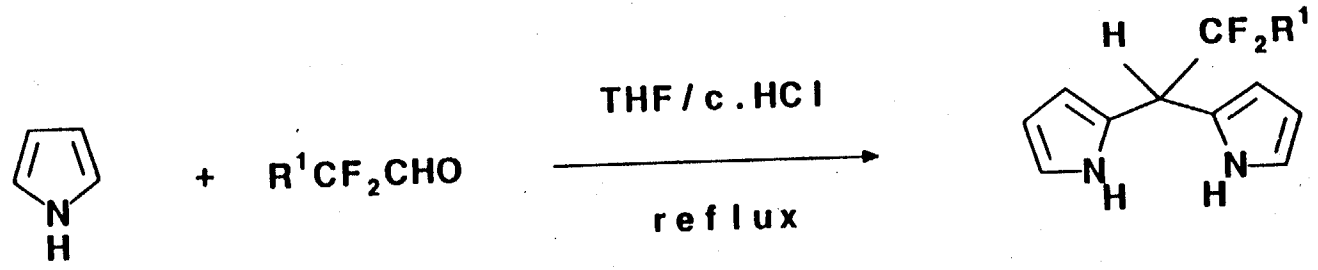
THF / c.HCl
reflux
+ R^1CF_2CHO
1
2a. $R^1=F$
2b. $R^1=CF_3CF_2$
3a. $R^1=F$
3b. $R^1=CF_3CF_2$

Scheme 1

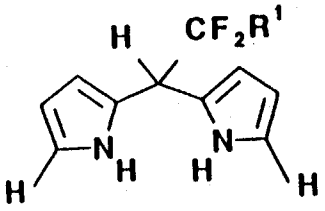

3a. $R^1=F$

3b. $R^1=CF_3CF_2$

+ R^2CHO

4a. $R^2=C_6F_5$

4b. $R^2=CF_3$

4c. $R^2=CF_3CF_2CF_2$

$\xrightarrow{H^+}$

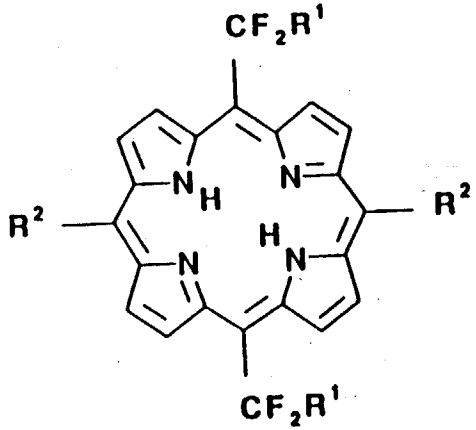

5a. $R^1=F$; $R^2=C_6F_5$

5b. $R^1=F$; $R^2=CF_3$

5c. $R^1=CF_3CF_2$; $R^2=C_6F_5$

5d. $R^1=CF_3CF_2$; $R^2=CF_3CF_2CF_2$

Scheme 2

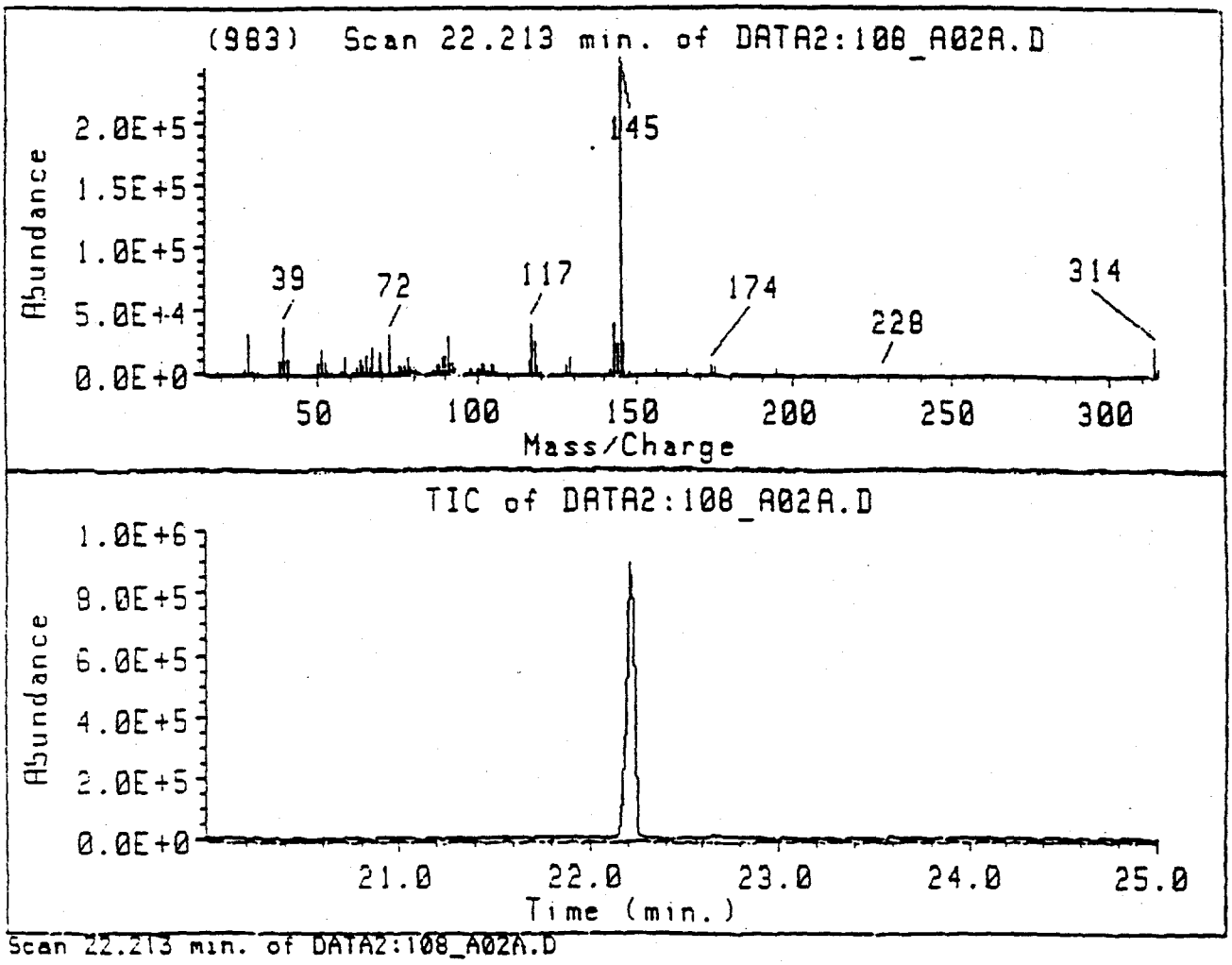

Figure 1:

GC Mass Spectrum of 5-Heptafluoropropyldipyrromethane [3b]

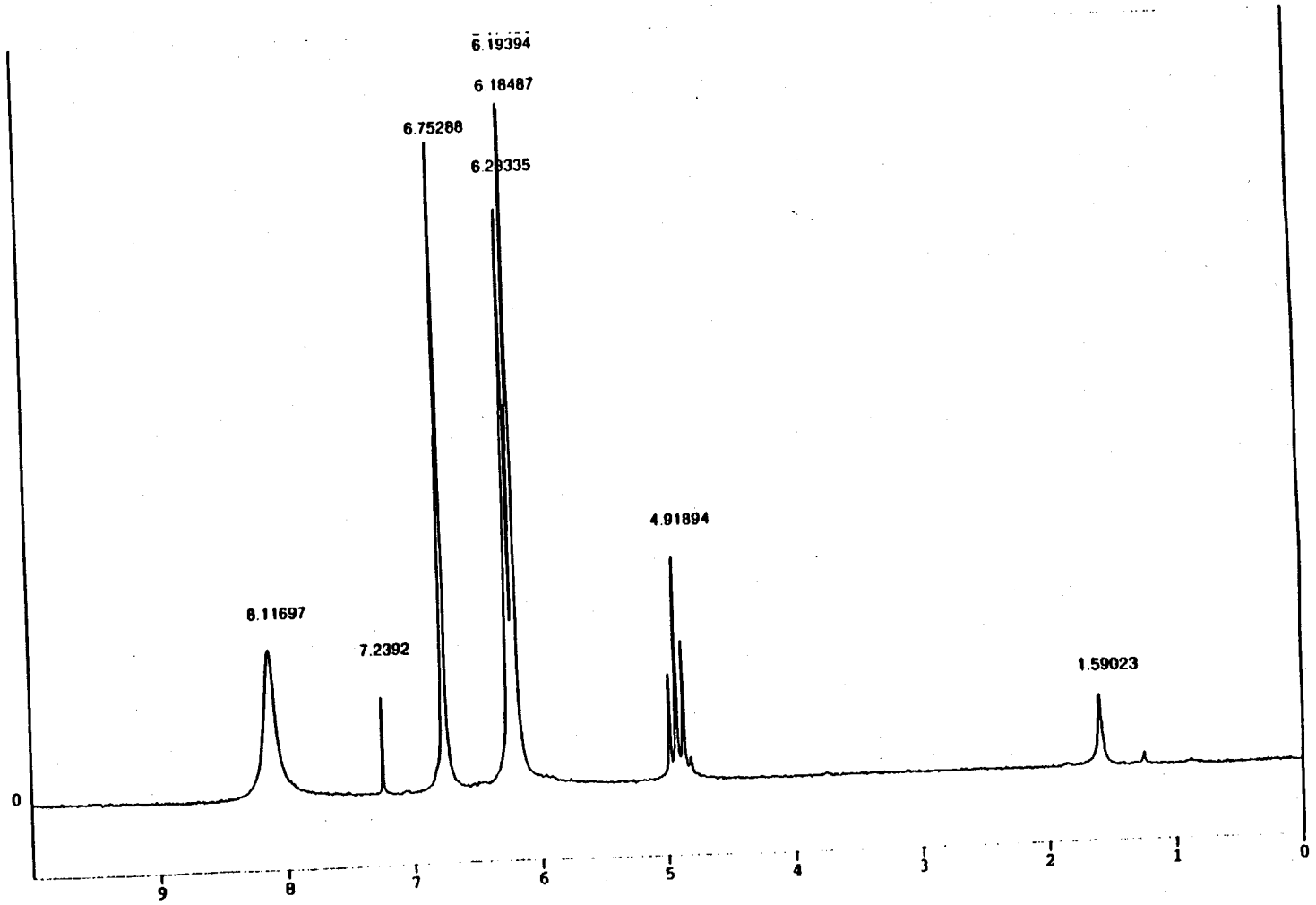

78

Figure 2:

^{1}H NMR Spectrum of 5-Heptafluoropropyldipyrromethane [3b]

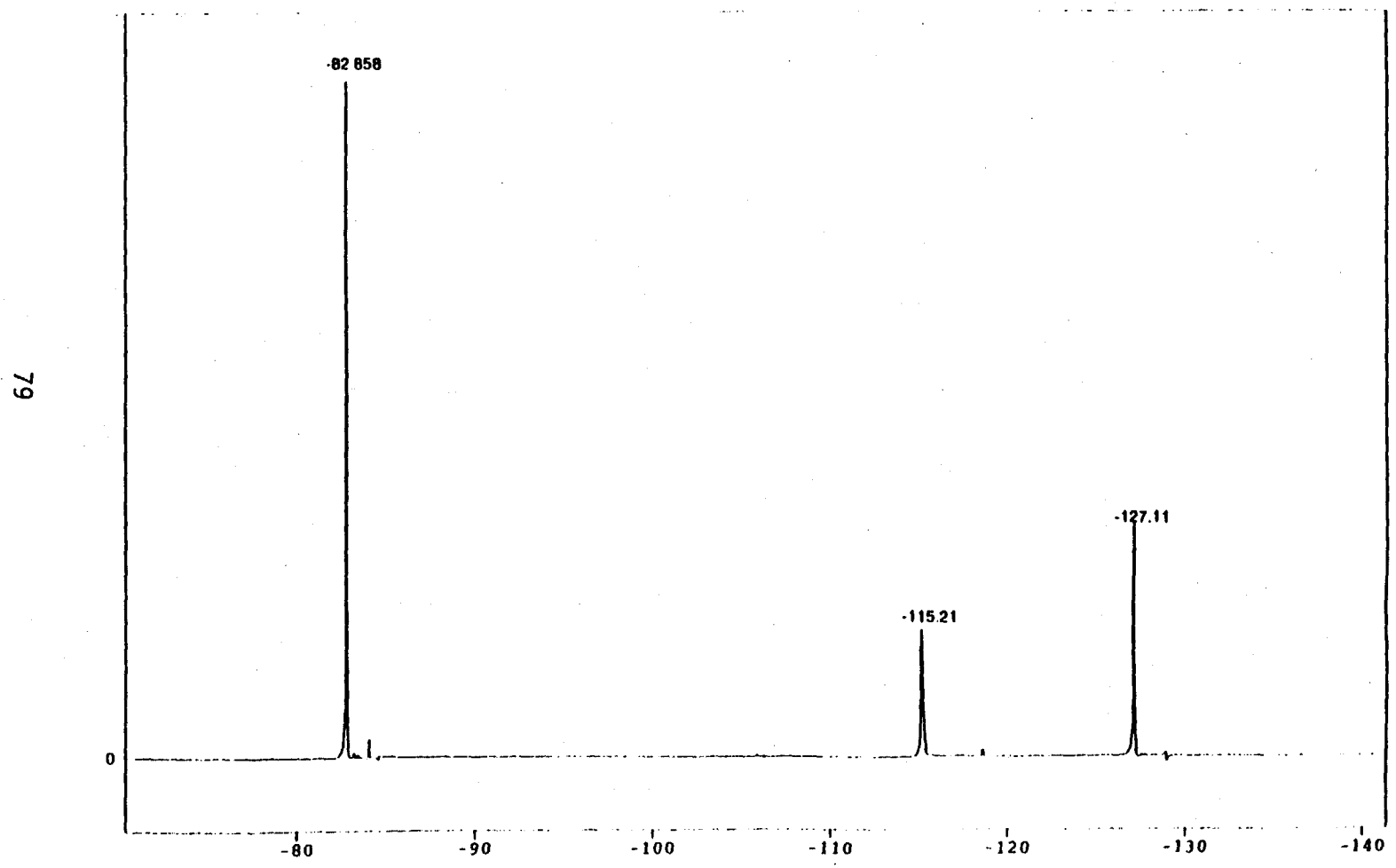

Figure 3:

^{19}F NMR Spectrum of 5-Heptafluoropropyldipyrromethane [3b]

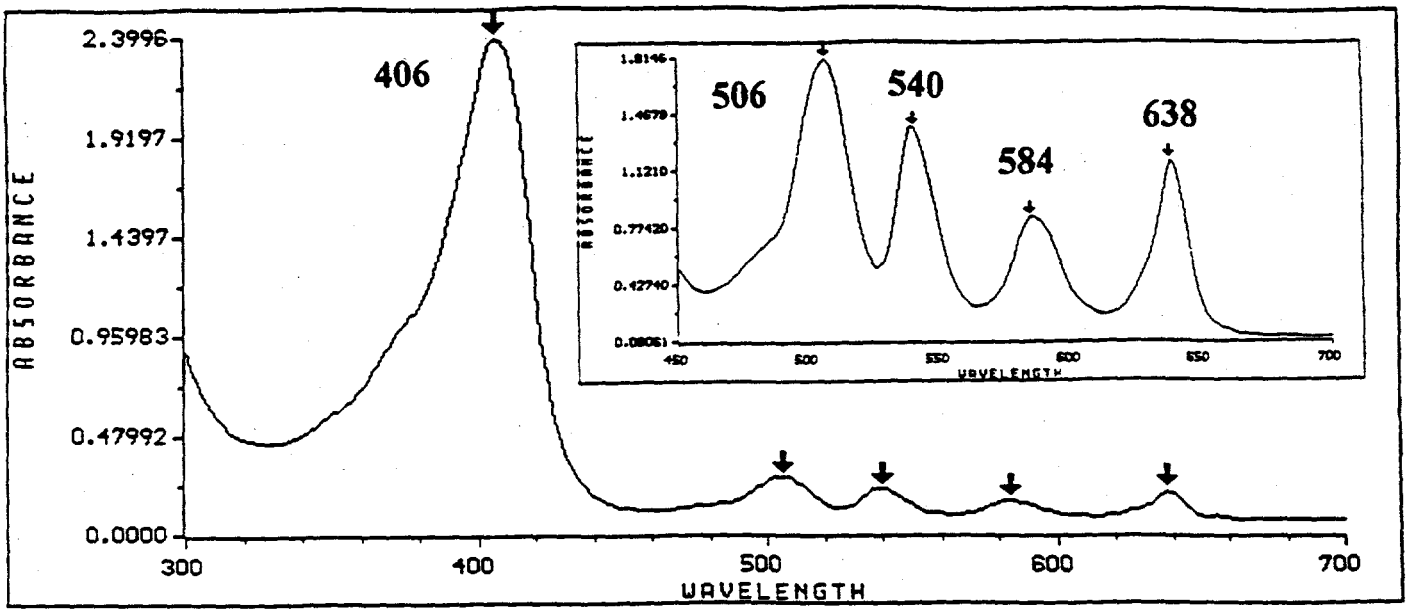

Figure 4: Absorption Spectrum of $F_{24}PH_2$ [5c]

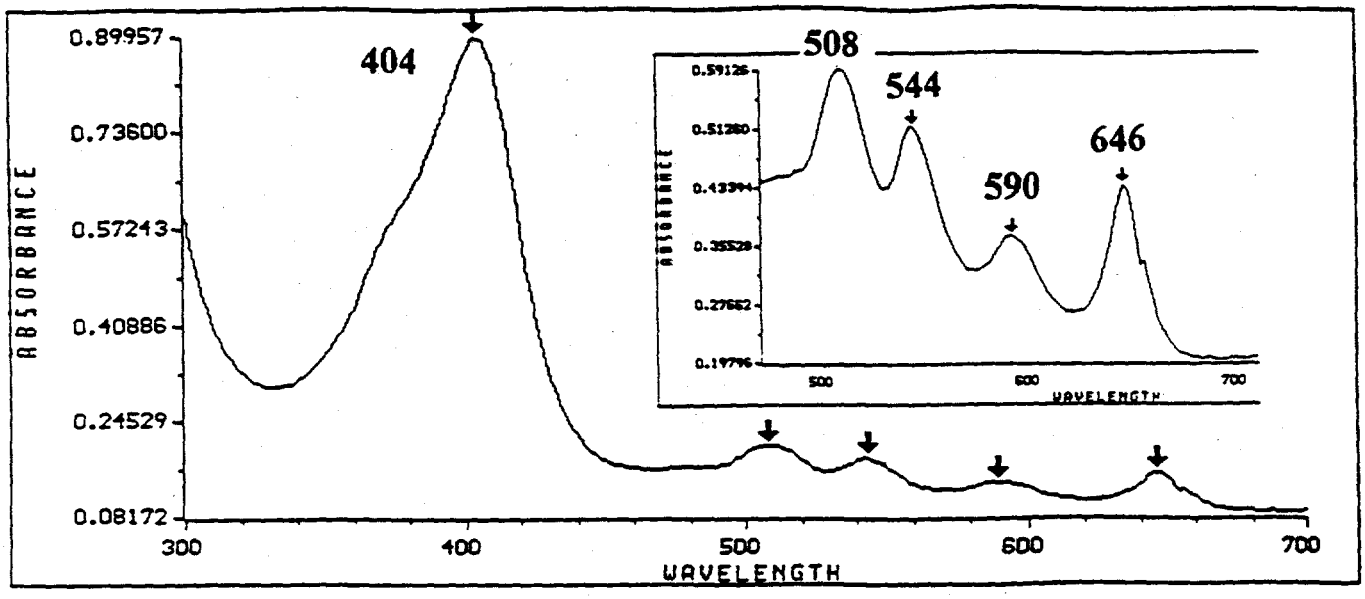

Figure 5: Absorption Spectrum of $F_{28}PH_2$ [5d]

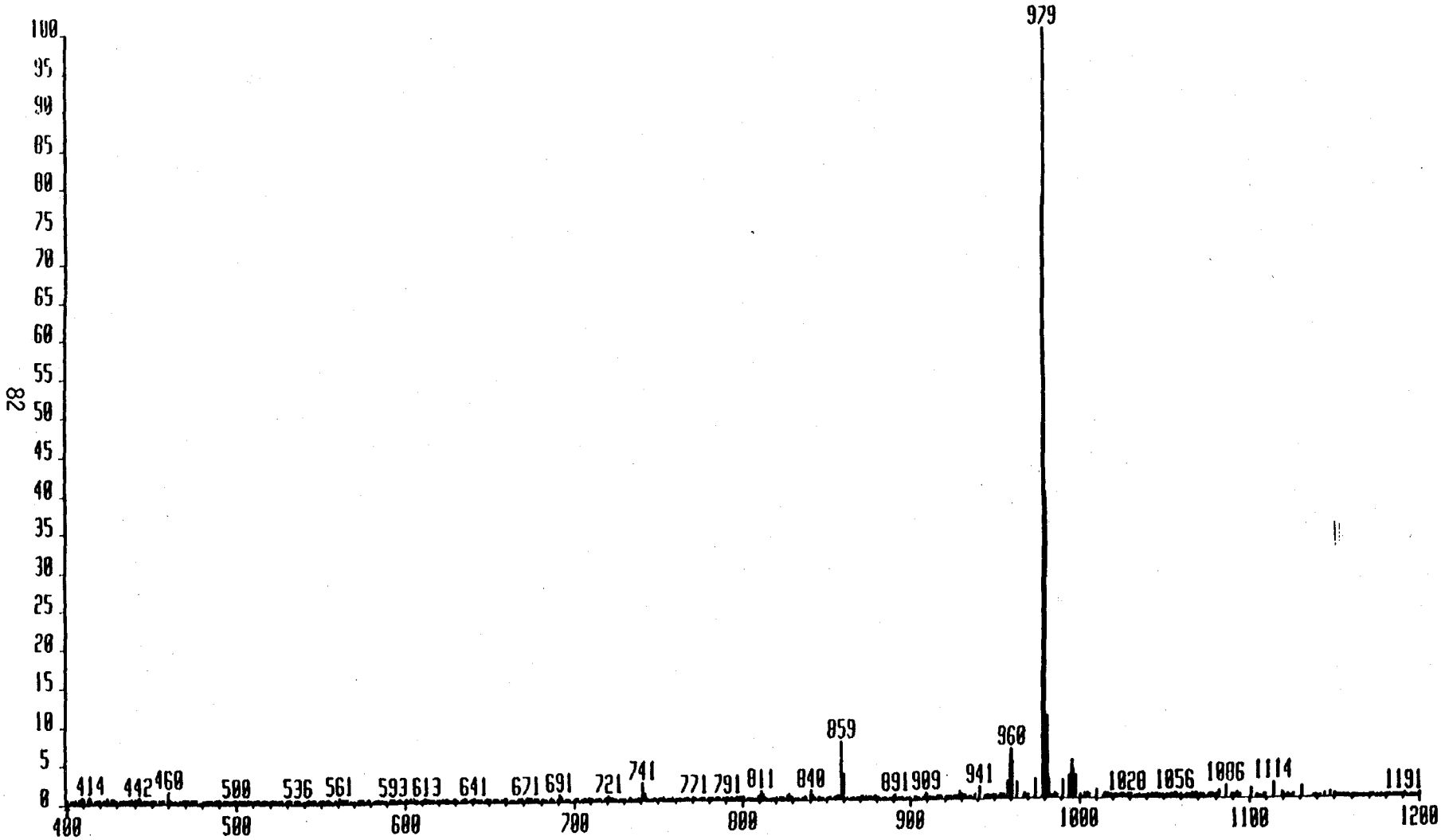

Figure 6: **FAB Mass Spectrum of $F_{24}PH_2$ [5c]**

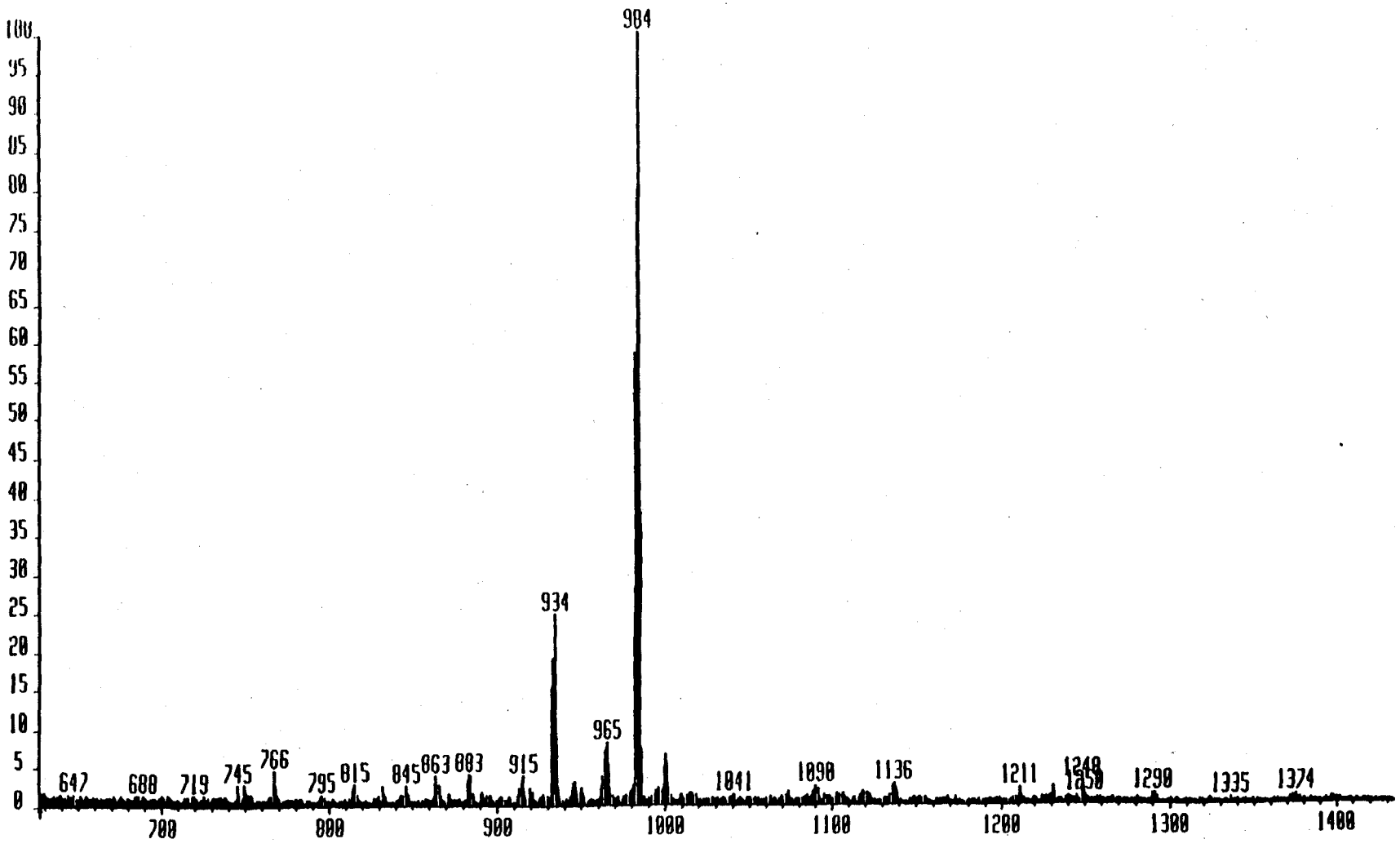

Figure 7: FAB Mass Spectrum of $F_{28}PII_2$ [5d]

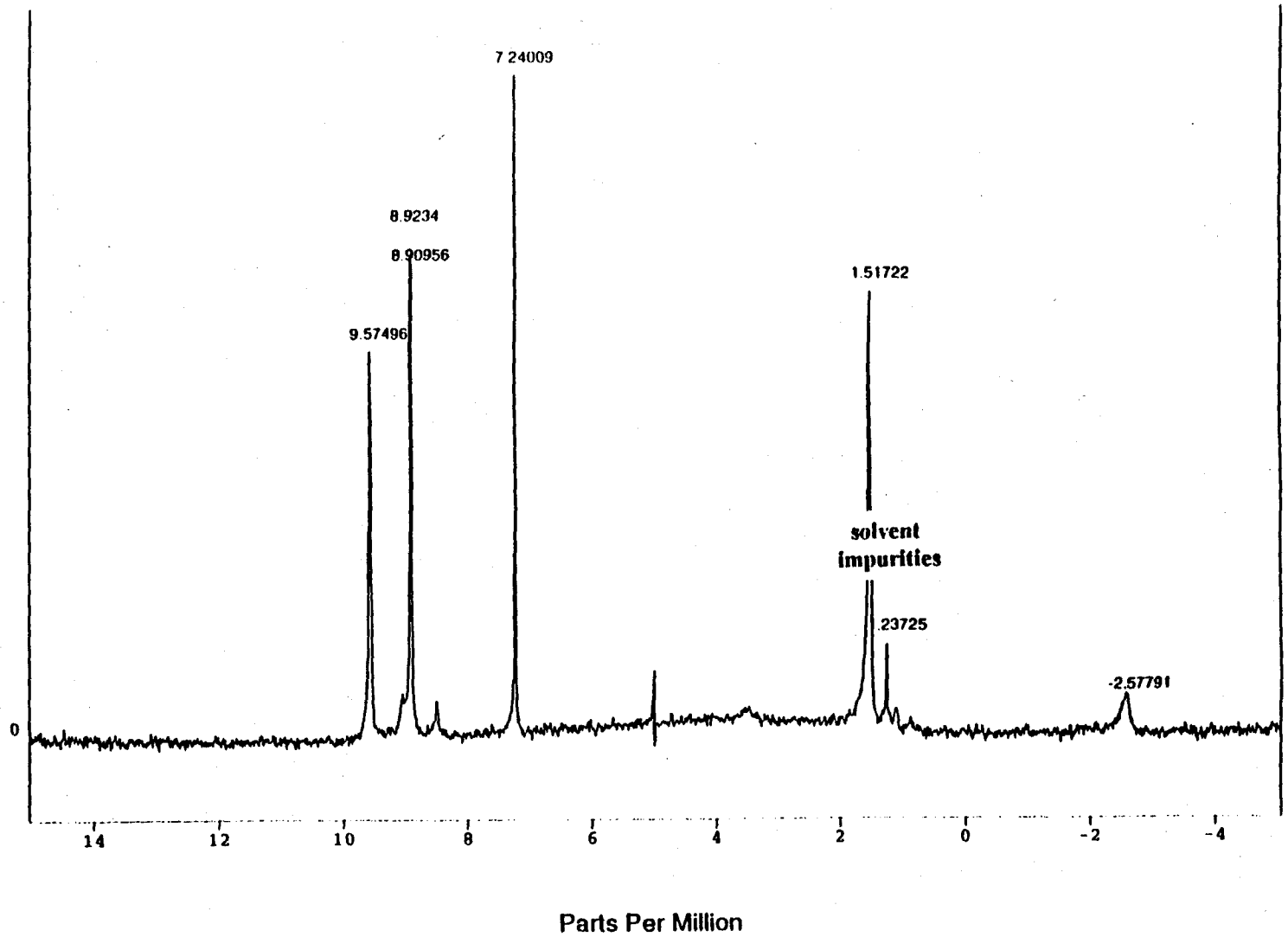

Figure 8: ^{1}H NMR Spectrum of $F_{24}PH_2$ [5c]

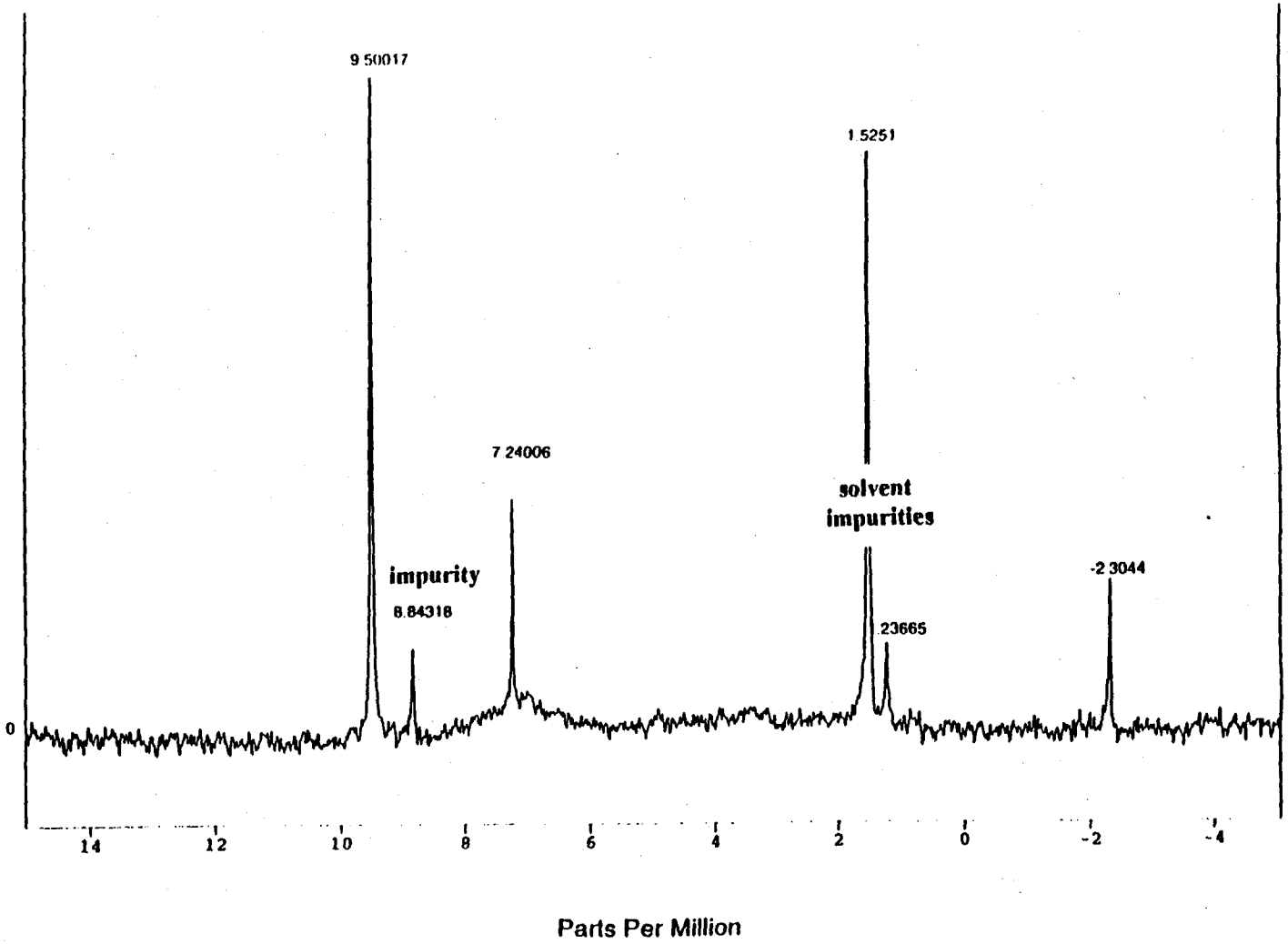

Figure 9: ^{1}H NMR Spectrum of $F_{28}PH_2$ [5d]

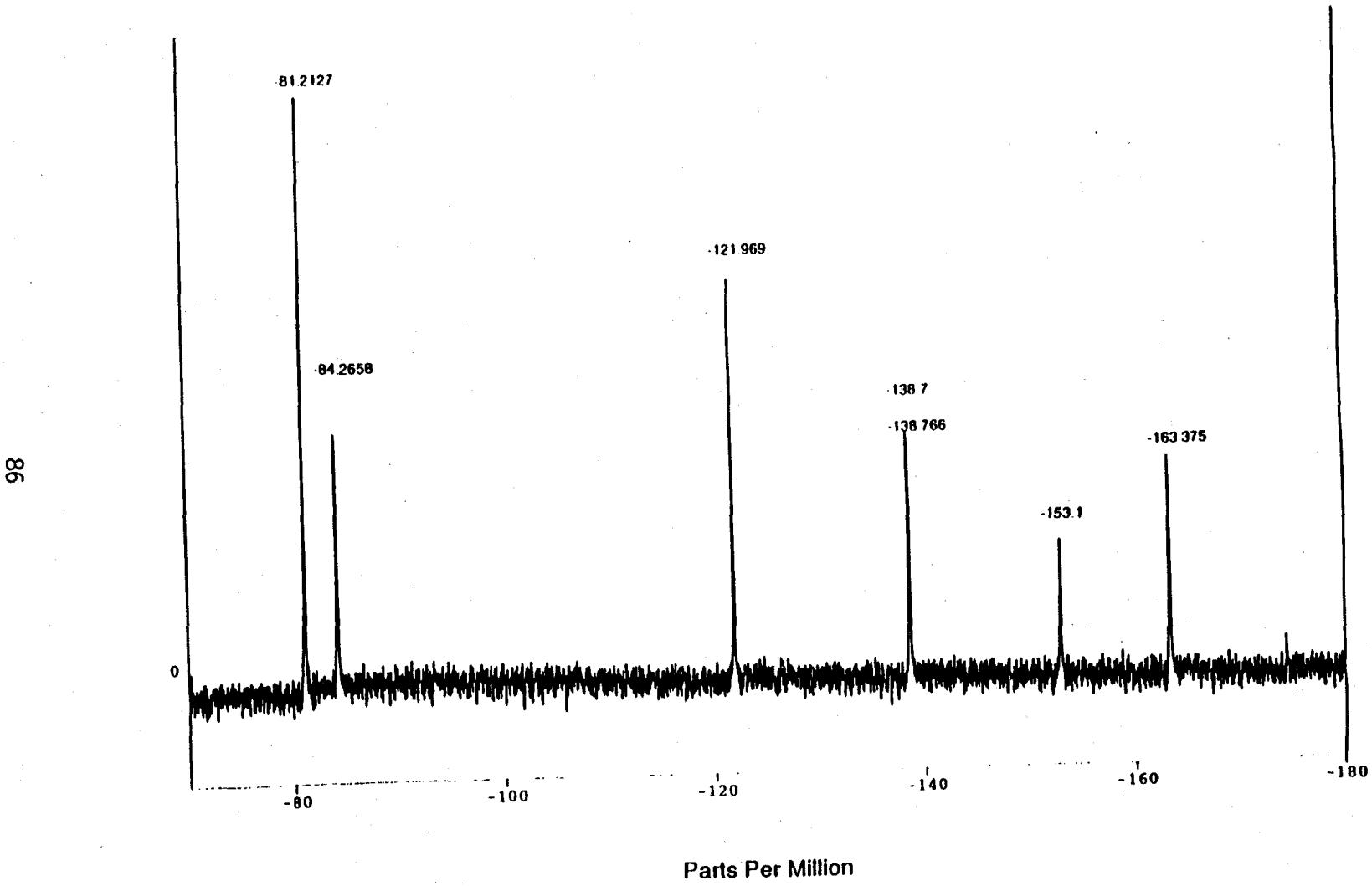

98

Figure 10: **^{19}F NMR Spectrum of $F_{24}PH_2$ [5c]**

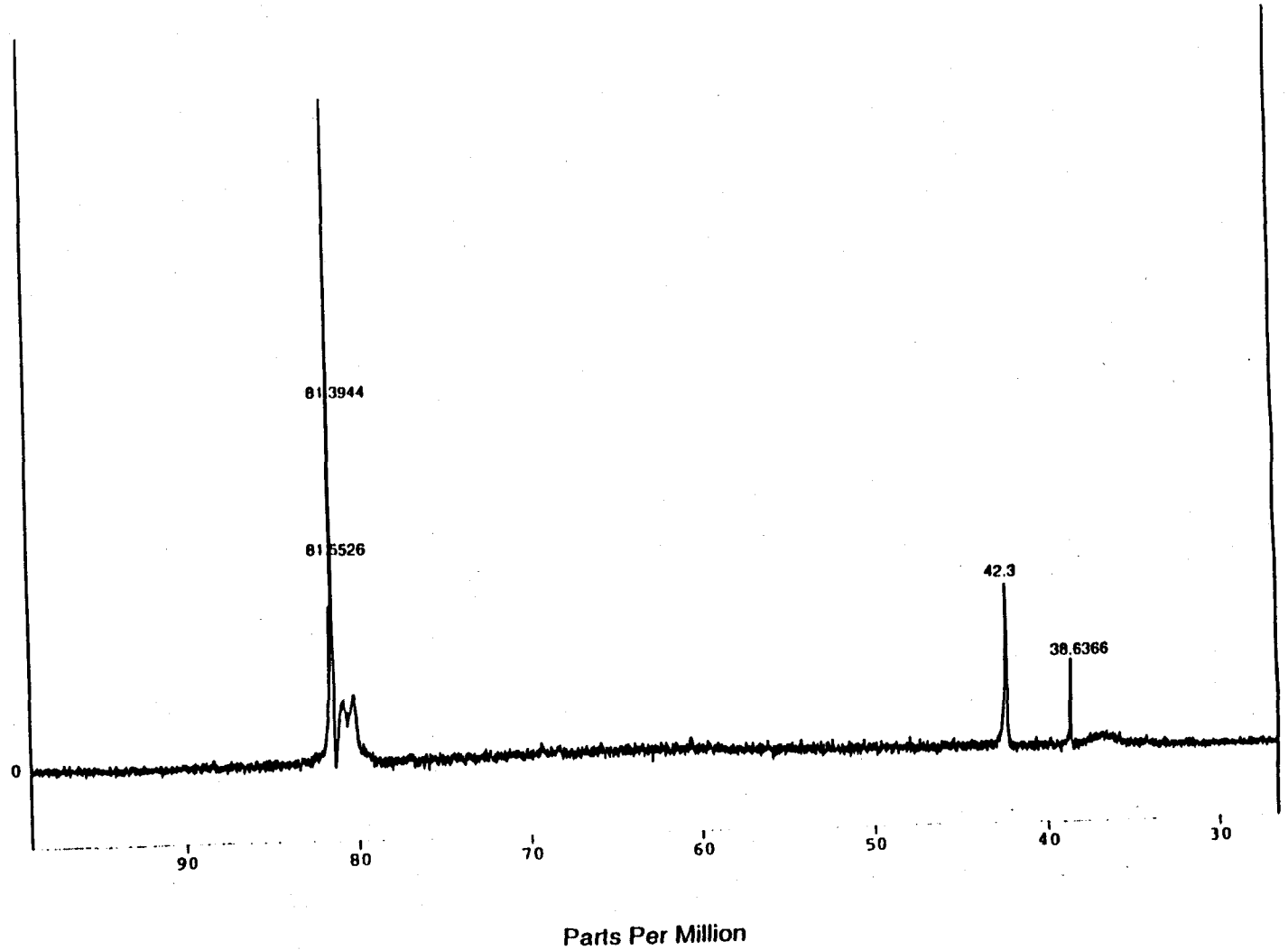

Figure 11: ^{19}F NMR Spectrum of $F_{28}PH_2$ [5d]

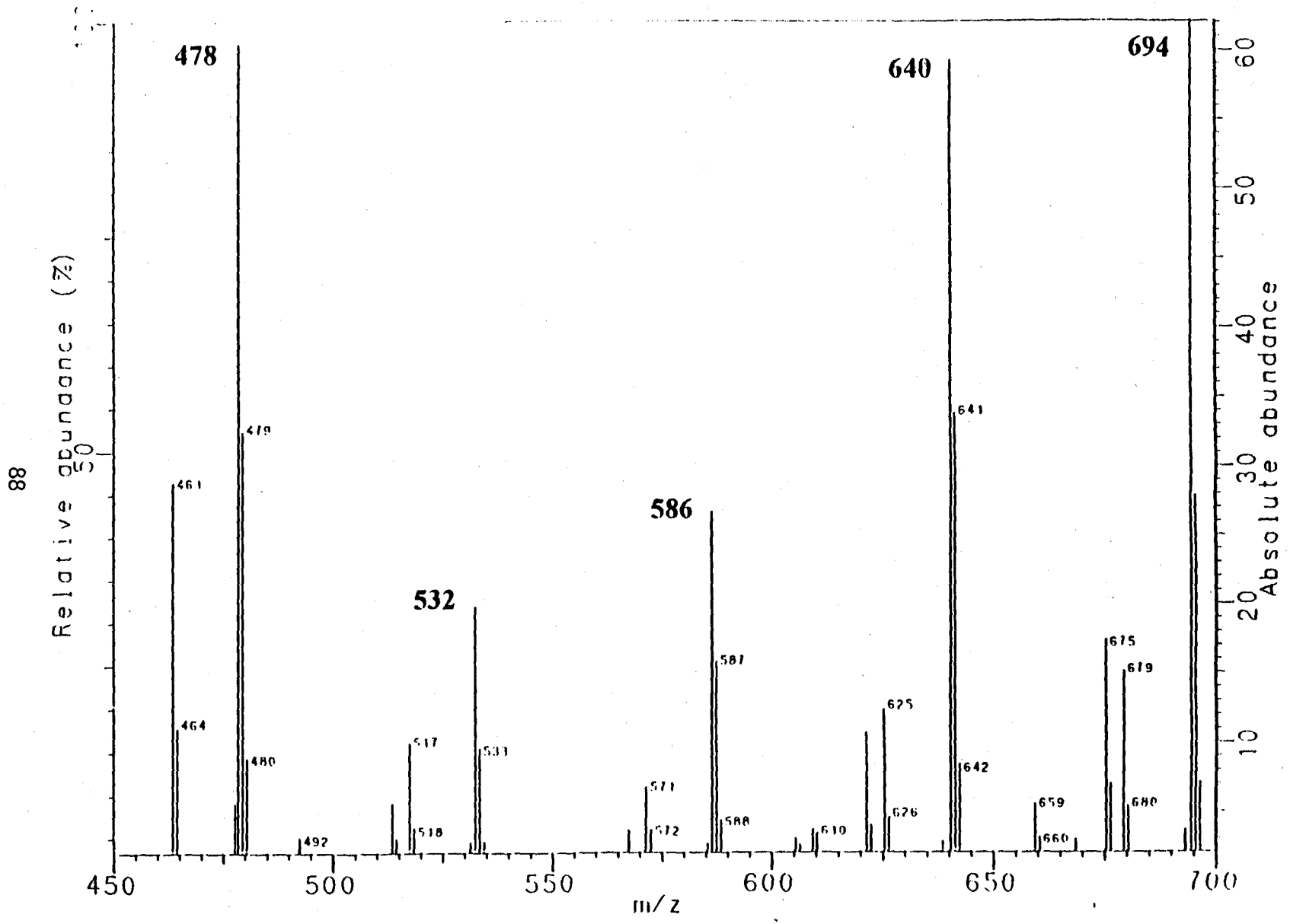

Figure 12: Laser Desorption Mass Spectrum of β-Trifluoromethylated Porphyrin Mixture

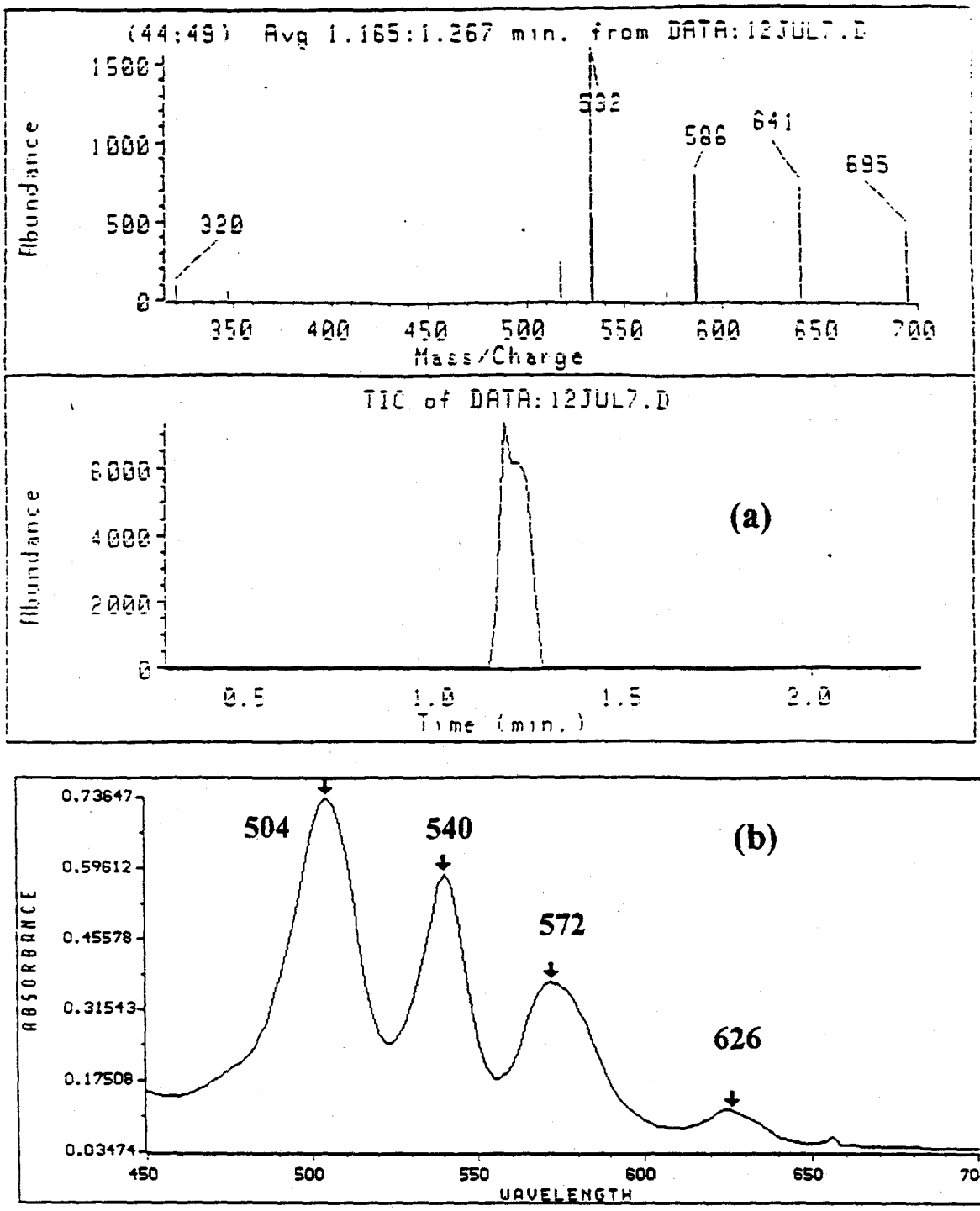

Figure 13: **(a). Electron Impact Mass Spectrum**

(b). Visible Range Absorption Spectrum

of the

Group I Porphyrin Mixture

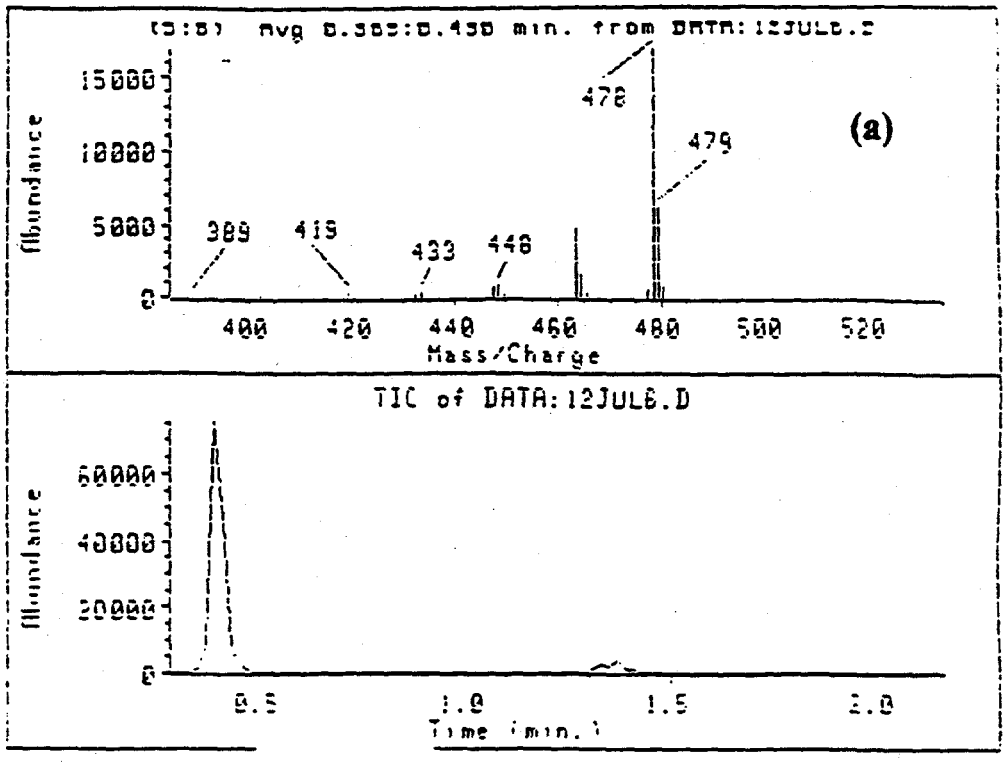

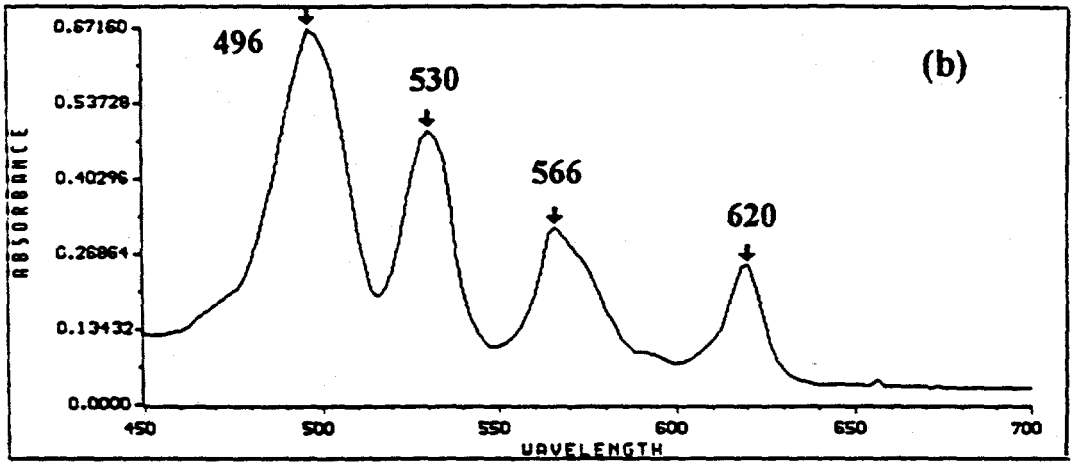

Figure 14: **(a). Electron Impact Mass Spectrum**

(b). Visible Range Absorption Spectrum

of the

Group II Porphyrin Mixture

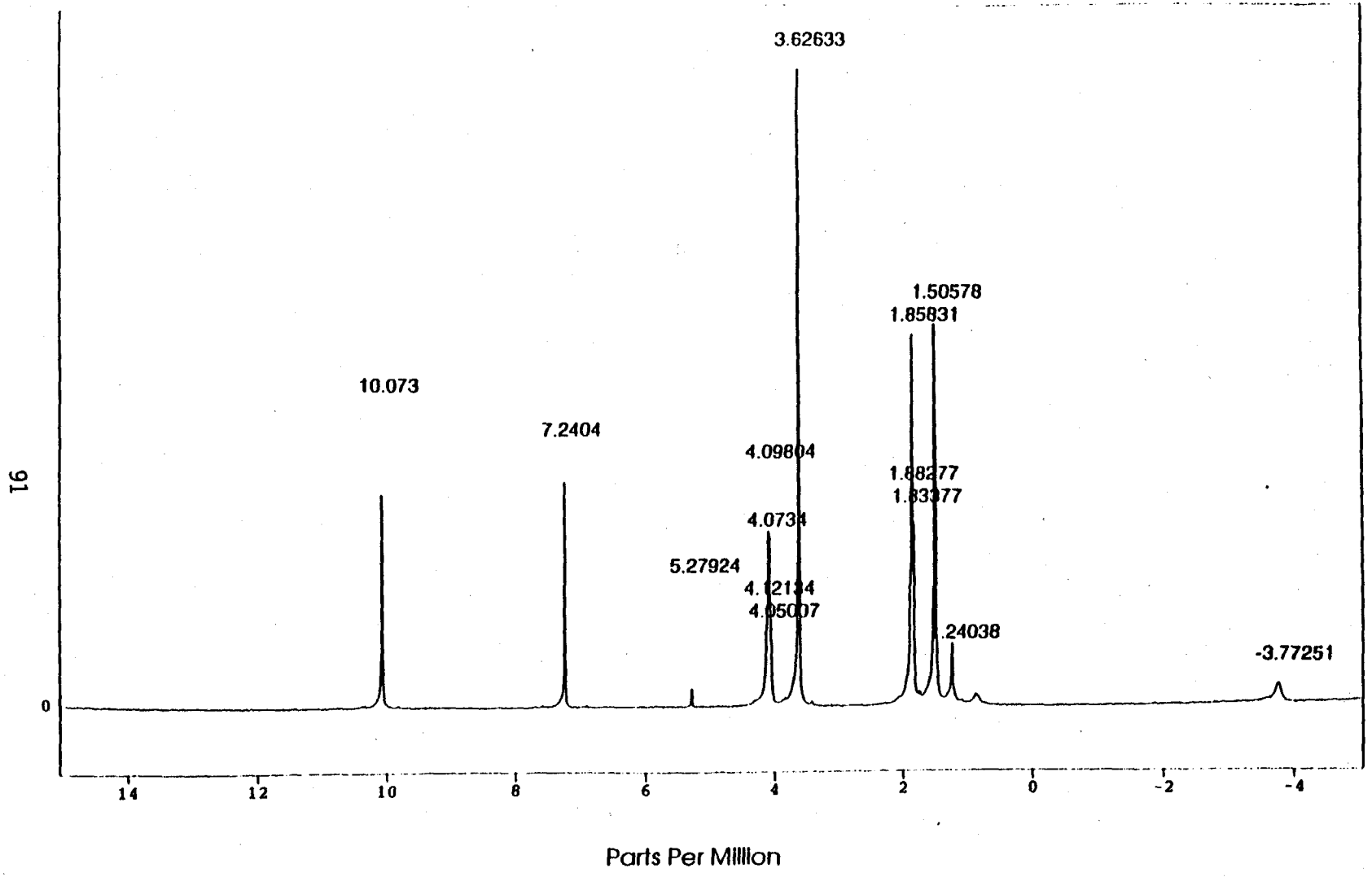

Figure 15:

^{1}H NMR Spectrum of the Group II Porphyrin Mixture

5.4 OXIDATIONS CATALYZED BY $F_{24}P$ AND $F_{28}P$ IRON COMPLEXES

Table 1 shows that isobutane can be oxidized at 60° C in the presence of meso-tetrakis (heptafluoro)porphyrinato iron hydroxide to give tert-butyl alcohol in high selectivity at good reaction rates. It is further seen that without halogenation of the porphyrin ring, entries 1,2, no oxidation activity is observed. Furthermore, one notes that the meso-heptafluoropropyl substituent entry 5, confers activity comparable to the meso-pentafluorophenyl substituent entry 3, after an initial induction period. This induction period is not evident when reactions are conducted in a metal reactor at 80° C, Figures 1-6. Inspection of Figures 2 and 6 indicate that the perhalopropylporphyrin complex is considerably more stable that the perhalophenyl complex as evidenced by the early departure of the latter curve from linearity.

6.0 HETEROGENEOUS CATALYSIS OF LIGHT ALKANE OXIDATION RESEARCH

V. A. Durante

6.1 SUMMARY

Supported metal complexes have been characterized and used in beginning studies to find structure-activity correlations between surface and compound characteristics and catalysis of the selective oxidation of alkanes. Conditions of interest were those of **heterogeneous** catalysis but at lower temperatures than those previously studied. Monometallic and dimetallic iron complexes were studied at low concentration on surfaces of varying hydrophobicity and surface texture. Single turnover experiments and pulse chemisorption of O_2 and CO as well as continuous oxidations of methane were conducted over several supported complexes at high pressure. New methodology for reactivity ranking was developed.

6.2 INTRODUCTION

We continue to synthesize, characterize, and examine surface supported metal complexes as potential catalysts for the vapor phase selective oxidation of methane, ethane, propane, and isobutane at relatively low temperatures compared to previous work. At the temperatures of interest, 100-380°C, the homogeneous vapor phase radical chain propagation rate is quite low and does not dominate the observed activity. Our aim is to determine structure-activity correlations for activation of dioxygen and catalysis of the selective oxidation of alkanes, particularly methane, by oxygenated mononuclear and binuclear metal complexes anchored to surfaces. We expect that modification of the surface characteristics will dramatically affect the overall selectivity to desired products such as alcohols and the ability and thermodynamic stability of the active sites and bound intermediates derived from oxygen and organic substrates.

TABLE 1

OXIDATION OF ISOBUTANE USING meso-PERFLUOROPROPYL PORPHYRINATO IRON CATALYSTS[a]

Complex	T,°C	t, hrs	TO[b]	TBA Sel, %[c]
Fe(O EP) Cl	60	6	0	--
Fe(TPP)Cl	60	6	0	--
$Fe[C_6F_5)_4P]Cl$	60	6	1100	90
$[Fe(C_6F_5)_2(C_3F_7)_2P]_2O$	60	6[d]	90	NA
		12	710	90
$Fe[(C_3F_7)_4P]OH$	60	6[e]	110	NA
		12	1110	81

a The catalyst, 0.013 mmoles, was dissolved in 25 ml benzene to which 7.0g i-C_4H_9 was added. Oxygen (to 100 psig) was added at reaction temperature and mixture sitrred for designated time. Product analysis by glpc.

b Moles O_2 taken up / mole catalyst after reaction time.

c (moles TBA formed / moles i-C_4H_9 reacted) X 100.

d Reaction had a 5 hour induction period.

e Reaction had a 3 hour induction period.

TABLE 2

DECOMPOSITION OF tert-BUTYL HYDROPEROXIDE CATALYZED BY meso-PERFLUOROPHENYL PORPHYRINATO IRON COMPLEXES[a]

Complex	T,°C	O_2 Evolution[b] in time t ,hr				RO_2H Conv.[c]
		1	2	4	24	%
$Fe[(C_6F_5)_4P]Cl$	80	1300	NA	NA	1375	92.5%
$[Fe(C_6F_5)_2C_3F_7)_2P]_2O$	80	1000	NA	1300	1390	94%
$Fe[(C_3F_7)_4P]OH$	80	1130	1260	1325	1400	>95%

[a] The catalyst, 0.60mg, was added directly to a stirred solution of tert-butyl hydroperoxide, 13.8g (dried thoroughly over activated 3A mole sieves prior to use) in tert-butyl alcohol, 18.1g, at 80°C. Oxygen evolution was measured manometrically. Liquid products were analyzed by glpc before and after the funs.

FIGURE 1

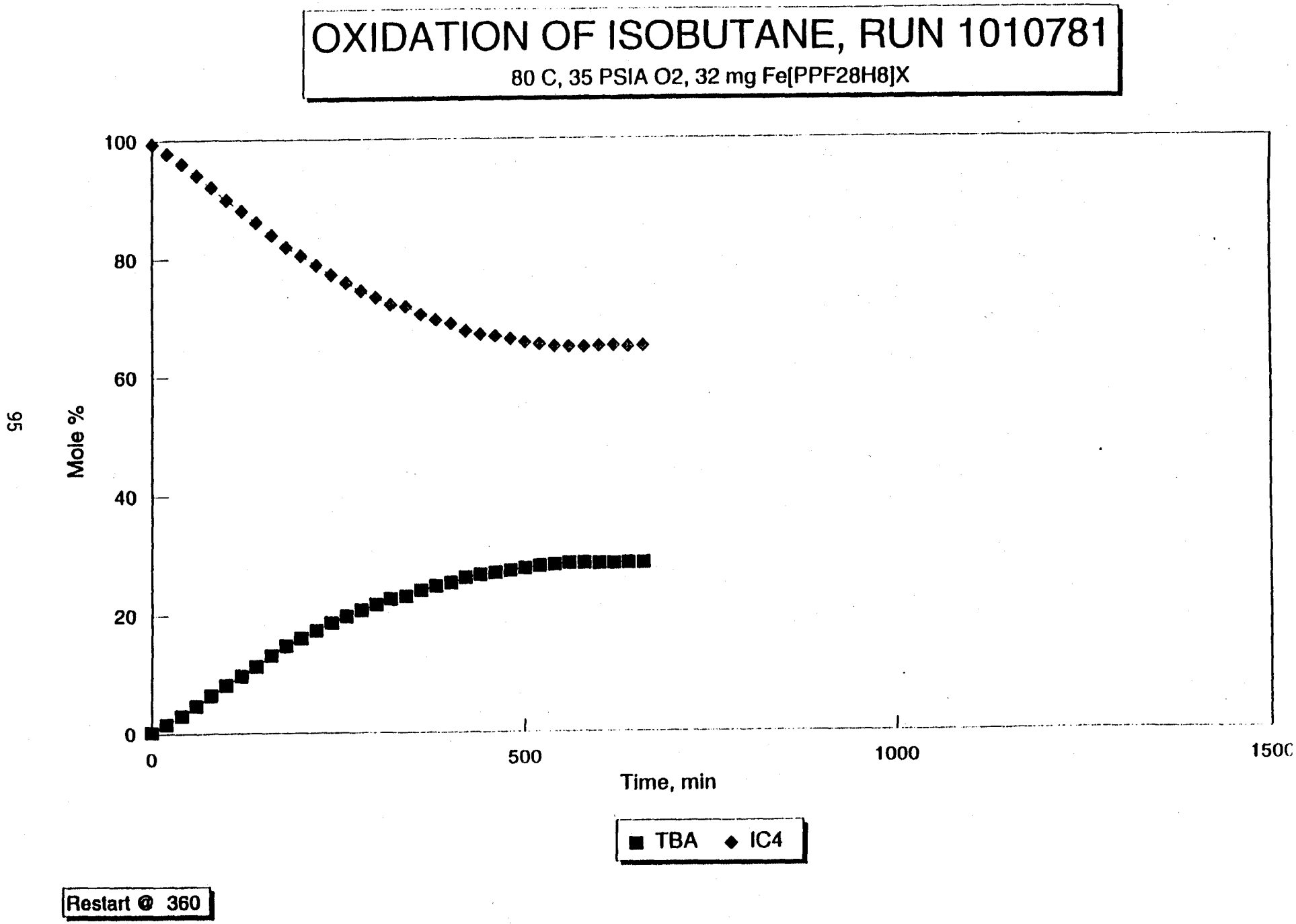
OXIDATION OF ISOBUTANE, RUN 1010781
80 C, 35 PSIA O2, 32 mg Fe[PPF28H8]X
100
80
60
40
20
0
Mole %
0
500
1000
1500
Time, min
TBA
IC4
Restart @ 360

FIGURE 2

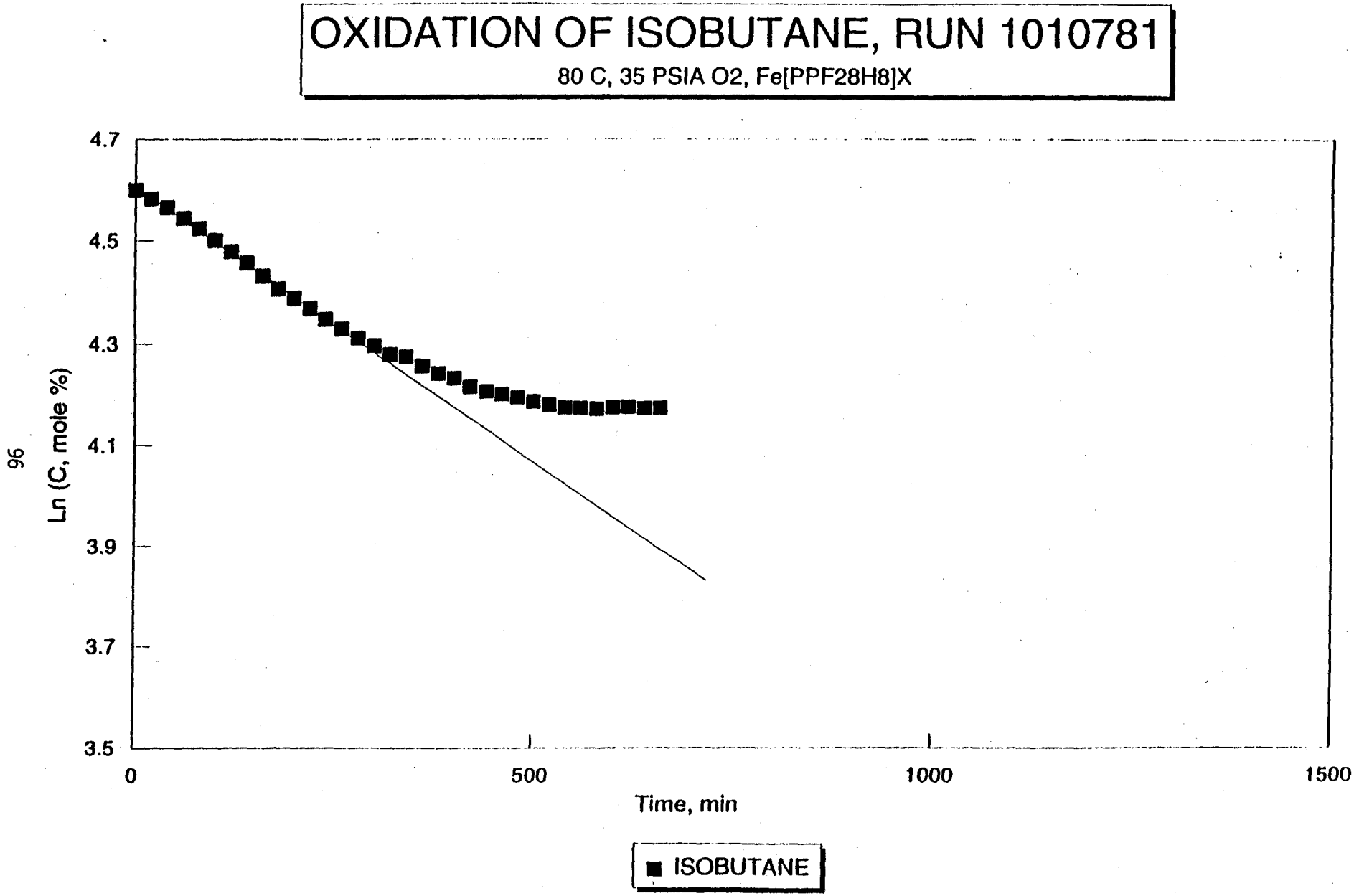
OXIDATION OF ISOBUTANE, RUN 1010781
80 C, 35 PSIA O2, Fe[PPF28H8]X
4.7
4.5
4.3
4.1
3.9
3.7
3.5
Ln (C, mole %)
96
0
500
1000
1500
Time, min
ISOBUTANE
Initial 1st order k=
-6.45E-02

FIGURE 3

OXIDATION OF ISOBUTANE, RUN 1010782

80 C, 35 PSIA O2, 32 mg Fe[PPF24H8]X

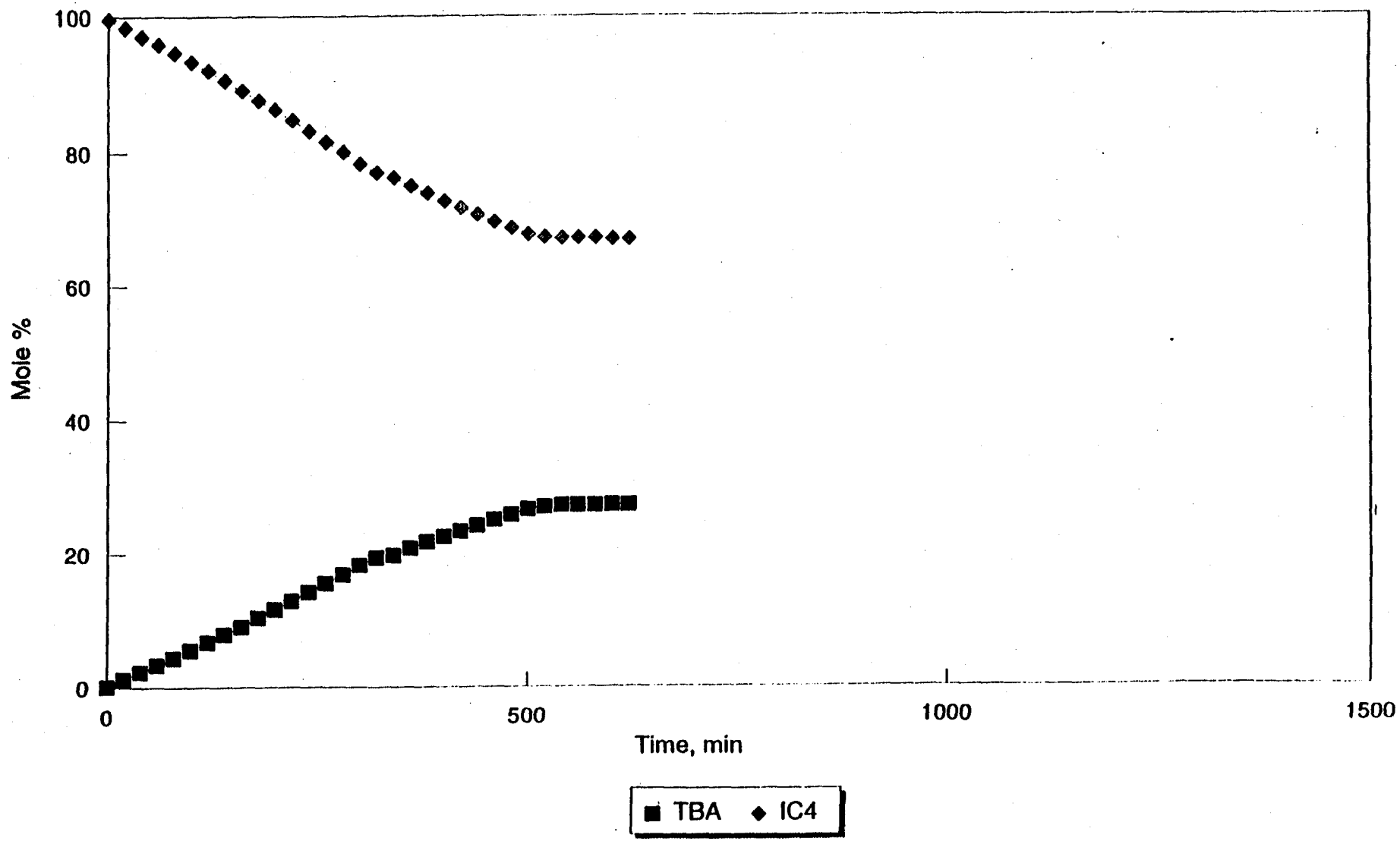

Restart @ 340

FIGURE 4

OXIDATION OF ISOBUTANE, RUN 1010782

80 C, 35 PSIA O2, 32 mg Fe[PPF24H8]X

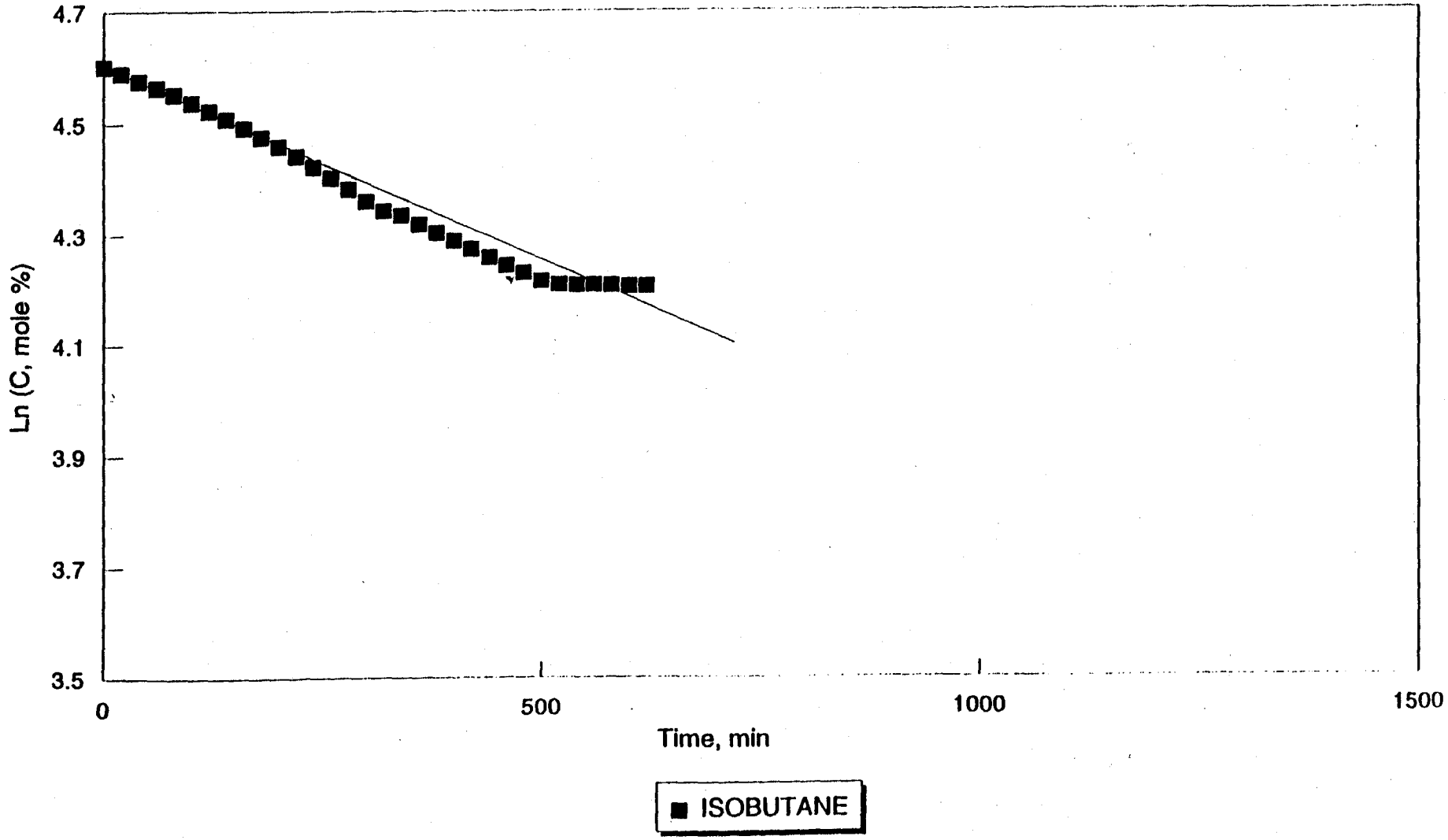

Initial 1st order k=
-4.19E-02

FIGURE 5

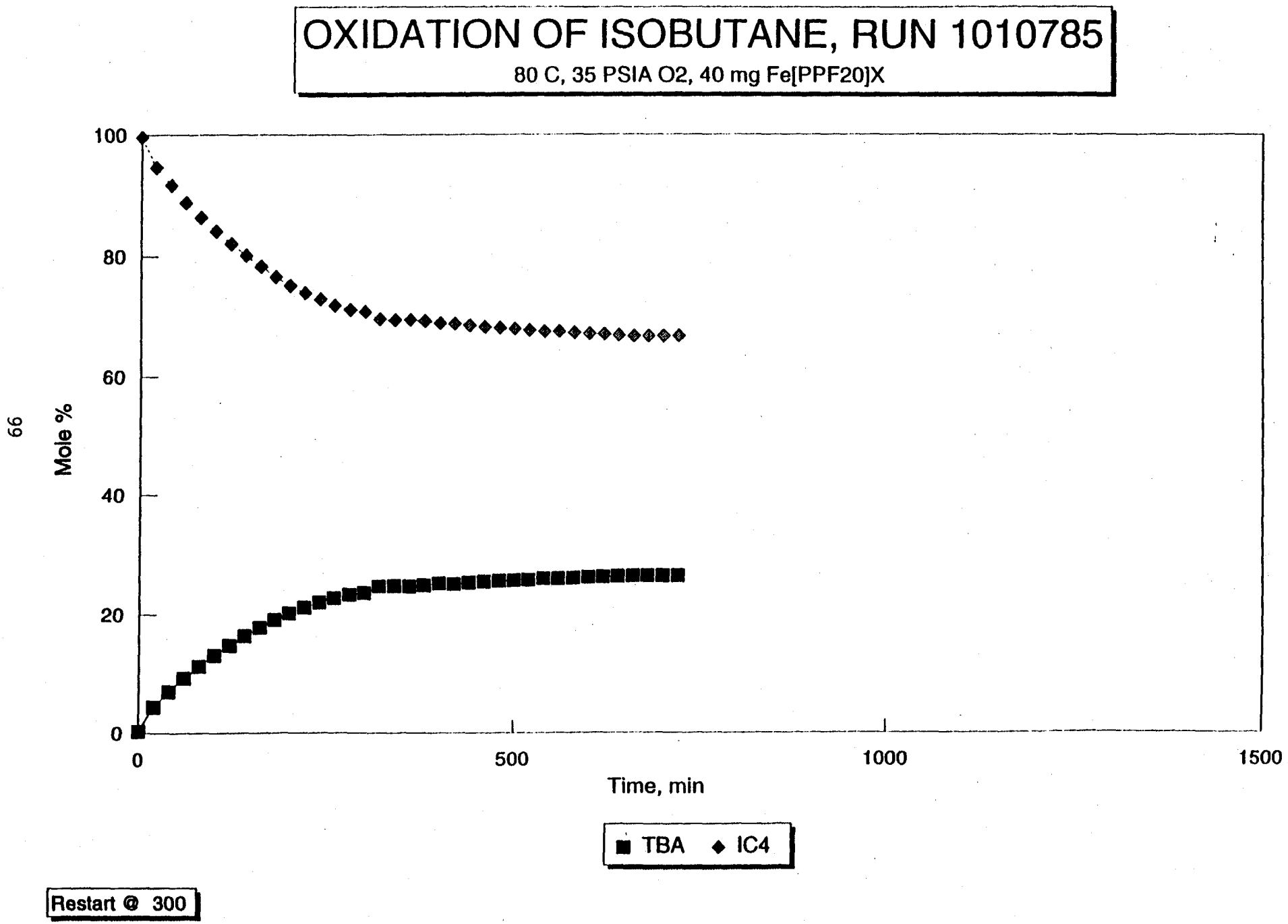
OXIDATION OF ISOBUTANE, RUN 1010785
80 C, 35 PSIA O2, 40 mg Fe[PPF20]X
100
80
60
40
20
0
Mole %
0
500
1000
1500
Time, min
TBA
IC4
Restart @ 300

FIGURE 6

OXIDATION OF ISOBUTANE, RUN 1010785

80 C, 35 PSIA O2, 40 mg Fe[PPF20]X

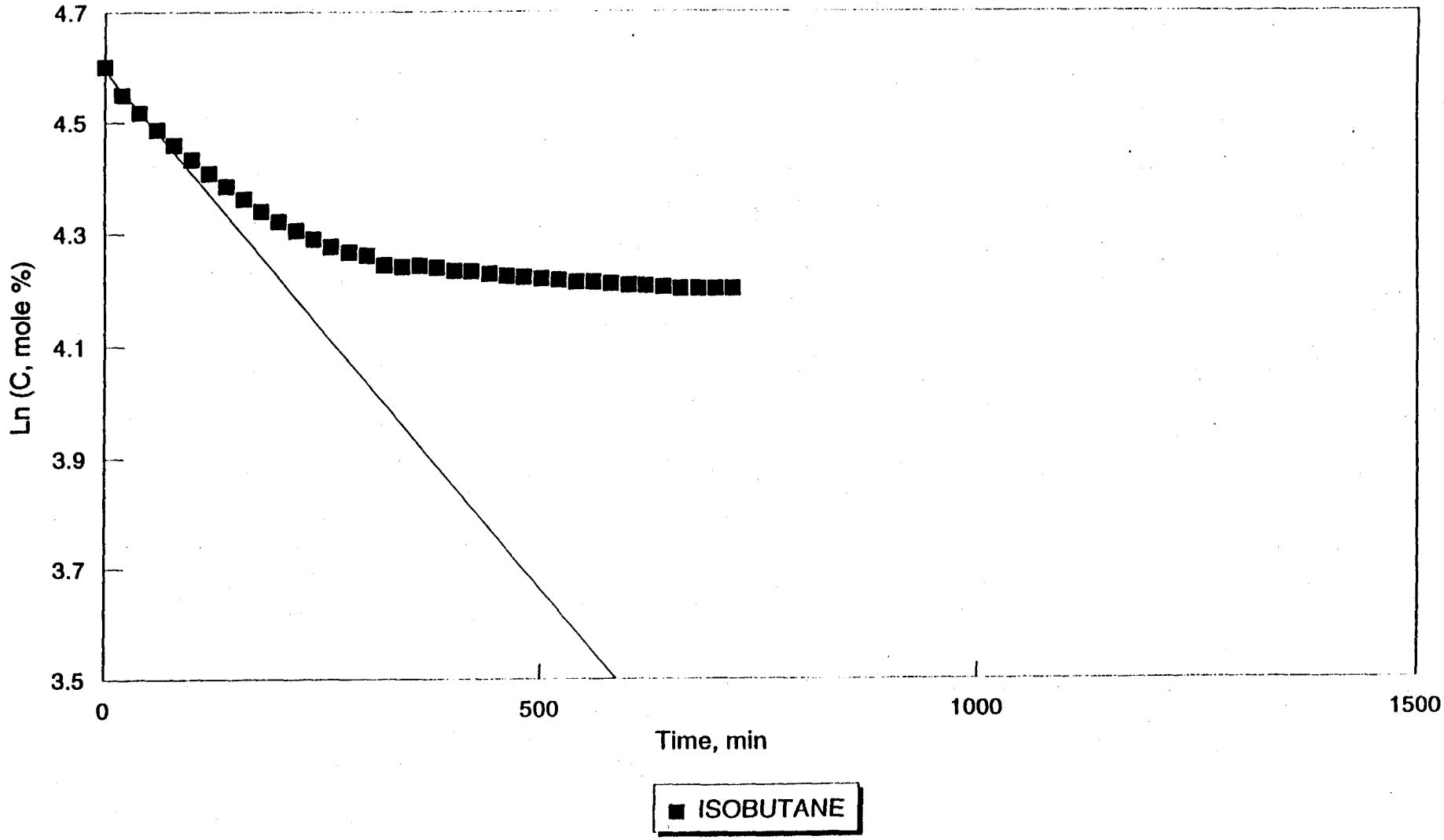

Initial 1st order k=
-1.12E-01

6.3 APPROACH

At this time, it is instructive to review the key features of our general approach: We draw on our underlying experience in the design of homogeneous catalysts for use in fluid solution, but the problems of synthesis and characterization of surface analogs is much more demanding than those encountered in fluid solution because systematic synthetic techniques are less developed in the solid state, techniques for phase purification are generally not readily available for solids so that low yield syntheses are not practical, and neither temporally resolved nor time-averaged techniques for the monitoring of many of the minority molecular surface species of interest are available in-house (and hard to find anywhere). Despite these difficulties, our focus is the comparison of characteristics of metal complexes--particularly those of iron in polydentate ligand frameworks into which electron withdrawing groups have been incorporated--when introduced into layered clays, molecular sieves, and other supports. The choice of support and its surface functionalization enables us to systematically vary eight parameters that we have identified previously or have reasoned to influence catalyst performance on a molecular level based on postulated catalytic cycles. These are:

- Fe-Fe atomic spacing [affects ability to bind oxygen]
- Density of accessible diiron sites on a surface [loading, dispersion]
- Geometric orientation of ligand plane of macrocyclic ligands with respect to the surface [parallel stacked vs. perpendicular edge-bound]
- Affinity of surface for alkane (methane) vs. alcohol (methanol)[hydrophobicity]
- Degree of mass transfer limitation [steric constraint] to a radical intermediate migration away from surface by variation of cavity portal or gallery size or surface-bound pendant groups in the vicinity of the active site [affects contribution of Eley-Rideal or "Rebound" reaction to the formation of alcohols versus the contribution of a homogeneous vapor phase process stemming from consequential reactions of a desorbed radical intermediate with molecular oxygen in the vapor phase away from the surface]
- Nature of the ligand system in the first coordination sphere of iron [affects electrochemical reduction potential and oxidative stability of complex]
- Surface acidity/basicity and nucleophilicity/electrophilicity [affects secondary decomposition processes of alcohols]
- Surface functionalization and nature of and rigidity of the bond of the iron sites or of the first coordination sphere ligands directly to the surface [affects ability to undergo surface migration and ability to maintain an "open" coordination site, i.e. coordinative unsaturation, in the presence of potentially bridging ligands other than dioxygen which are already in the vicinity of iron and formation of oxo-bridged diiron complexes on the surface].

If surface-bound complexes could be prepared and characterized, a number of the parameters listed above could be systematically varied using anionic complexes intercalated within the galleries of framework-modified, non-acidic anionic layered clays of the general class, hydrotalcites.

Precedented on published preparation methodology and characterization, we have argued that iron porphyrin, phthalocyanine, and other ligand complexes in which anionic functionalities such as sulfonato-groups are appended to the macrocycle can be ion exchanged into the interleaf galleries and anchored with the ligand plane perpendicular to the brucite layers. By variation of the ion exchange capacity of the brucite layers, one could, in principle, vary the proximity of mononuclear iron sites within the galleries. At some point of high exchange site density, iron-iron spacing could be brought within dioxygen binding distance but outside of the minimum distance conducive to formation of μ-oxo bridged Fe(III). That is, coordinative unsaturation could be maintained until a dioxygen bridge could be formed. In support of this concept is the published observation that pentacyano iron (III) would dimerize in fluid solution, but may remain as a monomeric species when generated at a hydrotalcite exchange site.

Although intercalated complexes with catalytic activity for the Merox oxidation are known, no one has studied the effect of iron-iron site proximity on oxidation catalysis as could be achieved by variation of the ion exchange capacity of the support. Such a study is intended as part of the present program. But our ultimate catalyst would probably require an ion exchange site density beyond the limits of known materials. Consequently, one of the objectives of the present research is to find ways to increase ion exchange capacity of layered clays. This poses a formidable synthetic challenge and may be one of the limiting rates to progress in the overall heterogeneous catalysis research program.

A related set of materials required for the systematic variation of iron-iron site density in the hopes of finding a structure activity correlation are supported **binuclear** metal complexes. That is, complexes in which the local geometry about the diiron site required for oxygen activation is presynthesized prior to emplacement of the formed "site" onto a surface. To this end, the synthesis of bimetallic complexes containing electron withdrawing non-porphyrin macrocyclic ligands and featuring labile ligands, displaceable by dioxygen, in other positions is also a critical part of our research.

Supported μ-oxo diiron complexes on surfaces, some of which have shown activity in fluid solution, are also of interest and are being prepared and tested in the present program. One interesting approach is to compare oxo bridged species as isolated sites formed in-situ within a cloverite zeolitic cavity to similar μ-oxo dimers formed on non-constraining supports such as silica gels. An expected limitation of this approach is the preparation of solids with high enough site density to both characterize and to produce sufficient initial oxidation activity to encourage further investigation.

Even prior to the introduction of metal complexes, the nature of support surfaces needs to be understood and methods for modification of properties developed. Preparation and characterization of such materials is also a part of our program, and work to this end is described here in.

Although we have in place many of the techniques for characterization and testing of catalyst candidates of the types described above, other techniques must be developed as part of this program. For example, a technique analogous to cyclic voltammetry to rank thermodynamic reducibility of supported metal complexes would be extremely useful in the development of structure-activity correlations. We are exploring the use of Temperature Programmed Reduction (TPR) and Oxidation (TPO) to this end. Pulse chemisorption techniques are also under development to characterize dispersions and oxygen absorption abilities of supported complexes. And in order to study catalytic cycles a step at a time in single-turnover experiments, double pulse techniques at high pressure are under development. Some of these are described below.

6.4. RESULTS AND DISCUSSION

6.4.1. **Pulse Chemisorption/TPD of Oxygen and CO**

A high pressure pulse chemisorption technique was developed using the CDS reactor system to monitor CO and O_2 uptake by supported metal complexes. This technique differs from typical chemisorption measurements normally conducted in the Omicron equipment in that it enables the use of high pressure to help shift absorption equilibria to more favorable positions than might normally be encountered under vacuum conditions used in the Omicron equipment. The actual run conditions are closer to those under which catalytic reactions proceed and, perhaps, the results are more representative of the state of affairs of the working catalysts. The high pressure technique uses flowing helium as the means to clean and desorb chemisorbed species rather than high vacuum. The technique relies on mass spectral monitoring to identify desorbed species and to differentiate relative absorbed amounts in competitive adsorption experiments. Unfortunately, the limit of detection of absorption for this technique is not as great as that of volumetric chemisorption in the Omicron instrument. Sensitivity is limited by the reproducibility of dosage volumes delivered in each successive pulse even though analytical sensitivity of the mass spectral detector is as low as picograms of material.

Under typical conditions successive pulses of the adsorbate are delivered by a computer controlled precision sampling valve and allowed to expand or compress into a flowing helium stream then passed over a pretreated solid catalyst in a quartz-lined reactor at high pressure. Typically, adsorption experiments are conducted at constant temperature, usually 10°C. Figure 1 shows a train of 6 successive pulses of CO when there is no adsorption as detected by a mass spectrometer coupled through an open-split interface via a heated silica capillary transfer line. The experiment was conducted at 815 +/- 4 psig; each pulse dose can be adjusted by adjustment of the temperature and pressure of the delivery loop; in this case, dosage was 205 micromoles of CO per pulse.

Adsorption is indicated by diminished peak areas during the titration until saturation is reached at which point peak areas return to full size. Total adsorption is the sum of adsorption found in individual pulses. The system is self-calibrating for any gas so long as saturation is eventually reached. After the adsorption, temperature is ramped upwards linearly to monitor the desorption of the adsorbate and the reversibility of the uptake.

In a self-consistent set of experiments, an iron perfluorophthalocyanine chloride complex was supported on Cabosil and subjected to pulse absorption of CO as a function of temperature. Although this complex shows little alkane oxidation activity in fluid solution at relatively low temperatures below 100°C, it was of interest to characterize this complex on supports because it is readily available, similar in structure to the non fluorinated iron phthalocyanine complex which has previously been studied by others, and because we hoped to observe some modest activity at the higher temperatures accessible **via** heterogeneous catalysis. The behavior of this complex could also be taken as a "control" for experiments with more active complexes.

Results of this study are plotted in Figure 2. Although the nature of the reaction between CO and this complex is unknown, it is possible that chloride is labilized and iron is reduced in the presence of CO. As temperature approached 150° or so, adsorption of CO dropped to near zero compared to a CO/Fe of 0.25 for this particular preparation at 9°C. Oxygen adsorption might be expected to correlate to CO absorption directionally at least. Thus, alkane oxidation catalyzed by such a complex is unlikely at the temperatures at which an oxygenated complex might show activation of dioxygen because adsorption equilibria for dioxygen are not favorable at those temperatures. Indeed, single turnover pulse experiments using ethane to attempt to reduce this supported complex after oxygen treatment at temperatures up to 350°C or the use of air to oxidize a CO treated complex at 245°C failed to generate significant quantities of oxidation products (**vide infra**). (Continuous oxidation may be required to generate any measurable activity).

CO uptake measurements at constant temperature may also be used as a measure of relative dispersion of supported complexes in a series at constant loading but on different supports. Table 1 lists results of CO and oxygen chemisorption measurements of the fluorophthalocyanine complex on several supports of varying water adsorption capacity and surface area. We expect that the equilibrium water absorption as listed is roughly correlated to surface hydrophobicity; a better measure would be water absorption capacity per unit surface area, but not all the surface areas have been measured as of this writing. The water absorption values are listed in Table 1 along with the uptake measurements. Note that in the series no correction was made for chemisorption by the support. The measurements therefore, represent upper limits, but the validity of the measurements is evinced by comparison of complexes on F-silicalite versus silicalite since these materials are expected to have similar CO absorptions despite differences in hydrophobicity of the supports. With the exception of fluorinated carbon, there is a roughly an inverse correlation between high water adsorption and higher CO uptake. We tentatively interpret this as a representative of the dispersion of the complexes. The fluorinated carbon showed very high CO uptake which undoubtedly was due to the support phase itself since values exceeding one were found for CO/Fe. If our interpretation is correct, then highly hydrophobic supports such as F-silicalite will not be readily usable to generate well dispersed complexes. Cabosil seems to be a good compromise support since it demonstrates relatively low

water absorption, yet it enables good dispersion. Future work with dispersion will involve the use of XPS techniques.

Also listed in Table 1 are oxygen uptake measurements by a tetra-sulfonated phenyl porphyrin complex ion exchanged into a high capacity hydrotalcite clay. It is interesting to note that initially low oxygen absorption is observed with this material, but after treatment at 200°C under hydrogen, oxygen uptake is greatly increased. If Fe(III) is reduced to Fe(II), this would be the expected result. However, reduction of the ligand or over reduction of the iron may also be possible. (See also Altamira TPR results).

That oxygen uptake is largely due to the metal complex may be surmised from the observation that O_2 uptake is nearly doubled when the complex is twice exchanged to give a higher loading on the clay. The quantitative two-fold increase is probably fortuitous, but the directional trend is significant.

Returning to Table 1, oxygen uptake by the fluorided carbon supported fluorophthalocyanine iron chloride complex is atypical of that found on other supports. Figures 3 through 5 show that oxygen absorption increases with each successive pulse and that carbon dioxide and water are formed at temperatures as low as 9°C, undoubtedly due to combustion of the support phase. It is interesting to note that under continuous oxidation conditions at higher temperatures, this complex is consumed in the reactor. The fluorinated carbon support is unsuitable for use to prepare oxidation catalysts.

6.4.2 Isothermal Single Pulse Experiments

We have developed a unique methodology to conduct single-turnover experiments with supported metal complexes using a pulse reaction technique under conditions of pressure and temperature that closely simulate those necessary for heterogeneous catalysis. After pretreatment of the metal complex in a helium stream held at reaction temperature and pressure, a first reagent is passed over the solid catalyst in excess (the "flood" pulse). After a short period to "clean-off" non bound reagent, a second, smaller pulse of a second reactant (reaction pulse) is passed over the catalyst and desorbed products monitored continuously by mass spec or by on-line GC or GC/MS of time resolved "slices" of the effluent. The time delay between flood and reaction pulses is computer controlled in our system. A linear ramp of increasing temperature or a sudden release of total pressure optionally can be incorporated into the protocol after the reaction pulse to generate further desorbed species or to conduct resolved TPD experiments. For metal complexes, this type of experiment was used with oxygen or air flood followed by ethane or isobutane pulse to monitor oxidation of ethane by oxygenated complex, and was used with CO flood followed by O_2 reaction pulse to study oxidation of bound CO.

Several supported complexes were studied by this technique as listed in Table 2. The fluorophthalocyanine iron (III) chloride complex on silica showed a small amount of carbon dioxide effluent in several experiments conducted between 250-350° no other oxygenates were detected, even in subsequent TPD experiments. On a carbon support, traces of CO_2 were detected coindent with the oxygen flood pulse, but not with the ethane reaction pulse. Similarly, no ethanol was observed over the $Fe(TPP(SO_3)_4$ singly exchanged into a hydrotalcite clay. The latter material may have been too dilute to observe any chemistry.

Oxygenation followed by isobutane reaction pulse of the $Fe[TPPF_{20}]_2O$ complex on Cabosil at 100°C similarly failed to generate t-butyl alcohol or acetone at levels beyond those of feed impurities.

6.4.3 Preliminary TPR/TPO Experiments in Altamira Instrument

Since we noted increased oxygen absortion by the supported fluorophthalocyanine complex after reduction by hydrogen, we used the Altamira instrument to study the TPR/TPO behavior of a couple of supported complexes at low pressure. This work is currently in progress, but some preliminary observations are encouraging: The iron fluorophthalocyanine chloride complex on silicalite shows a hydrogen absorption peak between 150 and about 210°C only in the first reduction run but not in a second run used to determine a baseline. Oxygen take-up is then observed for the reduced complex followed by renewed hydrogen absorption. Because these measurements were not quantitative, they must be considered preliminary but seem to indicate some degree of reversibility in a redox cycle.

The $Fe(TPPF_{20})Cl$ complex on Cabosil also show some take up of hydrogen, but at 50-80°C, a lower temperature than the fluorophthalocyanine complex. This is expected if the TPR temperature correlates with the half-wave reduction potential for the complex. Although preliminary, these results encouraged us to examine this technique further.

TPR /TPO OF Fe(FPc)/CAB-O-SIL

The TPR technique was used to study silicalite-supported Fe(FPc), and oxygen uptake measurements were conducted on the CABOSIL-supported complex. Since the Cabosil support is much more highly hydroxylated than the silicalite support, the probability of forming a surface bound complex is greater on Cabosil. We have now examined the Cabosil supported complex in TPR.

A sample containing 6.64 x 10-4 moles Fe per gram (VF) of Fe(FPc)/Cabosil was dried under vacuum 6 days at 120°C then subjected to reduction with 10 % hydrogen in the Altamira instrument. The temperature programmed reduction curve is depicted in Figure 1. Two major features observed are the maximum at 116°C and the broad underlying absorption centered at about 190°. Integration and calculation of the H/Fe ratios associated with these peaks, however, suggests that only a minor amount of hydrogen is taken up.

TP Reduction/Oxidation

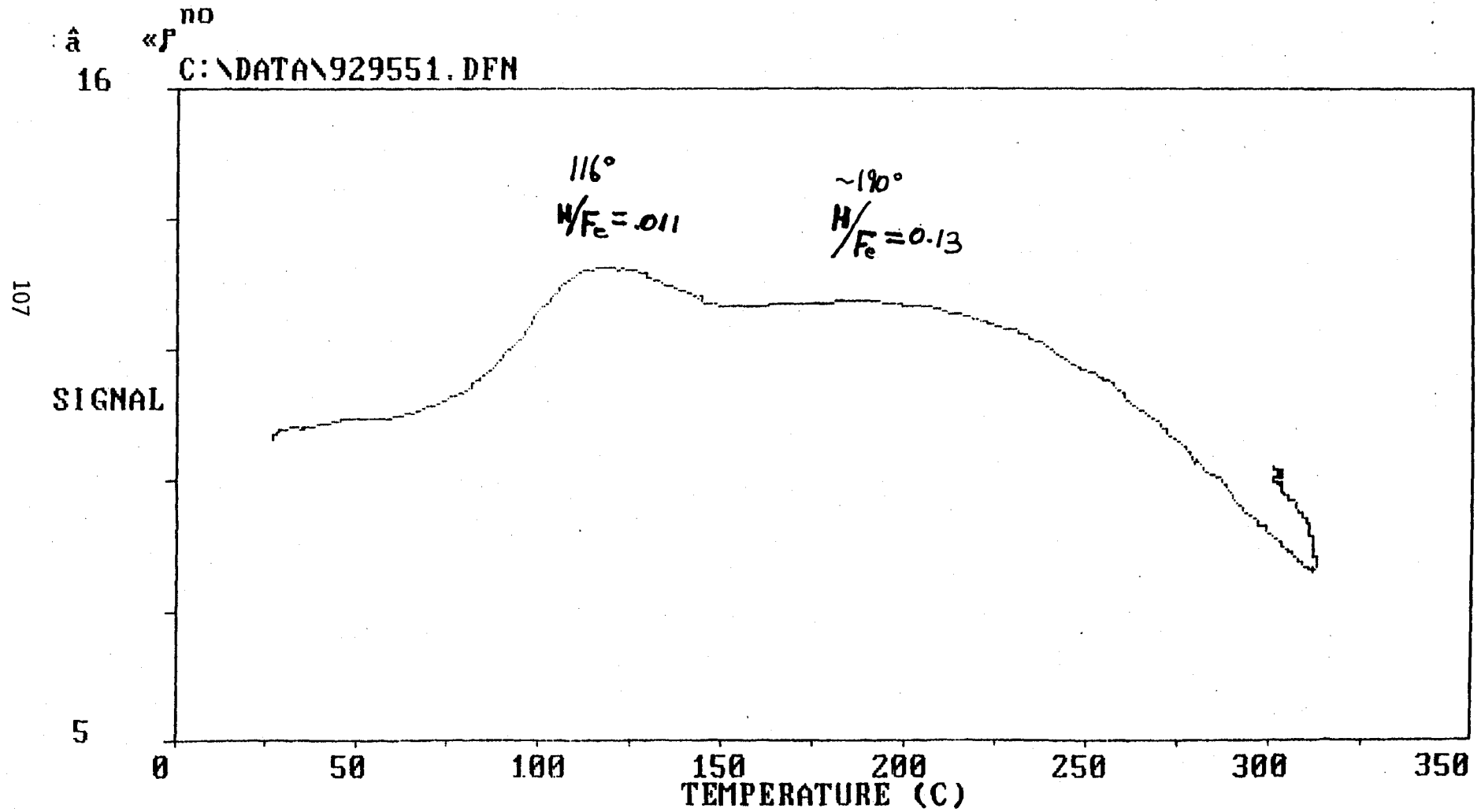

One rational explanation of our observations is that only a minor portion of the Fe(II)originally present is oxidized upon emplacement of the complex onto the surface. The result of oxidation of the complex could be either a mu oxo diiron species or a reaction product of a mononuclear iron complex with surface silanol groups. The major reduction observed using a silicalite supported Fe^{III}(FPc)Cl in the TPR experiment occurs at 192 degrees [see Quarterly Report 4th Quarter, 1993]. Because of the similar reduction temperature, it is likely that the broad absorption observed over the Cabosil-supported species is similar in nature to that occuring over the silicalite support. Since there are few silanols present on silicalite, it is most likely that the 190 degree peak corresponds to a reduction of a mu oxo diiron species. Hence, the broad reduction observed using the Cabosil-supported Fe(II) compound is probably a reduction of a mu-oxo species that is formed by air oxidation of the complex after deposition onto the surface. The lower temperature maximum (corresponding to the lower H/Fe value), is probably the reduction of the portion of the supported complex which is surface-bound as Fe(III):

Preparation of complex: }Si--OH + FeII(FPc)——> }Si--O-Fe^{III}(FPc) + H

TPR : }Si--OFe^{III}(FPc) + 1/2 H_2——> }Si--OH + Fe^{II}(FPc)*

The bulk of the complex must remain as Fe^{II}(FPc) which is refractory towards reduction.

6.4.4 Continuous Oxidation of Methane

Supported metal complexes were also studied as potential catalysts in isothermal steady-state continuous methane oxidation runs. In these experiments, a packed bed reactor was configured in our "Kung" protocol. A 0.7 cm ID X 17.1 cm long quartz liner was used to contain 1.4 ml of catalyst held in place by Pyrex wool (reactor was dimpled to hold wool in place) above a 2.5 ml heated void space and a 1.85 ml cooler void space. A thin thermocouple was inserted to monitor the bed temperature at the interface of the bed and the pyrex wool plug below the bed. Our standard water quench system and high pressure separator were utilized after the reactor. Premixing and preheating of feed was accomplished in a gold plated CSTR whose impeller was operated at high speed to ensure complete mixing at 364°C or operated at lower temperatures if the main reactor temperature was to be below 364°C. Control runs were conducted with silica gel in the main reactor at 100°C to ensure that no homogeneous reaction ensued in the preheater. Liquid aliquots were taken every 100 minutes and analyzed off-line in duplicate. Four gas samples were taken in the intervening time between each liquid sample, and the median analysis used to calculate reaction parameters and material balances. Gas chromatographs were independently calibrated; an internal standard method was used for methanol analysis. From time to time, liquid samples were analyzed by electrochemical differential pulse polarography at a mercury cathode in alkaline media to quantitate traces of formaldehyde. Data reported were normally those after 400 minutes on-stream time to ensure that steady-state was achieved. No induction periods beyond 400 minutes were observed in any of the runs reported here. Runs were conducted at 805 +/- 5 psig using a 3:1 methane:air feed at a total feed rate of 190 ml/min NTP; carbon balances of 96-104 were accepted, but balances usually fell within the range of 98-102.

NTP; carbon balances of 96-104 were accepted, but balances usually fell within the range of 98-102. Formaldehyde was not included in the material balance or selectivity calculations because it was never more than at least one order of magnitude smaller than methanol and made little difference in the result.

Figures 6 through 8 are plots of runs conducted in the range 200 to 410° for several supported metal complexes and for silica gel controls and for empty tube/pyrex wool and other controls. Figure 6 shows steady state methane conversion versus temperature. A curve is well defined for all complexes and controls taken together including runs at high temperature in which carbon supports were later found to have been consumed in the experiment. At lower temperatures, the reactor loading was replaced for EACH run, and each of these was replicated. The only significant deviation from the curve came from 300° runs over the iron fluorophthalocyanine complex on carbon, but even these were not major effects. Similar trends were observed with oxygen conversion and with methanol selectivity shown in Figures 7 and 8 respectively.

These results are expected based on the current hypothesis of reaction mechanism over the supported metal complexes. Generally higher loadings will be required of preformed binuclear complexes to observe the hypothesized low temperature (low) reaction rates of these systems with methane once oxygenated, and closer proximity of irons will be required for reactivity to be significant in the hydrotalcite intercalated catalyst series. The latter will require the synthesis of novel phases with ion exchange capacity exceeding levels present in currently known hydrotalcite compositions.

6.4.5 Conclusions

1. As temperature is increased from about 9°C to 150°C, CO and O_2 absorption by the coordinatively saturated iron fluorophthalocyanine complex does occur, but diminishes as temperature is raised to miniscule levels at temperatures of interest to catalysis.

2. Using the fluorophthalocyanine iron chloride complex as a prototype, we conclude that simple impregnation techniques on highly hydrophobic supports do not lead to good dispersion of neutral metal complexes. Surface functionalization must be considered as a means of anchoring complexes in future work. Cabosil is a good compromise support which is relatively hydrophobic yet enables reasonable dispersion of complexes by organic solvent impregnation to incipient wetness. Fluorosilicalite is the most hydrophobic support examined; although dispersion was poor on its surface, it still was adequate for some purposes. This support could be used as an external surface support even though the pore structure is too small to admit large metal complexes.

3. Some carbon supports, particularly fluorinated carbons, are highly reactive under oxidation reaction conditions and are unsuitable.

4. Known hydrotalcite phases are not of a high enough ion exchange capacity to bring mononuclear iron centers of functionalized porphyrins close enough together to activate dioxygen. Oxygen take-up by hydrotalcite supported Fe (III) complexes increased after hydrogen reduction at 200° and was sensitive to the loading on the support, as expected.

5. Oxygenation followed by isobutane pulses over the $Fe[TPPF_{20}]_2O$ complex on Cabosil at 100°C failed to generate any significant reaction.

6. Preliminary TPR experiments are encouraging. They show a variation of hydrogen absorption temperature with a variation of the complex on a surface and directionally change as would be expected from the Fe(III/II) reduction potential. Furthermore, some degree of reversibility is observed; that is, reoxidation followed by a second hydrogen reduction does show hydrogen absorption. Although it is not clear what the oxidized and reduced species are, if bulk hydrogenation were occurring, it would not likely be reversible in the fluorophthalocyanine complex.

FIGURE 1

File: C:\CHEMPC\DATA\992436.D
Operator: ELC
Date Acquired: 30 Mar 93 2:00 pm
Method File: PULSE.M
Sample Name: .196g Fe(FPc)Cl/Cab-O-sil;0.23mM/g;100285(
Misc Info: CO pulses at 200C; [Method 6COPULSE.S]
ALS vial: 1

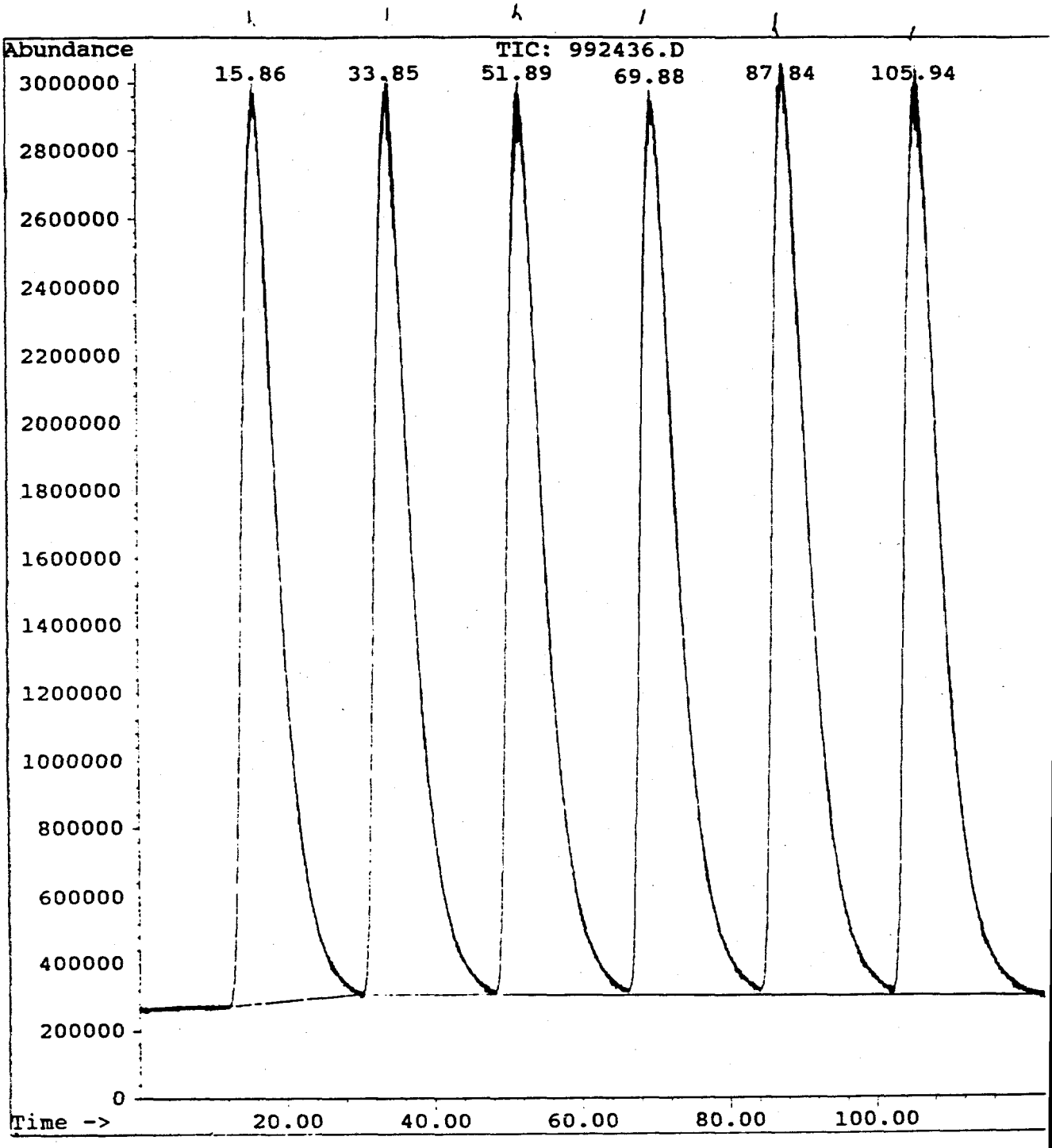

FIGURE 2

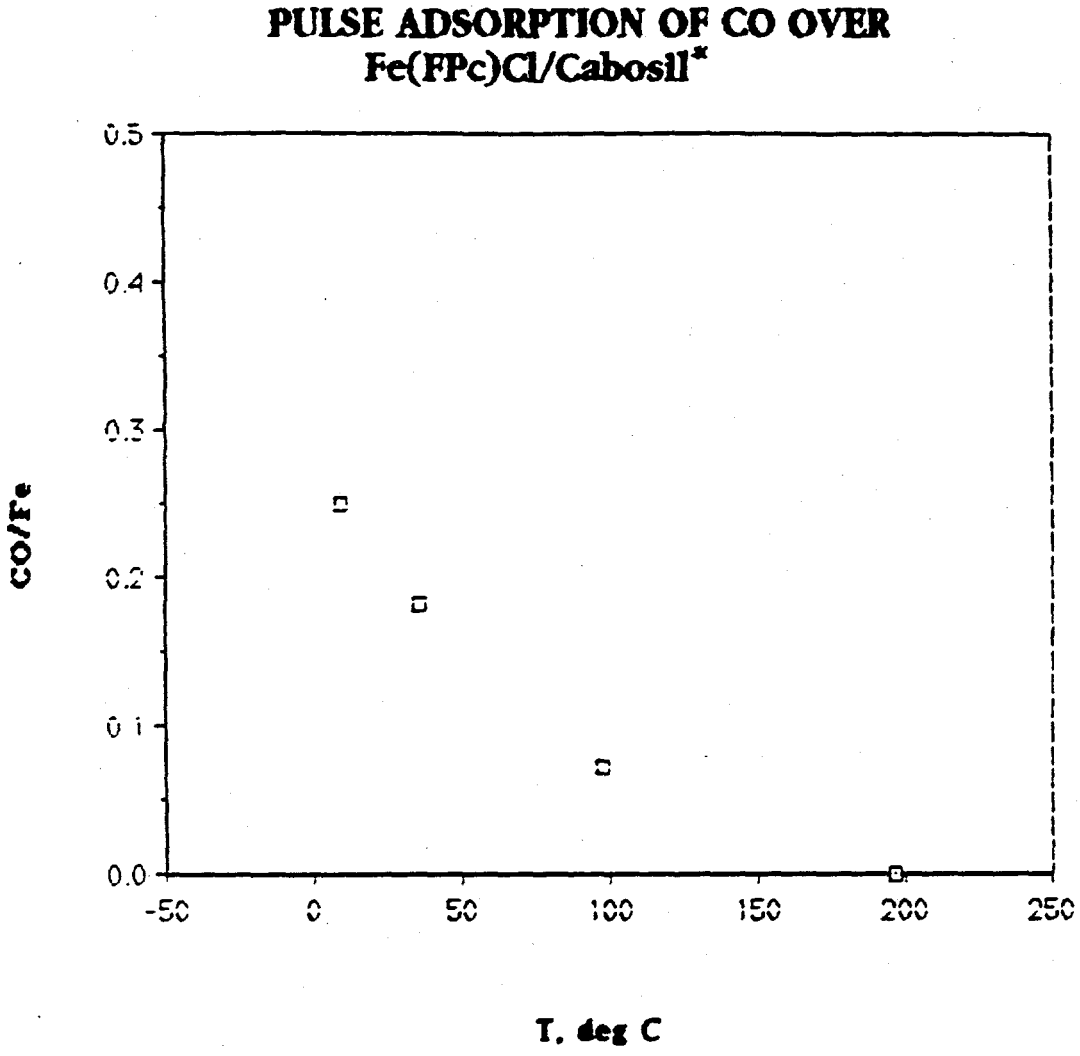

Flowing He 100 ml (NTP)/min; 45 moles Fe @ 0.23m mole/g; 815 p.s.i.

FIGURE 3

File: C:\CHEMPC\DATA\992441.D
Operator: ELC
Date Acquired: 27 Apr 93 11:04 am
Method File: PULSE.M
Sample Name: 0.193g F-graphite+Fe(PPc)Cl; 1002856-3
Misc Info: 6 OXYGEN pulses at 10 C.
ALS vial: 1

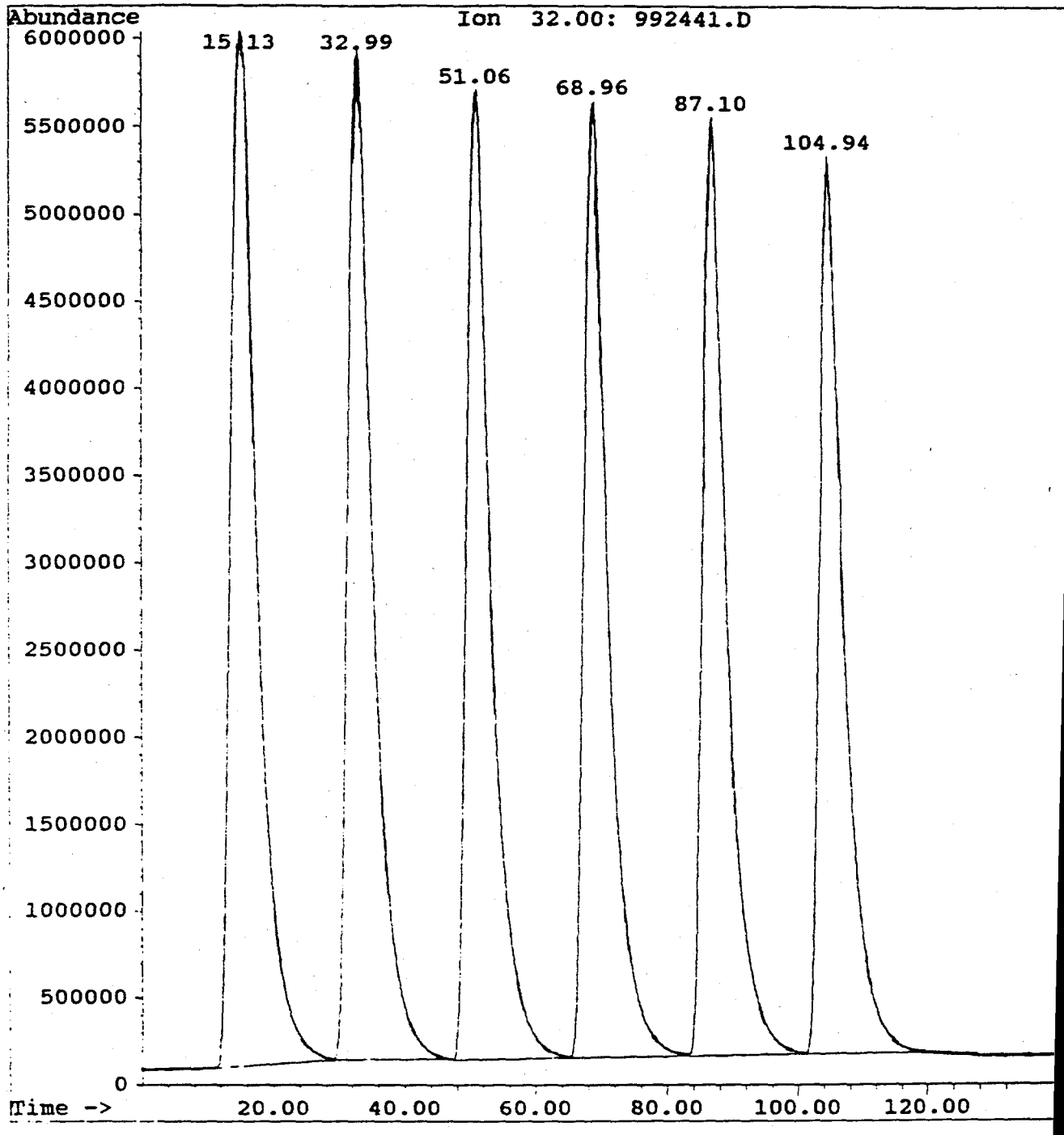

FIGURE 4

File: C:\CHEMPC\DATA\992441.D
Operator: ELC
Date Acquired: 27 Apr 93 11:04 am
Method File: PULSE.M
Sample Name: 0.193g F-graphite+Fe(PPc)Cl; 1002856-3
Misc Info: 6 OXYGEN pulses at 10 C.
ALS vial: 1

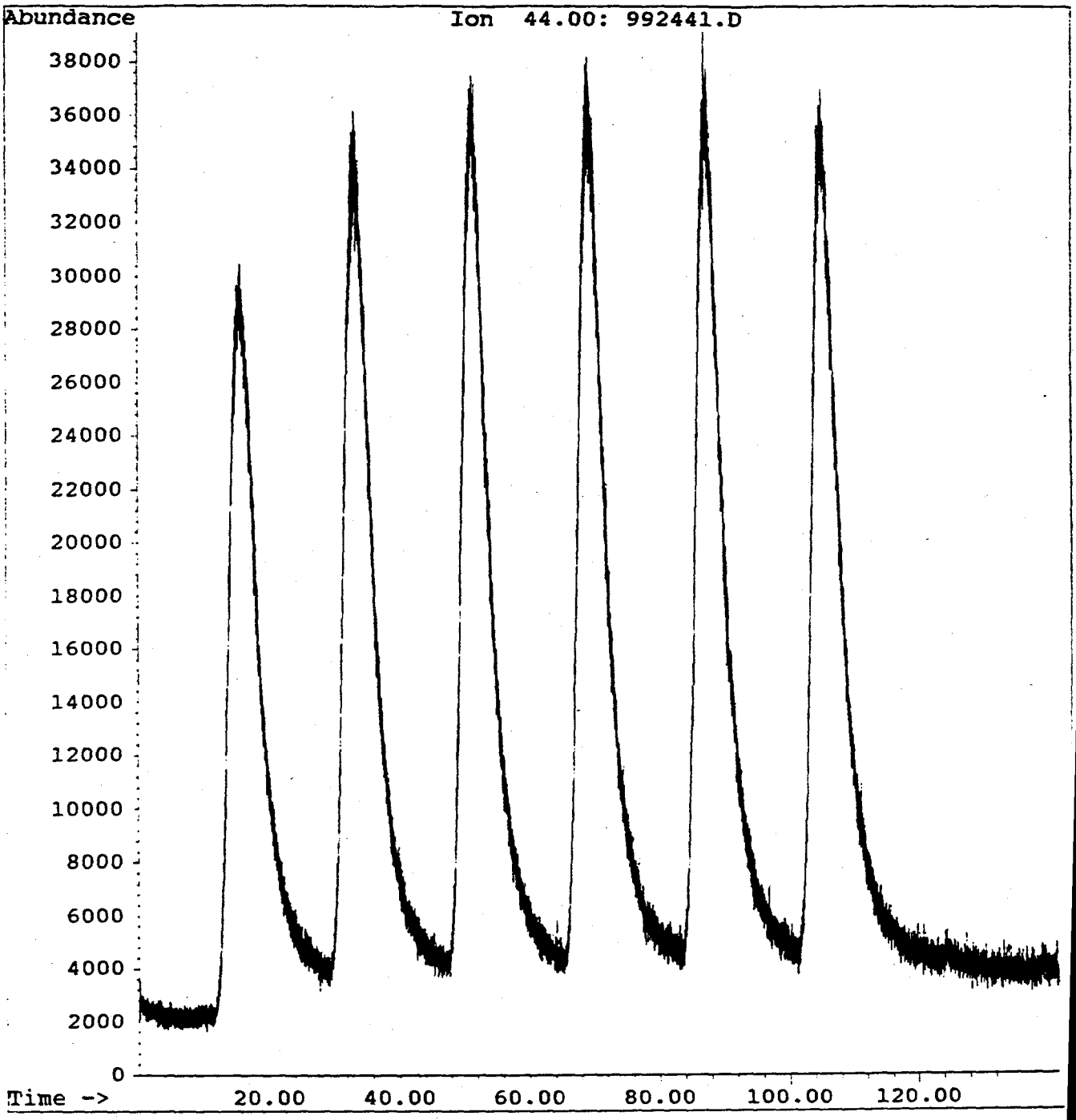

FIGURE 5

File: C:\CHEMPC\DATA\992441.D
Operator: ELC
Date Acquired: 27 Apr 93 11:04 am
Method File: PULSE.M
Sample Name: 0.193g F-graphite+Fe(PPc)Cl; 1002856-3
Misc Info: 6 OXYGEN pulses at 10 C.
ALS vial: 1

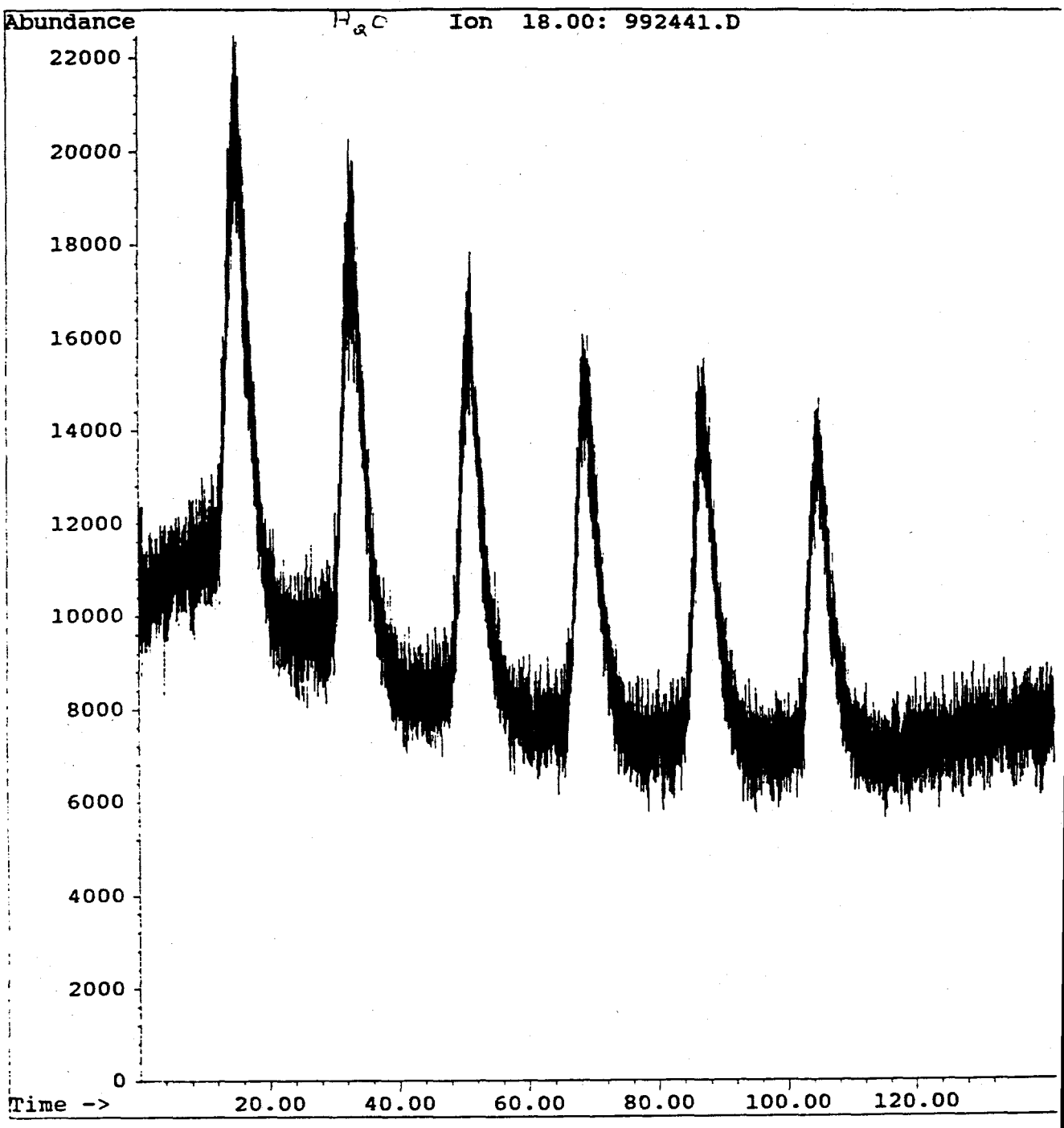

Figure 6 STEADY STATE METHANE CONV VS TEMP IN KUNG REACTOR RUNS

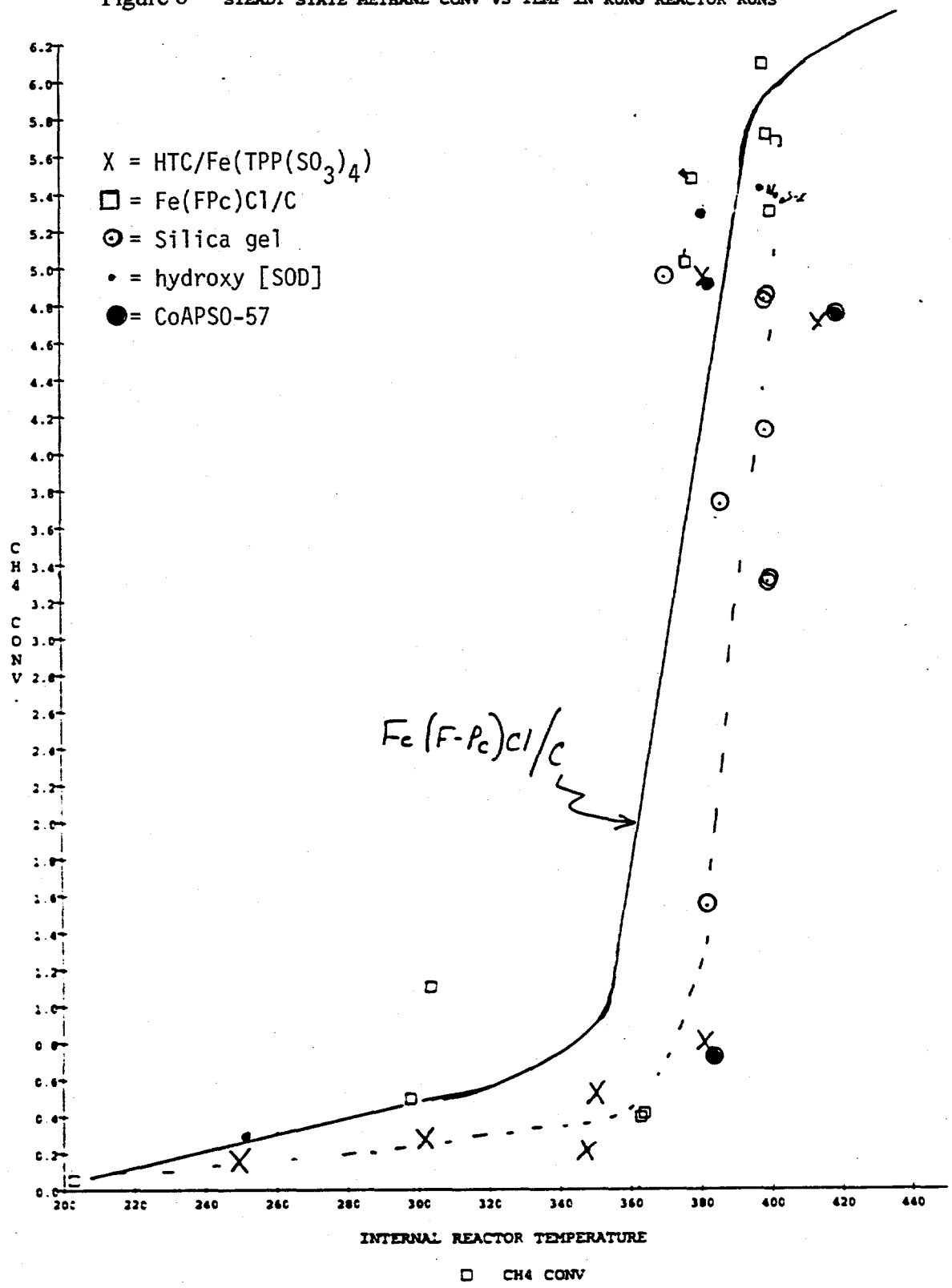

Figure 7 STEADY STATE O2 CONV. IN KUNG REACTOR RUNS

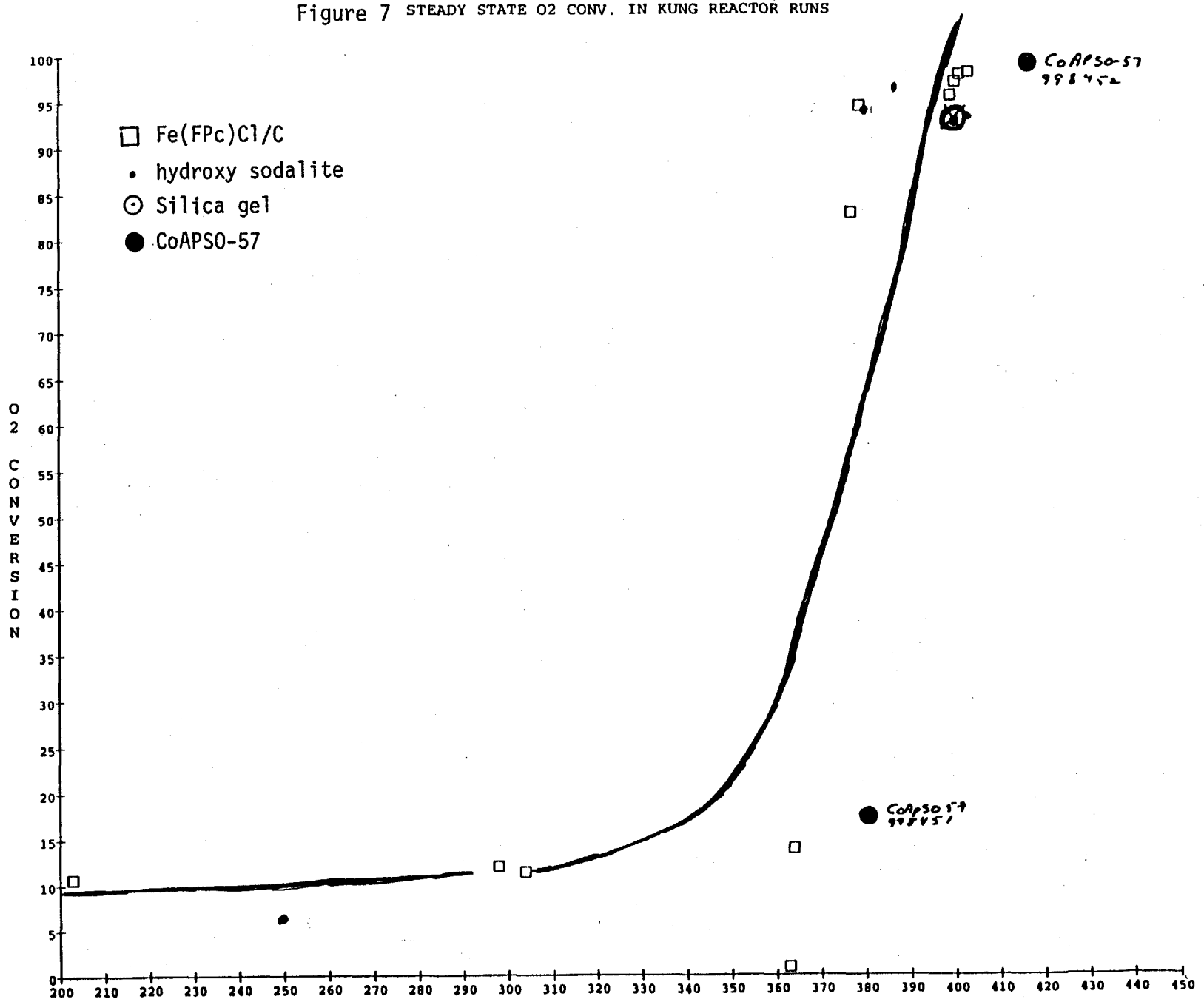

FIGURE 8 METHANOL SELECTIVITY AT STEADY-STATE IN KUNG REACTOR

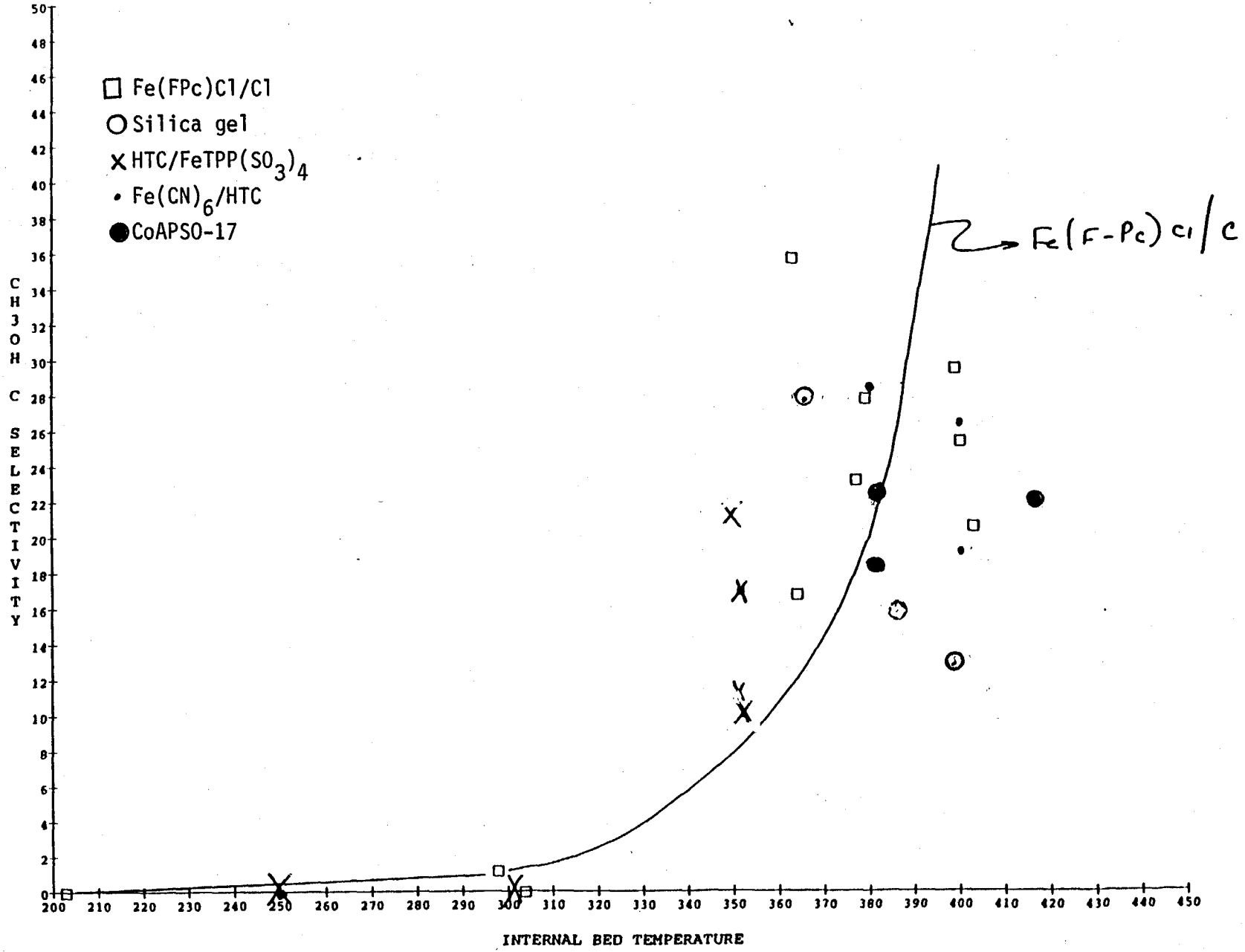

6.4.6 Testing of Supported Metal Complexes: Temperature Programmed and Isothermal Reactions with Gaseous Reagents

The technique of temperature programmed reduction, TPR, using the Altamira instrument for low pressure and the CDS reactor for high pressure work, was utilized to characterize supported metal complexes. The work described in this section is an attempt to understand the nature and stability of the surface species which result from the emplacement of several metal complexes on two hydrophobic surfaces using TPR protocols previously established in our laboratories or using related techniques. Among the complexes examined as of this writing were those which previously had been shown to catalyze hydrocarbon oxidations in the liquid phase. Surface supported versions were prepared using impregnation techniques, and, more recently, using direct condensation techniques to increase surface loading.

Silicalite-supported, fluorosilicalite-supported, and neat (unsupported) iron perfluorophthalo cyanine, iron $TPPF_{20}$, and related complexes were tested. Table I is a summary of our findings.

TABLE 1

TEMPERATURE PROGRAMMED AND ISOTHERMAL PULSE REACTIONS OF SUPPORTED METAL COMPLEXES WITH GASEOUS REACTANTS

Exp. Type	Run #.	Compound	Support	Loading (umol Fe/g)	Pretreatment Reagent		T Max (°C)	H/Fe (corr)[a]	O/Fe	Delta Wt%[b]
TPR	929511	None	F-Silicalite	—	Ar/20°/15m	10% H_2	~45			
TPR→300°	929508	Fe(TPPF$_{20}$)Cl	F-Silicalite	12.8	Ar/20°/15m	10% H_2	~40	~0		
						150°	11.8			
TPR→300°	929521	Fe(TPPF$_{20}$)Cl	F-Silicalite	12.8	Ar/20°/15m	10% H_2	~40	<<0.3		
						130	6.8			
TGA	929521	Fe(TPPF$_{20}$)Cl	F-Silicalite	12.8	None	100% H_2	47			-35%
						148				-221%
TPR→300	929522	Fe(TPPF$_{20}$)Cl	Silicalite	13.8	TPR→300	10% H_2	45	1.15		
TGA		Fe(TPPF$_{20}$)Cl	Silicalite	13.8						
TPR		Fe(TPPF$_{20}$)Cl	Silicalite	13.8	NONE	100% H_2	53			88.4%
		+ KOH	Silicalite	13.8	Ar→80	10% H_2	36	1.6(uncorr)		
							~140	~0		
							~210	~0		
TPR	929510	[Fe(TPPF$_{20}$)]$_2$0	NONE	23.6mg	Ar/25/10m	10% H_2	<25	Trace		
H_2 PULSE	929515	[Fe(TPPF$_{20}$)]$_2$0	NONE	34.3mg	Ar/22/3m	100% H_2	@22°	0.008		
H_2 PULSE	929516	[Fe(TPPF$_{20}$)]$_2$0	NONE	34.3mg	H_2/22	100% H_2	@22°	0.007		
H_2 PULSE	929497	[Fe(TPPF$_{20}$)]$_2$0	Silicalite	13.8	5% 0_2/112°	10% H_2	@45°	0		
TPO	929509	Fe(TPPF$_{20}$)Cl	F-Silicalite	12.8	TPR→300	5% 0_2	NONE		0	
TPO	929523	Fe(TPPF$_{20}$)Cl	Silicalite	13.8	TPR→300	5% 0_2	NONE		0	
TPR	929525	Fe(FPc)	Silicalite	79	Ar/25°/5m	10% H_2	35	0.032		
							192	1.116		
TPR	929526	Fe(TPP)Cl	Silicalite	12.4	Ar/20°/5m	10% H_2	42	0.22		
TPO	929496	[Fe(TPPF$_{20}$)]$_2$0	Silicalite	13.8	H_2/60°/	5% 0_2	~150		(4.5)	

a Corrected for absorption of H_2 by support using data from control experiences.

b Weight % reduction (or gain) as % of mass of starting material complex (not including support).

** Little hydrogen absorbed

*** V-UV of sublimate indicates presence of free base and monomeric FeCl complex.

TABLE 2

STOICHIOMETRIES FOR VARIOUS POSSIBLE REACTIONS OF IRON MACROCYCLIC COMPLEXES WITH HYDROGEN

L = FPc or $TPPF_{20}$	H/Fe
$L\ Fe^{III}Cl + H_2 \rightarrow Fe^{II}\ L + H\ Cl$	1/1
$[L\text{-}Fe^{III}]_20 + 1/2\ H_2 \rightarrow 2Fe^{II}\text{-}L + H_20$	1/1
$Si\text{-}0\text{-}Fe^{III}L + 1/2\ H_2 \rightarrow\ Si\text{-}0H + Fe^{II}L$	1/1
$L\text{-}Fe^{III}\text{ - }0H + 1/2\ H_2 \rightarrow LFe^{(II)} + H_20$	1/1
$L\ Fe^{III}\ Cl + H_2 \rightarrow LFe\text{-}H + HCl$	2/1
$Fe\text{-}N_4 + H_2 \rightarrow N_3\ Fe\text{-}H + H\text{-}N$	2/1
$[L\text{-}Fe^{III}]_20 + 2H_2 \rightarrow 2Fe(H)L + H_20$	2/1
$2L\text{-}Fe^{III}Cl + 3\ H_2 \rightarrow 2\ Fe(0) + 2\ H_2\ L + 2HCl$	3/1
$[L\text{-}Fe^{III}]_20 + 3\ H_2 \rightarrow 2\ Fe(0) + 2\ H_2L + H_20$	3/1
$L\ Fe^{III}Cl + 4H_2 \rightarrow Fe\ L\text{-}\beta\text{-}H_8$	8/1
$2\ Fe^{III}(TPPF_{20})Cl + 21\ H_2 \rightarrow 2\ Fe(TPP) + 40HF + 2\ HCl$	21/1

On fluorosilicalite, the most hydrophobic support known to us, the F_{20} porphyrin iron complex does not absorb much hydrogen in TPR experiments until temperatures in the range of 130-150°C are reached. At these relatively high temperatures, very high hydrogen-to-iron ratios are measured (H/Fe=7-12), indicating either massive hydrogenation of the complex or spill over onto the support phase, a phenomenon which is not observed in control experiments with the support alone. TGA experiments confirm the involvement of the support since weight losses were observed which greatly exceeded the available weight of the iron complex. Traces of HF were also measured by on-line mass spectrometry. Visual examination of the sample holder after hydrogen exposure indicated that colored compounds had sublimed from the support and condensed in a cold region outside the furnace. Analysis of the sublimed material by electronic spectroscopy and mass spectrometry indicated that the sublimate contained both the free base and the monomeric $Fe(TPPF_{20})$ species as well as the hydrogenated ligand, in some experiments. We conclude that on the fluorosilicalite support, the iron complex acts to transfer hydrogen to the support to liberate HF or to otherwise hydrogenate the support as well as to possibly become itself reduced. The reduced species is probably the volatile component which sublimes as more heat is applied. This view is consistent with further observations made on non-fluorinated supports, described below. Hence, although quite hydrophobic, the fluorosilicalite support is unsuitable for our purposes since its use complicates the interpretation of the redox chemistry of the supported complex.

On the non-fluorinated support, silicalite, we did observe a low temperature hydrogen absorption peak in TPR experiments with a corrected H/Fe ratio of 1.15. Corresponding TGA analysis indicated that sublimation occurred at 53 °, a temperature just above the 45° hydrogen absorption. In this case, the apparent reduction of the supported complex was not masked by hydrogen spillover onto the support, and a self-consistent interpretation of the observations was possible: The low temperature hydrogen absorption at 45° could represent the reduction of Fe(III) to Fe(II) followed by sublimation of the reduced iron complex. Further reductions of the iron to oxidation states lower than +2, whether from the *-oxo bridged diiron species or from the monomeric species, would have resulted in larger H/Fe stoichiometric ratios in the TPR experiments, assuming that the original surface-bound iron species was in the +3 oxidation state (see Table 2). We are in the process of conducting in-situ reduction experiments in the fore-chamber of an XPS instrument to attempt to determine the initial and final oxidation states of the surface compounds.

Further interpretation of the nature of the reaction with hydrogen requires knowledge of the structure of the surface species originally present. Possible compositions of Fe(III) species include $LFe^{III}Cl$, $[LFe^{III}]_2O$, $LFe^{III}OH$ (L= porphyrinato ligand) or a surface bound species originating from the reaction of the monomeric complex with a silanol group:

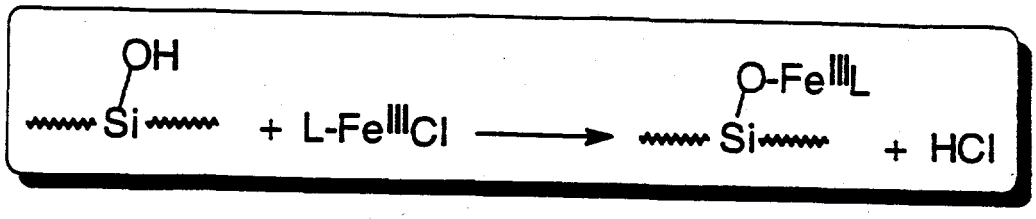

The latter moiety could then react with hydrogen to regenerate a surface silanol and a reduced iron species, requiring a H/Fe stoichiometric ratio of 1:

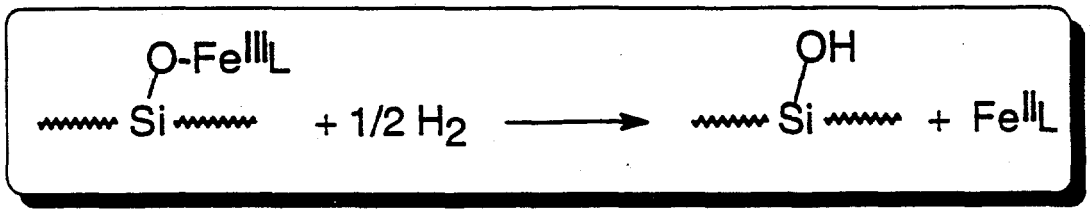

The other Fe(^{III}) candidate structures could react according to the possibilities shown in Table 2. An attempt was made to decipher whether the surface species of interest existed as a dimer or as a monomeric complex containing a chloride ligand. In this regard we note that no HCl was detected in TPR experiments as an effluent, but this negative result does not rule out the presence of low levels of a chloride ligand. Furthermore, treatment of a sample of the Fe(TPPF$_{20}$)Cl/silicalite with KOH (run 992495 in Table 1) did not quench the low temperature hydrogen absorption in a subsequent TPR experiment. However, neither TPR nor isothermal hydrogen titrations of the neat μ-oxo diiron compound or of a supported version (runs 929510, 515, 516, and 992497 in Table 1) failed to result in significant hydrogen absorption despite the high sensitivity (low level of detection) possible in the hydrogen titration experiments. Either hydrogen only reacts with the external surface of the neat dimer, yet more fully with a dimer formed by KOH treatment of the surface-supported Fe(III) chloride compound; or hydrogen cannot reduce the dimer, whether on a surface or not, but can reduce a monomeric hydroxy-ligated iron (III) species formed on the surface by KOH treatment. Although the neat compounds display distinctive infrared absorption bands [Jayarj et. al., Inorganic Chem. (1986) **25**, 3516,] neither the μ-oxo diiron species or the monomeric chloride was distinguished conclusively in DRFTIR difference and ratio spectra of the supported catalysts. Examination of the spectral region where surface silanol vibratory modes are expected was similarly unproductive. Hence, we cannot differentiate the possibilities for the nature of the reaction between hydrogen and supported electron-deficient iron porphyrin species at this time.

Examination of run 929526 in Table 1 reveals that the silicalite-supported non-halogenated porphyrin iron chloride shows a sub-stoichiometric low temperature hydrogen absorption at 42°. This compound would be expected to be less responsive to hydrogen than the electron-deficient versions above, showing a reduction peak at higher temperatures but of similar stoichiometry. No higher temperature peak was observed up to 300°C. One possibility is that this compound has a less labile chloride ligand than that of the electron-deficient analogs above, hence the non-halogenated porphyrin compound may be less prone to form a silanol-bound species than the halogenated porphyrin compound by the route shown in equation (1), above. This interpretation is consistent with the known

reduction potentials and steric constraints of the two compounds. The TPR observation could then be rationalized if the surface-bound ---but not the chloride---species were reducible.

In contrast to the porphyrin systems, the perfluorophthalocyanine iron (II) compound, formed by condensation directly onto silicalite was well behaved. This material showed a clean reduction peak at 192°C with a H/Fe stoichiometry of 1 (see Figure 1 and Table 1). Although this compound starts out as iron (II), it is unlikely that hydrogen reduces the Fe(II) to a lower oxidation state and still retains a bound phthalocyanine ligand. The observed stoichiometry is not consistent with a reaction such as (3) or (4) which would require a H/Fe ratio of 2; and the density of silanol sites is far too low to give rise to the stoichiometric formation of a surface-bound species such as formed by route (5), which could subsequently be reduced with hydrogen as in (2), above:

(3) $Fe^{II}(FPc) + H_2 \longrightarrow H^+[H\text{-}Fe^{II}(FPc)]$

(4) $Fe^{II}(FPc) + H_2 \longrightarrow H\text{-}Fe^{III}(FPc) + H^\bullet$

(5) $Fe^{II}(FPc) + Si\text{-}OH \longrightarrow Si\text{-}O\text{-}Fe^{III}(FPc) + H^\bullet$

A more probable explanation of the observed hydrogen reduction is that the Fe(II) species formed by condensation directly on the silicalite surface reacts with atmospheric oxygen (and water) after its deposition to produce the μ-oxo diiron species which could then react with hydrogen in the TPR experiments to liberate water and Fe(II) monomer with a 1/1 stoichiometry.

More extensive characterization of related phthalocyanine complexes is in progress. In addition, future work will be conducted on a different siliceous support, Cabosil, which features a significantly greater concentration of surface hydroxyl functionalities, ca. 1.13 milliequivalents per gram. Direct condensation of the phthalocyanine compound onto this support is expected to result in a somewhat different TPR behavior, if dispersion of the iron complex by surface condensation with silanol groups is important to the reduction results.

FIGURE 1 TEMPERATURE PROGRAMMED REDUCTION OF
Fe(FPc)/SILICALITE AFTER AIR EXPOSURE

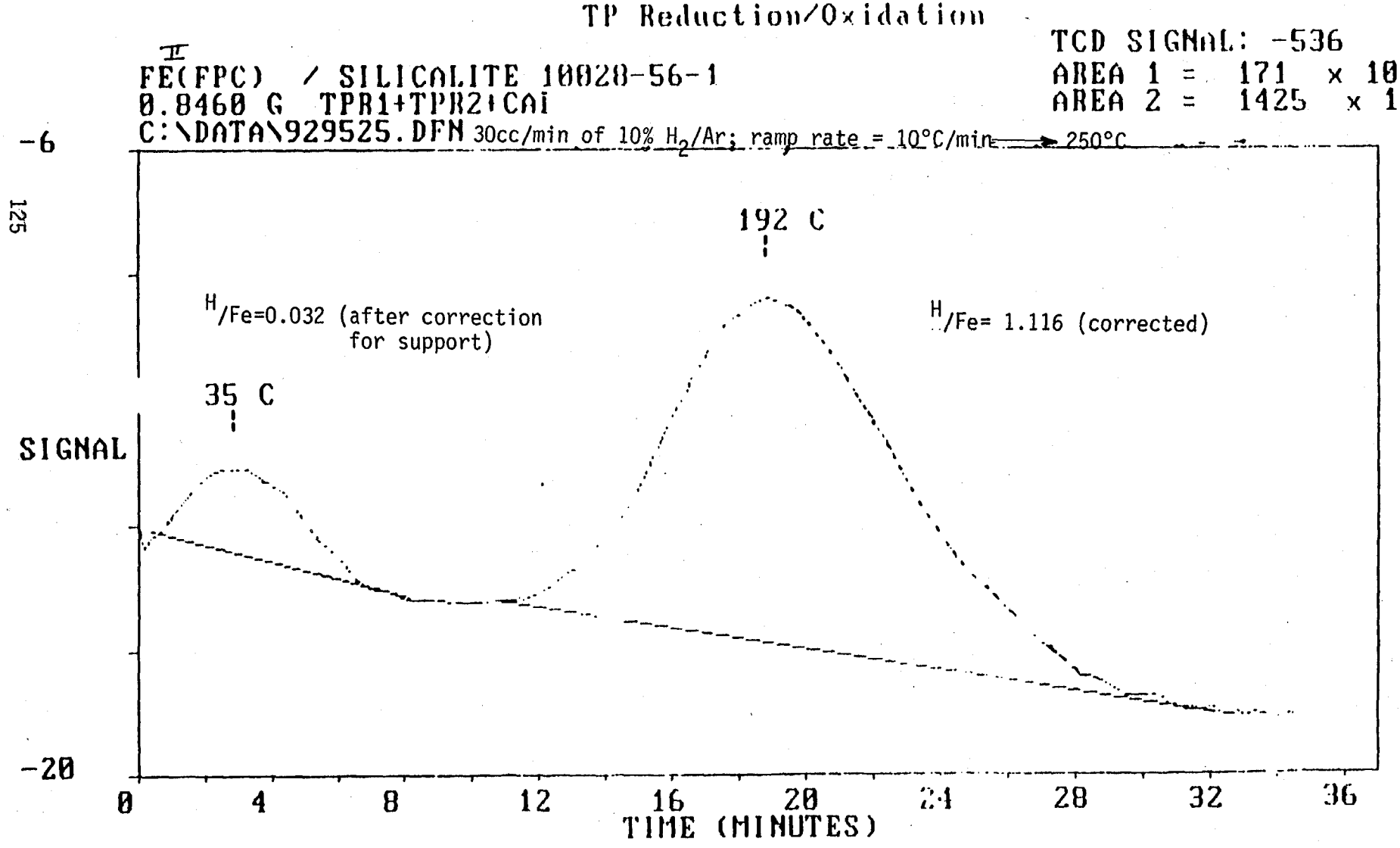

OXYGEN ABSORPITON ISOTHERM OVER Fe(II)(FPc)Cl/C

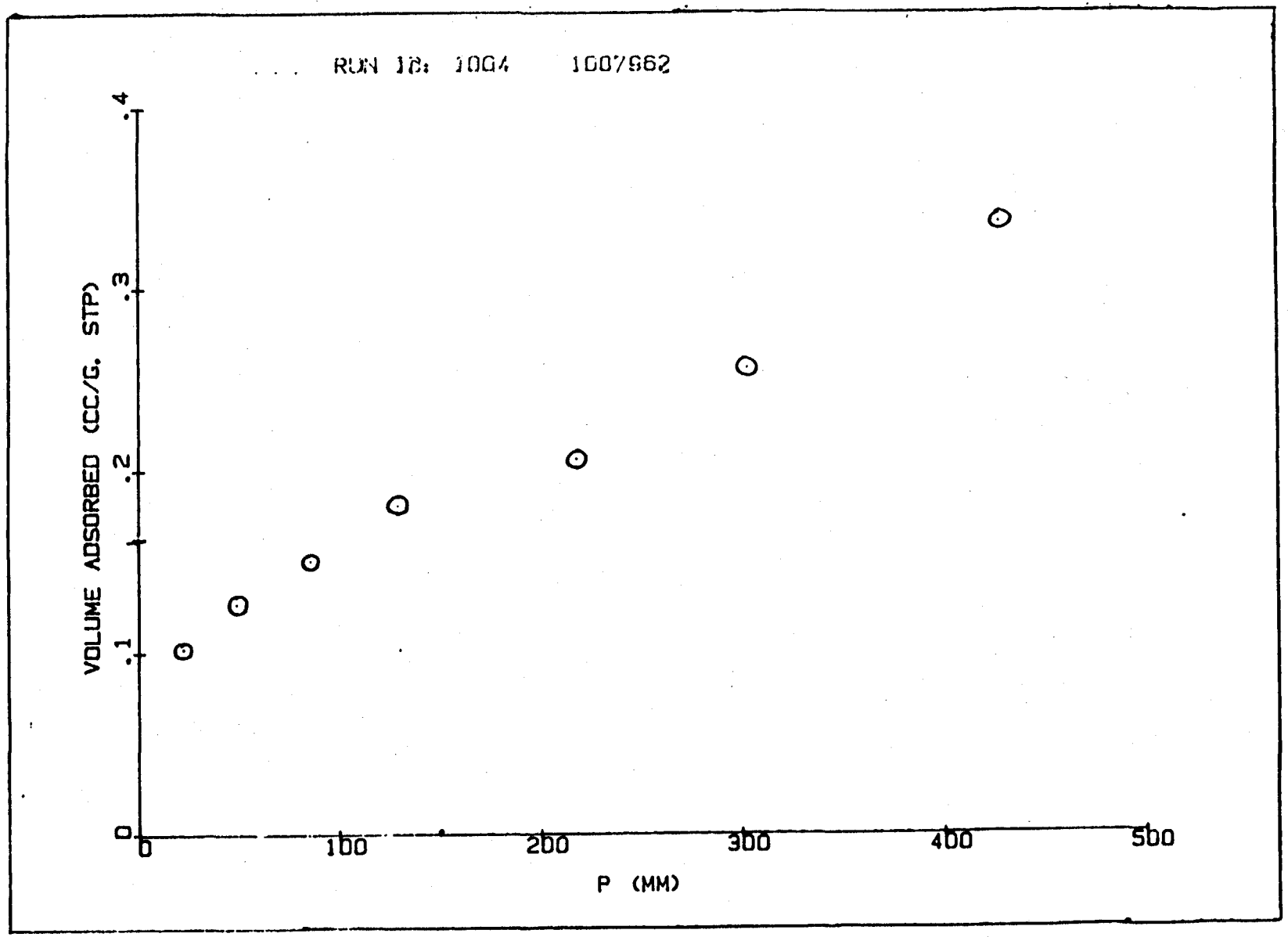

6.4.7 Oxygen Absorption Studies

A sample of FeII(FPc)/cabosil containing 56.85 wt. % complex on a volatile-free basis was subjected to volumetric oxygen chemisorption using the static chemisorption protocol in the Omicron 360 instrument at 26°C after evacuation and flowing hydrogen treatment at 175°C. After correction for helium absorption in the automated sequence, an isotherm for oxygen take-up was plotted, shown in Figure 2. A slight breakpoint was noted in the plot between 129 and 218 torr. Extrapolation of this "knee" point curve to 0 pressure resulted in an apparent monolayer capacity of 0.165ml STP/g which translates to 0.011 O_2/Fe(II). Assuming a stoichiometry of 1 O_2 per Fe(II) (to form a superoxide complex) and that all of the exposed iron reacts with oxygen quantitatively, this calculates to an apparent dispersion of 1.1%. If the equilibrium constant to bind oxygen is low, however, then the assumption of complete reaction is poor, and the low value of O_2/ Fe(II) reflects the small value of the equilibrium constant for binding at room temperature. Using a value of 201 angstrom^2 for the footprint of the Fe phthalocyanine complex, [Herron and Tolman], one may calculate an apparent surface area of 8.9 m^2 complex per gram of solid. If oxygen binding is the required prerequisite for catalysis of selective oxidation, then the fluorinated complex is expected to do a poor job of catalyzing such reaction because of the low concentration of active species formed at temperatures at which oxidation might proceed.

We expect that electron donating, rather than electron withdrawing, substituents will enable improved oxygen binding, and hopefully, also improved catalysis of the selective oxidation of alkanes by Fe^{II}(Pc-X) complexes. To this end, we shall examine complexes prepared by Paul Ellis containing electron donating substituents after their deposition onto standard surfaces.

6.4.8 Recent Alkane Oxidations Over Fe(FPc)/ CABOSIL

The Fe(FPc)/cabosil catalyst, prepared by direct condensation of the Fe(II) complex onto the support rather than by impregnation, a catalyst which was described above as having the potential to contain a surface-bound iron species, was examined for its ability to catalyze vapor phase oxidations of isobutane and of propane in the CDS reactor in the continuous mode.

At temperatures as low as 128°C, isobutane was oxidized at about 0.4% conversion to a mixture of TBA and acetone without generating detectable quantities of CO, CO_2, and water over the catalyst of interest. At higher temperature (272°C), CO, CO_2, H_2O, and CH_4 were observed in addition to TBA and several other unidentified products. Propane was not oxidized at temperatures as low as were suitable for isobutane, but at 288°C, a temperature which is still quite low, methanol, acetone, carbon oxides, water, and other unidentified products were detected. The methanol formed was 0.7% of the feed propane. Although these results are not spectacular, they suggest that the fluorophthalocyanine iron (II) system is capable of catalysis of alkane oxidations at relatively mild conditions.

6.5 SYNTHESIS OF BENZENE-SOLUBLE SCHIFF BASE COMPLEXES WITH ELECTRON WITHDRAWING FUNCTIONALITIES

In addition to porphyrins and phthalocyanine-type ligands, we have considered other ligand systems to have the appropriate characteristics needed to activate a coordinated metal such as iron, ruthenium, or manganese such that the complexed metal ion would become competent to catalyze reactions of interest to this program. Among characteristics which could be altered by modification of ligand substituents are the tuning of the Fe (III/II) reduction potential and rate and extent of oxygen binding. Because of the ease of preparation of various derivatives and their relatively low cost, Schiff base ligands were considered as targets for this research.

Since attachment of metal complexes to surfaces by ion exchange techniques is thought to be desirable as one means to maintain dispersion and to control the concentration of active catalytic centers, charged complex ions may be preferred over neutral species. However, to compare reactivity on an ion exchanged surface with reactivity in fluid solution in non-polar solvents, both charged and uncharged complexes of the same chelating ligand would be required, ideally, because the charged complexes would be strong electrolytes and not likely to be soluble in non-polar solvents. To achieve the broadest range of applicability, it is important to be able to vary the charge on the complex ion without alteration of the formal oxidation state of the central metal. Additionally, the ability to form cis configuration chelates, which the planar porphyrins and phthalocyanines cannot do, may be important to reactivity tuning. Tripodal or tetrapodal non-macrocyclic Schiff-base ligands afford the ability to add additional attachments to the metal to adjust charge (i.e., the complexes are not coordinatively saturated by virtue of the chelate alone) and may be tailored to provide stable cis complexes by adjustment of steric interactions of the ligand backbones. A wide range of functionalization with electron withdrawing as well as electron donating substituents is also possible within a series of Schiff base ligands. Accordingly, we have studied in the past, and continue to investigate, a number of both mononucleating and binucleating Schiff base ligands and their corresponding metal complexes.

Although iron and ruthenium complexes of Schiff base (imino-linkage) chelating ligands had been prepared in the past, the earlier preparations were either strong electrolytes or contained nitro substituents and had been found to be largely insoluble in organic solvents. The present work was focussed on the preparation of soluble mononuclear complexes or their ligand precursors which incorporated varying degrees of electron withdrawal in the macrocyclic ligand system. Such complexes are potential catalysts for low temperature alkane oxidations and hydroperoxide decomposition in fluid solution and as heterogeneous catalysts once deposited onto solid supports. The solubility characteristics of these complexes (soluble in non-polar solvents and possibly insoluble in polar solvents) enables their facile emplacement onto surfaces by incipient wetness impregnation techniques yet improves their stability towards migration or removal in the presence of water or steam which is either a feedstock component or formed as a product of oxidation. Ion exchange techniques cannot be used to attach these complexes to surfaces, but exchangeable analogs can be made which contain the same chelating ligand by variation of the other (non-chelating) charged ligands such as chloride.

Two types of Schiff base ligands were prepared. Those based on the SAP structure (tridentate) and those based on the SALOPH structure (tetradentate):

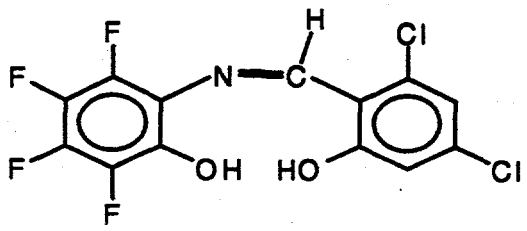

F_4, Cl_2 - SAP

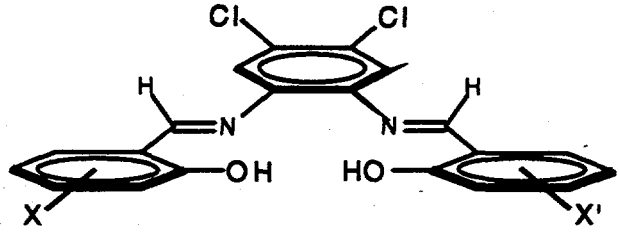

Cl_2, X_2 - SALOPH

Synthesis of the fluorinated salicylaldehyde precursor of the SAP-type ligands was described previously. The general methodology of ligand synthesis is illustrated by the preparation of one of the ligands as detailed below.

A. SYNTHESIS OF N,N'-BIS(-3,5-DICHLOROSALICYLIDENE)-PHENYLENE-4,5-DICHLORO-1,2-DIAMINE
alt. name: 1,2-BIS (3,5-DICHLORO-2-PHENOLIMINYL)-4,5-DICHLOROBENZENE
alt.name: 4,5-DICHLORO-1,2-PHENYLENEDI-(1-IMINYL-3,5-DICHLORO-2-PHENOL)
alt. name: Cl_6 SALOPH

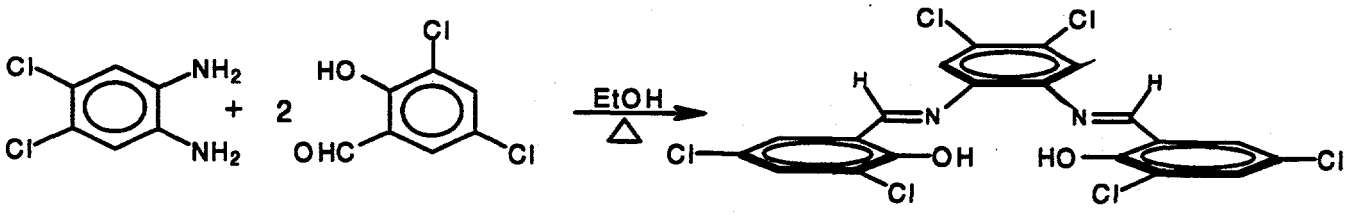

This ligand and other analogs were prepared by the classical Schiff base condensation. The preparation of the ligand was conducted in dry ethanol in glassware exposed to air in several batches at the 0.01 or 0.1 mole scale. A typical preparation was as follows:

Ligand precursors were purchased and used as received. Dichlorophenylenediamine (Aldrich D7,160-7) [1.77g, 0.01m] was dissolved into 50 ml of EtOH with heating and magnetic stirring on a hot plate. 3,5 dichlorosalicylaldehyde (Aldrich 26,181-5) [3.82 g., 0.02 mole] was dissolved into 30 ml EtOH in a separate beaker with heating and stirring. The brown amine solution was added dropwise to the yellow aldehyde solution while hot and stirred for 0.25 h. An orange precipitate formed immediately, and the liquor was then cooled to room temperature. The precipitate was collected on a medium frit, washed with cold EtOH [3x, 15 ml], and air dried. A second crop formed in the filtrate and was collected separately and air dried. The air-dried products were then dried further in a vacuum oven [2h, 80*], labelled 920193-1 (1st crop) and 920193-1B (2nd crop). Yield of the first crop was 61-70% in various preparations. Small portions of the ligand were recrystallized from EtOH/acetone or from ACN/EtOH.

B. SYNTHESIS OF NEUTRAL IRON COMPLEXES

Iron (II) complexes of the ligands were prepared using $FeCl_2.4\ H_2O$ as a synthon for neutral complexes. $FeCl_2.4H_2O$ (Aldrich 38,002-4) [0.199g, 0.001 m] was partially dissolved in 10 ml of EtOH in an erlenmeyer flask with heating and stirring under N_2. Cl_6SALOPH (920193-1) [0.523g, 0.001m] was similarly dissolved in 2:1 acetone:EtOH (v:v). Upon combining the two solutions, an immediate green color formed despite the incomplete dissolution of the iron chloride compound. The combined solution was evaporated to dryness with mild heating in a N_2 stream, and the resulting solid extracted with benzene [2x, 30 ml]. The benzene extract was transferred to a separatory funnel and back washed with water to remove any non-complexed iron compounds. The benzene solution was then evaporated to dryness in a stream of N_2, and the resulting solid dried in a vacuum oven at ca. 70*C overnight and labelled 920194-1. Yield was 12%.

Attempts to synthesize iron complexes using $Fe(BF_4)_2$ did not result in soluble products.

The benzene soluble complexes may be formulated either as **i** or **ii** below.

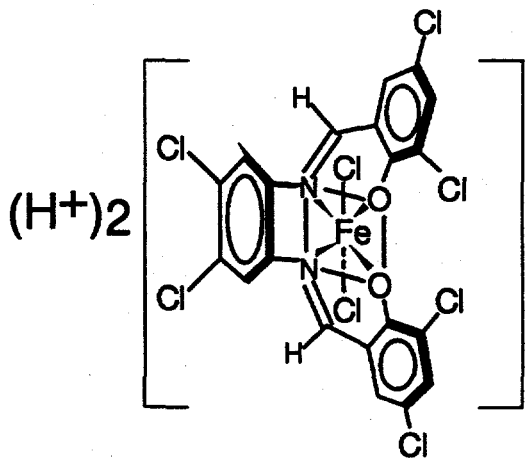

cis- or trans

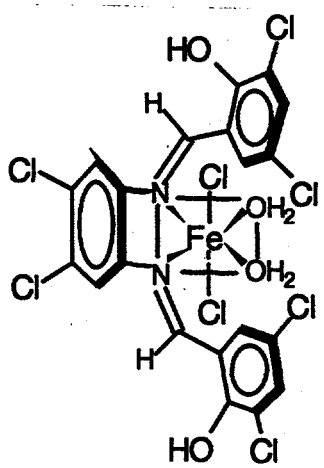

6.5.1 Conclusions

Several conclusions can be made from work in each of the areas described in this report.

1. Although quite hydrophobic, fluorosilicalite is an unsuitable support for metal complexes for alkane oxidation because hydrogen atom spillover complicates the redox chemistry of interest.

2. On silicalite and on Cabosil, surface deposited iron complexes can exist either as a μ-oxo diiron species or as a mononuclear surface tethered moiety. The mode of attachment of iron-pyrrolic-type macrocyclic compounds to siliceous surfaces of both the porphyrin or phthalocyanine ligand type may involve attachment via Si-O-Fe linkages if the chloride ligand of the iron is labile and the concentration of silanol hydroxyls on the surface is high. Otherwise, dimeric complexes may be formed. Although other interpretations cannot be excluded with certainty, it seems that surface μ-oxo diiron species of $TPPF_{20}$ and of FPc behave differently towards reduction by hydrogen, the latter being more easily reduced. Further investigation is necessary to elucidate the implications with regard to catalysis.

3. Oxygen binding of the FeII(FPc)/Cabosil system is quite low at room temperature as measured by volumetric chemisorption techniques. Electron donating substituents may aid in improving this characteristic.

4. Despite poor oxygen binding, low level (phenomenological) catalysis of propane and isobutane oxidation to alcohols (and other products) is possible over Fe(FPc)/Cabosil at temperatures below those needed to initiate thermal reaction in the vapor phase.

5. Substituted Schiff-base ligands based on the SAP or SALOPH structures containing electron withdrawing groups have been prepared. Three benzene-soluble Schiff-base iron complexes have also been prepared using $FeCl_2.4H_2O$ as a synthon .

6.6 SYNTHESIS OF ADDITIONAL SCHIFF BASE MONONUCLEAR LIGANDS AND IRON COMPLEXES

A. Synthesis of N,N'-bis-(-4-methoxysalicylidene)-phenylene-4,5-dichloro-1,2-diamine
alt name: Cl2,-(OMe)2-SALOPH
alt name: DMSDCP

A Schiff Base synthesis previously described was adapted to the preparation of the named compound from the appropriate purchased reagents:

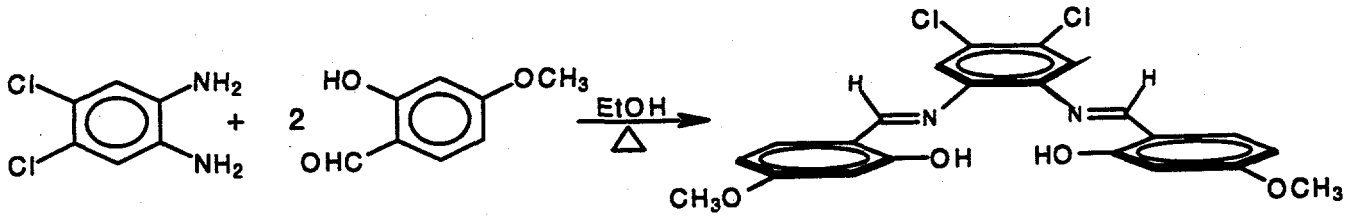

The synthesis was conducted on a 0.01mole scale, realizing a 50.6 % yield of the Schiff base product. Recrystallization of the yellow product from hot ethanol followed by washing with cold ethanol and vacuum drying afforded the ligand, 920200-1R, for preparation of the iron complex, below.

B. SYNTHESIS OF Fe(DMSDCP) or (DMSDCP)Fe-O-Fe(DMSDCP)

The title compound was prepared from the disodium salt of the Schiff base ligand and $Fe^{II}SO_4 7H_2O$. DMSDCP in ethanol [920200-1R, 0.1 mmol, 0.0445g] was titrated with 1N NaOH (aq) [0.2 ml, 0.2 mmol] to generate a partially insoluble salt. $FeSO_4 7H_2O$ [0.1 mmol, 0.028g] was dissolved in a water/ethanol solvent mixture and the solution added to the dissolved ligand with stirring and warming in air. Additional water was added to partially dissolve the brown precipitate. The aqueous solution was then extracted with benzene [2x, 30 ml] in a small separatory funnel. The benzene layer became reddish-brown in color and was separated from the aqueous layer and a lightly colored precipitate remaining therein. A brown solid was recovered by evaporation of the benzene layer, labelled 920202-1.

Although the compound formed was undoubtedly neutral in charge since it was able to dissolve in benzene, it could be formulated either as $Fe^{II}L$ or as LFe^{III}-O-$Fe^{III}L$ where L is DMSDCP coordinated in a tetradentate fashion. No characterization has been conducted as of this writing, but the sample will be examined as a potential catalyst for isobutane oxidation and hydroproxide decomposition in fluid solution prior to testing for methane oxidation.

6.7 Progress in the Synthesis of a Binucleating Polyimidazole Ligand with Electron Withdrawing Substituents, BIMP-X

Several intermediates along the way to the preparation of the BIMP ligand system functionalized with either chlorine atoms, or with -CN or $-NO_2$ substituents were prepared.

A. ATTEMPTED NITRATION OF N-METHYLIMIDAZOLE

Nitration of imidazole derivatives normally requires the use of refluxing concentrated fuming nitric/sulfuric acid and a difficult workup [K. Hofmann, Imidazole and Its Derivatives, Part I of Chemistry of Heterocyclic Compounds, Interscience, NY, 1953, pp.127ff.]. However, given the success of the reagent, N_2O_4, at nitrating prophyrin ring systems without oxidative cleavage of the product, we hoped to use this reagent to prepare nitrated BIMP ligands from the previously synthesized non-functionalized parent compound under relatively mild conditions with an easy workup. Since we have only a small quantity of the BIMP ligand, we first studied the nitration of N-methylimidazole at the 4 and 5 positions using N_2O_4 reagent as a model for nitration of the BIMP ligand system. If this reaction were successful on the methylimidazole monomer, similar reaction conditions could have been applied to the precious BIMP ligand, a polyimidazole.

N-methylimidazole [0.5 g] was dissolved into 75 ml of methylene chloride. Dinitrogen tetroxide liquid was weighed from a cylinder into an open beaker [8.4 g] at room temperature. Then the nitrating agent was added slowly at room temperature to the methylimidazole solution with magnetic stirring in an open beaker and stirring continued for 1 hour. A small amount of water was added to "quench" the reaction, and the reaction mixture cooled further in the refrigerator. Two layers had formed; ^{1}H-NMR of the organic layer indicated that no nitrated substituent was present; the spectrum was consistent with the formation of a salt, $[HMeIM]^+ NO_3^-$. Since there was no evidence for any nitration at all using the model compound, no attempt was made to nitrate the actual BIMP ligand.

B. SYNTHESIS OF 5-CHLORO-1-METHYLIMIDAZOLE-2-CARBOXALDEHYDE

The procedure was modelled after our successful synthesis of 1-methyl-2-

residue was vacuum distilled at 4 torr through a Vigreaux column. A fraction was collected at 74° and 4 torr which solidified at room temperature; the starting material is reported to boil at 89° at 14 torr. ^{1}H NMR ($CDCl_3$) showed the characteristic aldehyde resonance at 9.58 ppm and other peaks at 7.13 and 3.87 ppm in addition to peaks due to DMF and starting material contaminants. Yield was %.

C. SYNTHESIS OF OTHER SUBSTITUTED METHYLIMIDAZOLE ALDEHYDES

6.8 METALS IN MONO- AND BINUCLEATING MACROCYLES

Vincent A. Durante and Bonnie Marcus

In past reports we have discussed the potential benefits of binuclear surface sites for activating and cleaving the dioxygen molecule. This could be achieved by making di-metal derivatives of binucleating macrocycles and depositing these on or in a surface support material. As discussed in recent reports, we have been engaged in activities oriented toward synthesizing complexes of metals in binucleating ligand systems and supporting them on hydrophopic support materials. Simultaneously with this activity, we have been supporting stable mononuclear macrocyclic complexes on hydrophobic and other support materials. The rationale for the latter activity is that although mononuclear superoxo complexes are unlikely to be active catalysts for the oxidation of alkanes at low temperatures in solution, they may be active catalysts for oxidation of alkanes at high temperatures on a surface, Figure 1. The following sections detail attempts at synthesis and support of metal complexes of both the mononuclear and binuclear type.

Figure 1 Hypothetical Superoxide Oxidation Mechanism for Site Isolated Mononuclear Complexes on Surfaces at 80<T<400°C[a]

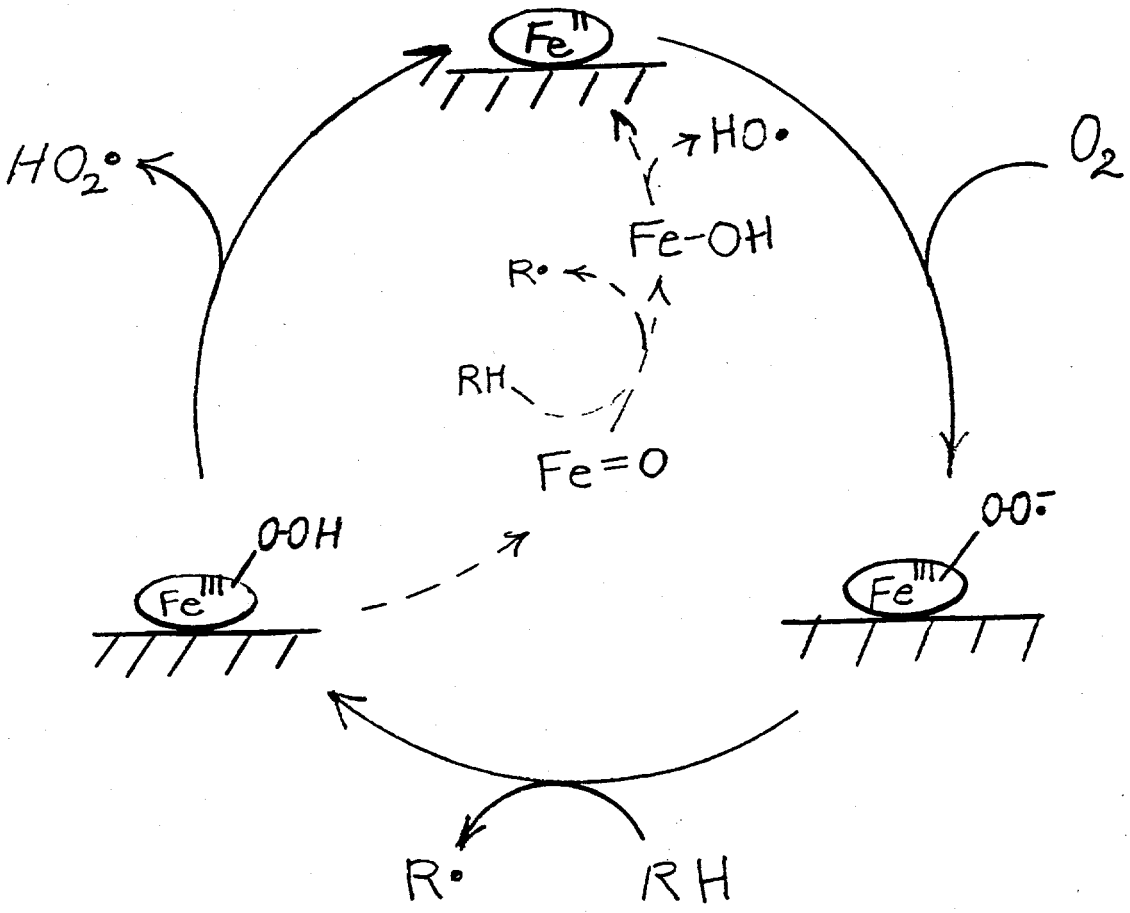

[a]RXN of superoxide w/alkane is normally slow in liq. phase @ Low T, but it is faster at elevated T's on surface μ-oxo dimers can't form on surface.

6.8.1 Introduction

We continued to investigate two approaches outlined in the program plan: supported mononuclear complexes and supported binuclear complexes. The first approach, involving the use of supported mononuclear complexes, has been delayed because of our inability to successfully characterize oxidation states of the previously prepared supported iron fluorophthalocyanine complexes in the anticipated manner by XPS (because of the interference of the F atom with the Fe binding energy measurement) and because of the unavailability of supported phthalocyanine complexes of types containing electron donating substituents forcing us to examine other types of ligand systems. We shall give greater attention to the first approach in the coming quarter. The second approach is the longest range one in our plan but also the one with the greatest odds of success. It is also the one that gave the most progress in the synthesis of intermediates leading to electron deficient binucleating ligands of the BIMP-X type.

We have continued to synthesize a range of SALOPH type mononuclear ligands with electron donating and withdrawing substituents using the general procedures previously described in detail. We have prepared a dimethyl, tetramethoxysaloph ligand which is an acyclic tetradentate ligand which binds with two imine nitrogens and two phenoxy oxygens as a 2^- anionic species. This is the most electron donating ligand ever made in the SALOPH series. The successful synthesis via a Schiff base condensation was confirmed by FAB-MS, but a high molecular weight impurity was found in the unrecrystallized material. Recrystallization of the compound as well as of a series of 8 other ligands of this general type which had been prepared previously is currently under way. These ligands are of interest to prepare iron, ruthenium, and manganese complexes which will be used as oxidation catalyst candidates for methane conversion to methanol once supported on solids.

6.8.2 Synthesis of Binucleating Macrocyclic Ligands with Electron Withdrawing Substituents

We have moved ahead with the preparation of a new round of intermediates which are the precursors to novel polyimidazole binucleating ligands with electron-withdrawing groups: 2,5-bis[bis((5-chloro-1-methylimidazol-2-yl)methyl)amino)-methyl]-4-methylphenol, **{Cl_4-BIMP}**, a ligand with one chlorine atom per imidazole, and **{Cl_8-BIMP}**, the corresponding ligand with 2 chlorines per imidazole.

The key new compounds we have now prepared cleanly are the synthons to a number of later imidazole derivatives leading to the binucleating **BIMP-X** ligands and related ligands. Previous efforts resulted in impure compounds in poor yields and required more tedious purification procedures. We have also prepared several new substituted chloroalkyl phenols, previously unknown compounds, which will be used as the backbone of the polyimidazole ligands to bring together the chlorinated imidazole arms of each ligand. We are particularly interested in a non-symmetrical difluoro compound as a building block for a molecularly engineered binucleating ligand.

6.8.3 The synthesis of the ligand:
2,6-Bis-((bis((4,5-dichloro-1-methylimidazol-2-yl) methyl)amino)methyl)-4-methylphenol

Cl_8-BIMP

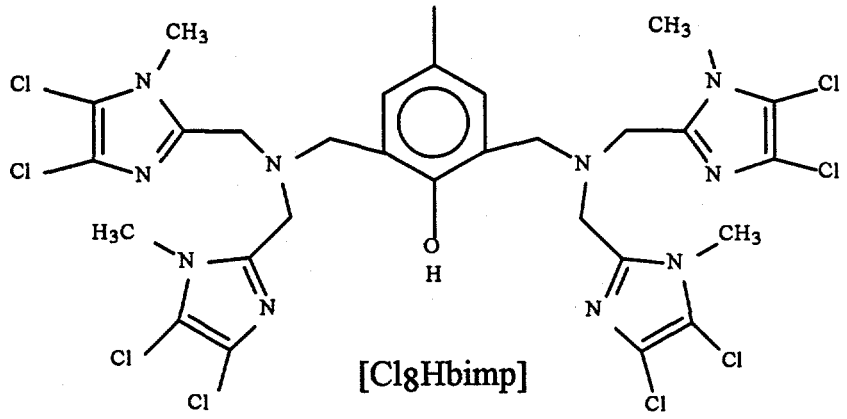

[Cl8Hbimp]

2,6-Bis((bis((4,5-dichloro-1-methylimidazol-2-yl)-methyl)amino)methyl)-4-methylphenol

Previous work in our laboratory had been directed towards the synthesis of homo and heterobinuclear metal complexes of Fe(II) and other transition metal ions. Among the binuclear complexes prepared previously were those based on the known polyimidazole ligand, BIMP. After considerable effort, we have now prepared, purified, and characterized a polyimidazole binucleating ligand with electron withdrawing chlorine atoms appended to the 4,5 imidazole positions, Cl_8-BIMP. This and other binucleating ligands with electron withdrawing groups will be used to prepare a variety of metal complexes which may be active as catalysts for selective oxidation of light alkanes when supported on surfaces or in liquid solution. The synthesis of the novel ligand, 2,6-*bis*-((*bis*((4,5-dichloro-1-methylimidazol-2-yl)-methyl)amino)methyl)-4-methylphenol, Cl_8-BIMP, is described below:

1) 4,5-dichloro-1-methylimidazol-2-carboxaldehyde (MW 179.01).

8.92 g of 4,5-dichloro-1-methylimidazole (MW 151) were dissolved in 600 ml of dry ethyl ether and cooled to 0°C. 40 ml (27.14 g) of n-butyl lithium (MW 64.06) was slowly added *via* syringe, and the mixture was allowed to stir for approximately 2 hours. 7.3 ml (6.9 g) of dimethyl formamide (MW 73.10) was dissolved in 20 ml of ethyl ether and quickly added to the solution *via* an addition funnel. The solution was then stirred over night at 0°C. 10 ml of water were added over a 15 min. period to quench the system followed by addition of 65 ml of 4 N HCl. The layers were separated and the ether layer evaporated under reduced pressure. The resulting yellow crystals were dried in a vacuum oven with a yield of 9.443 g (89.4%), 10.562 g theoretical yield. ^{1}H NMR showed peaks at 9.6 and 4 ppm representing the aldehyde and methyl hydrogens respectively, with a ratio of 1:3.3.

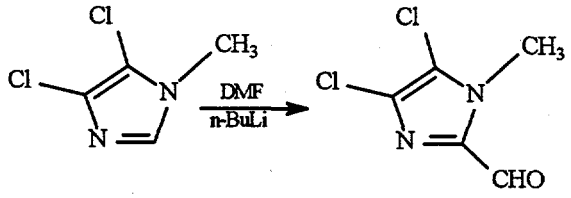

Compared to the procedure previously used to synthesize the non-derivatized imidazole ligands, the synthesis of the present compound required several modifications to avoid contamination with unreacted DMF. The boiling point of the 4,5-dichloro-1-methylimidazole- -2-carboxaldehyde is too high for use of even vacuum distillation as a purification technique; therefore, several attempts were made at isolation of the product through chloroform extraction. Although the best results were achieved with the procedure above, residual contaminants including DMF and others were not completely removed by the chloroform extraction procedure. Solubility of DMF is as follows: ethyl ether < water < chloroform. A key factor to ensure success was the use of fresh *n*-butyl lithium and

dry ethyl ether. The material was characterized by IR and ^{1}H-NMR in comparison to the non chlorinated derivative prepared previously; however, due to the similarity of the IR spectra of DMF and that of the aldehyde in the aldehyde stretch region, only the NMR measurement was considered definitive evidence of product formation.

2) 4,5-dichloro-1-methylimidazol-2-carboxaldehyde oxime (MW 194.02).

4 g of 4,5-dichloro-1-methylimidazol-2-carboxaldehyde (MW 179.01) were dissolved in 10 ml of ethanol. 1.527g of NH_2OH•HCl (MW 69.49) were dissolved in 20 ml of water along with 1.184 g of Na_2CO_3 (MW 105.99). The two solutions were combined and cooled to *ca.* 0°C. Crystals formed and were filtered off and washed with water. The clear crystals were dried in a vacuum oven, yielding 3.112 g (71.8 % of theoretical yield). 1H-NMR at 300 MHz confirmed the product: CH3-Im, 3.81 ppm(3), NOH, 7.50 ppm(1), CH=N, 8.04 ppm(1).

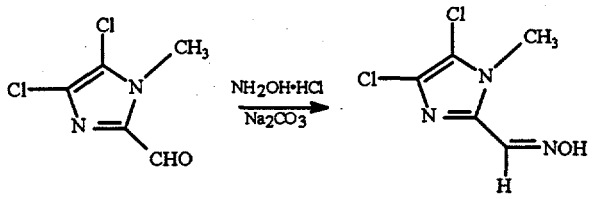

The procedure above was not altered from the original procedure used to prepare the non-chlorinated oxime previously except for the use of additional ethanol to dissolve 4,5-dichloro-1-methylimidazol-2-carboxaldehyde.

3) 4,5-dichloro-1-methyl-2-aminomethylimidazole dihydrochloride (MW 252.96).

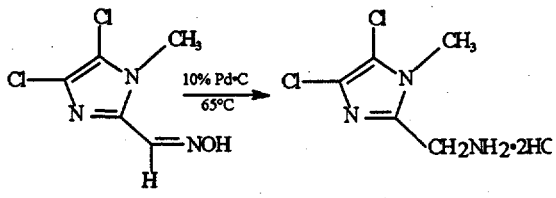

3.0 g of 4,5-dichloro-1-methylimidazol-2-carboxaldehyde oxime was dissolved in 100 ml of methanolic HCl (95:5). The solution was heated to 65°C and hydrogenated by bubbling hydrogen through the solution for 4 hours at atmospheric pressure with 0.76 g of 10% Pd on carbon used as a catalyst. The catalyst was filtered off and washed with 10 ml of MeOH•HCl. The filtrate was evaporated to 30 ml and coled to -20°C. The resulting crystals were filtered and washed with two 10

File # 1 : MB346P

Memo: MB346,BRU,10000831,DCMIMCAO,CDCL3,H1CHL1,9/7/94

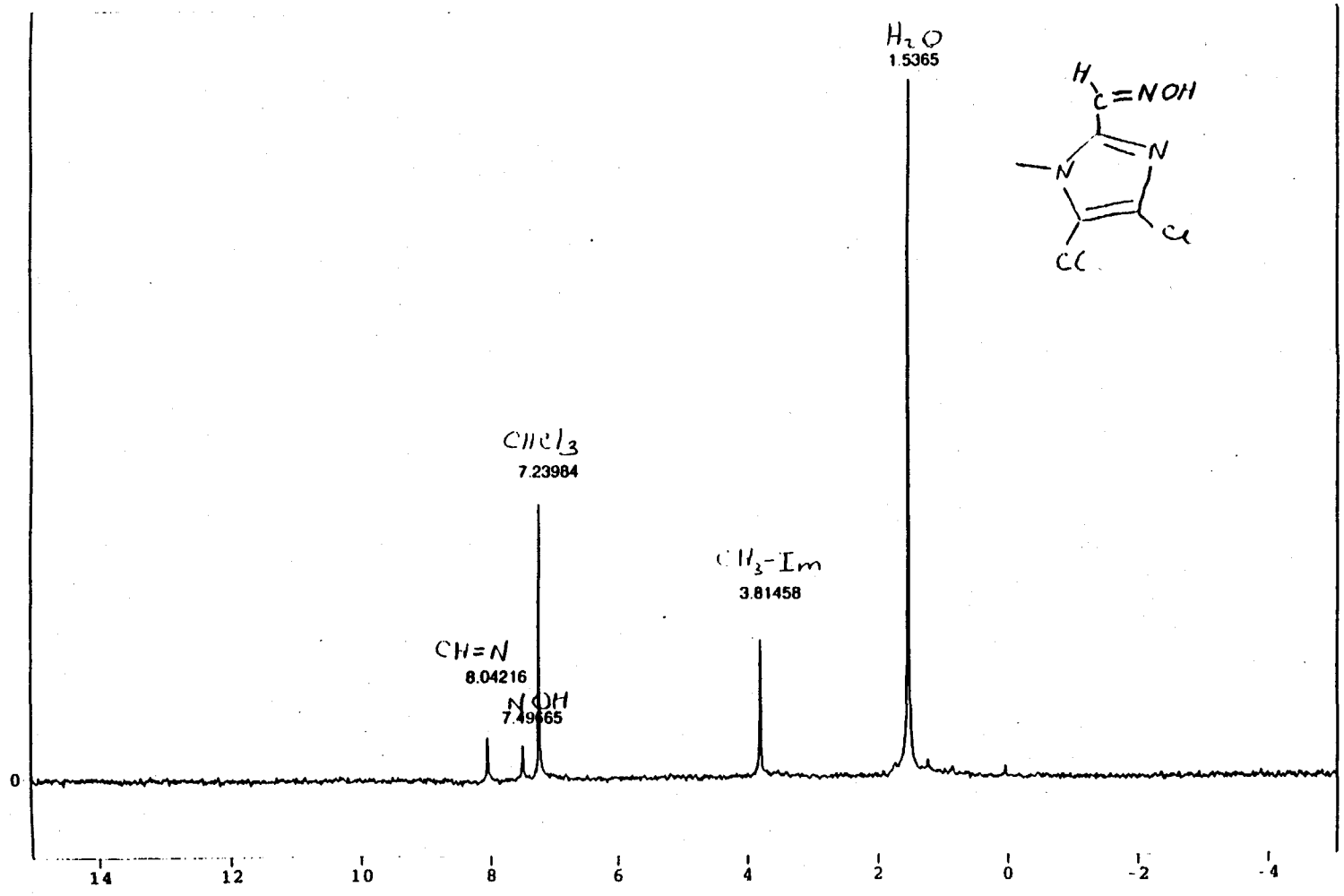

portions of MeOH•HCl. The resulting crystals were dried to yield 0.995 g (25.4% of theoretical yield).

When the hydrogenation procedure above was applied to the **mono**chloroimidazole derivative, the chlorine was lost, yielding a non-chlorinated product. Although the **di**chloro derivative was found to be more robust, we were unhappy with the low 25% yield. Hence, we sought an alternative procedure for reduction of the oxime to an amine which did not require the use of molecular hydrogen. Although not tested in our laboratory for the dichloro derivative, an alternative method based on a reduction with $LiAlH_4$ was developed for the monochloro derivative and could probably be adapted to the dichloro derivative in future preparations:

0.7 g of 5-chloro-1-methylimidazole-2-carboxaldehyde oxime (MW 159.57) was dissolved in 5 ml of ether and cooled to -40°C under nitrogen. 5.7 ml of 1M $LiAlH_4$ solution (MW 37.95) was added and the mixture allowed to stand for 30 min. 10 ml of water were added cautiously followed by 2 ml of 10 N NaOH. The layers were separated and the ether layer was dried and evaporated under vacuum to yield the amine, with a theoretical yield of 0.639 g of the 5-chloro-1-methyl-2-aminomethylimidazole (MW 145.59).

4) Bis-(2-(4,5-dichloro-1-methylimidazolyl)methyl)amine trihydrochloride (MW 54.44).

1.0 g of 4,5-dichloro-1-methyl-2-aminomethylimidazole dihydrochloride (MW 252.96) and 0.22 g KOH were dissolved in 25 ml of methanol. 0.71 g of 4,5-dichloro-1-methyl- imidazole carboxaldehyde was dissolved in 25 ml of methanol. The solutions were combined and hydrogenated over 0.6 g of Pd on carbon for at least four hours. The catalyst was filtered off, and the solvent was reduced to about 10 ml, then the KCl was filtered off. The solution was diluted with 50 ml MeOH•HCl and cooled to -20°C, and the precipitate was filtered and washed with MeOH•HCl. The yield was undetermined, since the MIMA•3HCl was immediately converted to MIMA without weighing. The theoretical yield was 1.98 g.

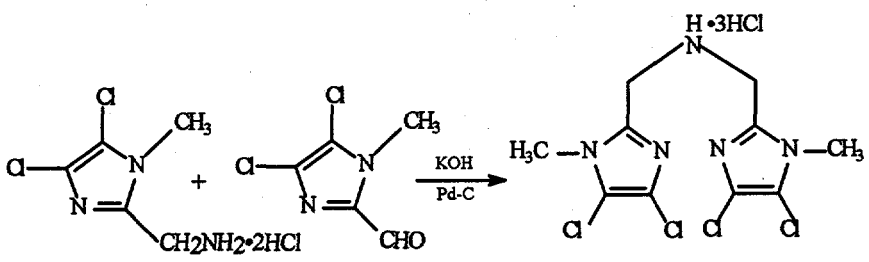

5) *Bis*-(2-(4,5-dichloro-1-methylimidazolyl)methyl)amine (MW 345.06) [Cl_8MIMA].

The reaction product of the Cl_8MIMA•3HCl was dissolved in a saturated potassium carbonate aqueous solution. The solution was then extracted two times with 75 ml of chloroform. The combined chloroform layers were dried with magnesium sulfate and evaporated under vacuum.

6) 2,6-B*is*-[bis-(2-(4,5-dichloro-1-methylimidazol-2-yl)methyl)amino) methyl]-4-methyl-phenol. {Cl_8-HBimp} (MW 818.25)

0.66g of bis-(2-(4,5-dichloro-1-methylimidazol-2-yl)methyl)amine and 0.195g triethylamine were dissolved in 15 ml of methanol and combined with a solution of 0.197g of 2,6-bis-(chloromethyl)-p-cresol in 5 ml of methanol. The combined solution was allowed to stir for ~4 hours. The methanol was removed under reduced pressure. The residue was dissolved in ~75ml of a chloroform/water (1:1) mixture. The layers were separated and the chloroform was washed with water several times. The chloroform solution was dried with $MgSO_4$ and removed under pressure to yield the desired product. 0.408g of Cl_8HBimp was recovered (51.8%), with a theoretical yield of 0.787g. Confirmation of the product was based on 1H-NMR [Figure] and IR.

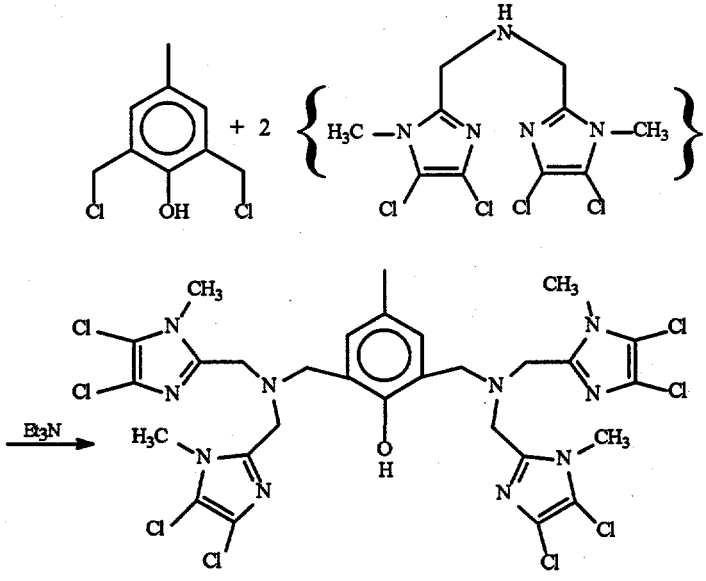

Memo: MB336,BRU,1000836,BIMP-CL8,CDCL3,H1CHL1,8/25/94

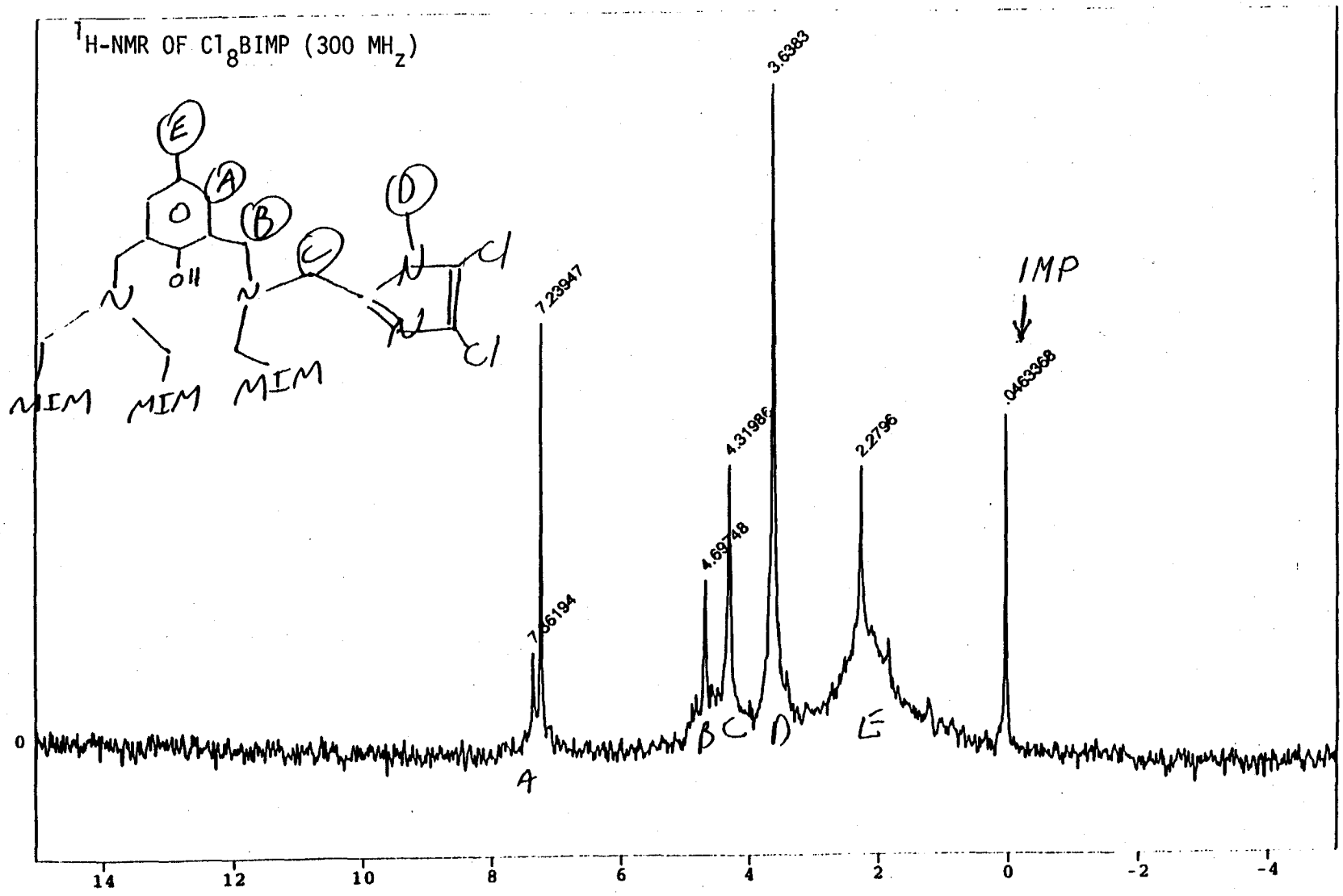

II. SYNTHESIS OF SUBSTITUTED BIS-CHLOROMETHYLPHENOLS

It was of interest to us to prepare *non-symmetrical* binucleating ligands that were also oxidatively stable. Hence, we examined the possibilities for synthesis of a series of ring- halogenated phenols with the appropriate appended chloromethyl arms to form the backbone of ligands similar to BIMP. Unfortunately, the work with phenols is incomplete as of this writing. The procedure previously used for the methylation of ρ-cresol was performed on several different substrates; it was adapted from Ullmann and Brittner, *Chemische Berichte*, 2539-48 (1909). The range of substrates explored were as follows: 3,5-dichlorophenol, 3,5-difluorophenol, 3,4-difluorophenol, and α,α,α,-trifluoro-ρ-cresol. The 2,6-bis-hydroxy- methyl-3,4-difluorophenol was the only compound successfully synthesized. The procedure was as follows:

7) 2,6-bis-(hydroxymethyl)-3,4-difluorophenol (MW 190.15)

0.772g of sodium hydroxide and 1.0g of 3,4-difluorophenol (MW 130.10) were dissolved in ~2 ml of water. 1.40g of formaldehyde (32.94%) (MW 30.03) was added to the solution and the mixture was allowed to stand for three days at ambient temperatures. The crystals were filtered off and washed with brine. The crystals were dissolved in water and neutralized with glacial acetic acid. The resulting crystals were filtered off and washed with brine. 0.65 g of orange crystals were recovered (44.5%), with a theoretical yield of 1.46g.

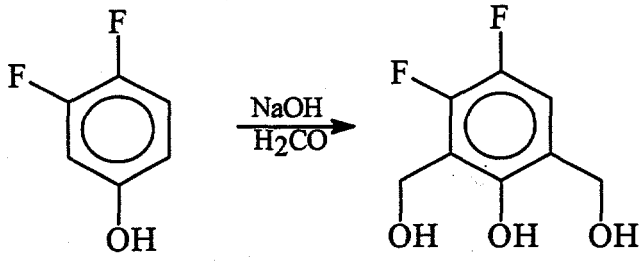

This procedure was used unsuccessfully with the other phenolic substrates. The 3,5-dichlorophenol and the 3,5-difluorophenol reacted; however, products other than those desired were formed. The α,α,α,-trifluoro-ρ-cresol reacted exothermally with the sodium hydroxide to form a polymer.

8) 2,6-bis-(chloromethyl)-3,4-difluorophenol (MW 227.04)

This compound was not successfully synthesized; however, several attempts were made. The first procedure was similar to that of Zeigler, *Chemische Berichte*, 77B, pp 731-735 (1944). The procedure was as follows:

A two phase mixture was made with 0.65g of 2,6-bis-(hydroxymethyl)-3,4-difluoro- phenol (MW 190.15) in 5ml of benzene. 0.49g of HCl was added to the mixture with vigorous stirring. The mixture was allowed to stir until the water layer became clear. The benzene was separated and dried with magnesium sulfate. The benzene was removed by rotary evaporation. The orange crystals that were recovered were found to be unreacted starting material.

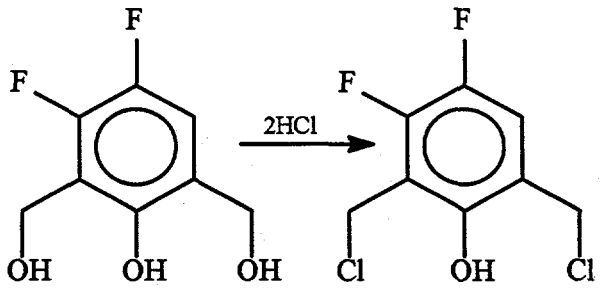

A second procedure was attempted with the use of thionyl chloride in place of the HCl, however this too was unsuccessful:

A two phase mixture was made with 0.45g of 2,6-bis-(hydroxymethyl)-3,4-difluoro- phenol in 10 ml of methylene chloride. 0.49g of thionyl chloride was dissolved in 10 ml of methylene chloride. The thionyl chloride solution was added to the 2,6-*bis*-(hydroxymethyl)- 3,4-difluorophenol mixture with vigorous stirring. The mixture was allowed to stir over night. The resulting solution was poured over water to neutralize the unreacted thionyl chloride and neutralized with sodium hydroxide. The layers were separated, and the water layer was extracted with methylene chloride. The combined organic layers were dried over magnesium sulfate and rotary evaporated (theoretical yield = 0.542g).

III. POST-SYNTHESIS CHLORINATION

9) Chlorinated bis-(2-(1-methylimidazolyl)methyl)amine.

The MIMA compound was chlorinated in an attempt to bypass the need to work with intermediates derived from 5-chloro- or 4,5-dichloro-1-methylimidazole. This chlorination produced a mixture of products of varying degrees of chlorination as shown by ^{1}H NMR A typical procedure was as follows:

0.5 g of bis-(2-(1-methylimidazolyl)methyl)amine was dissolved in 50ml of chloroform. The solution was heated with stirring to 40°C. A slow flow of chlorine gas was admitted into the system for 15s. The solution was allowed to stir with gentle heating for four hours. The chloroform was removed by rotary evaporation to yield 0.323g of a green oil.

IV. SYNTHESIS OF OTHER BINUCLEATING LIGANDS

10) 2,6-*BIS*(N-(5-NITROPYRIDIN-2-YL)-AMINOETHYLAMINOMETHYL)-*P*-CRESOL {BNPEC}

The novel binucleating ligand BNPEC was designed to provide several features not found in other ligands: an electron withdrawing group on a pyridine binding site, a flexible tetradentate linkage for each metal ion, no imine linkage which could potentially act as a radical quenching site--unlike Schiff base ligands--, and a net anionic coordination to help reduce the net charge of the electropositive metal ions.

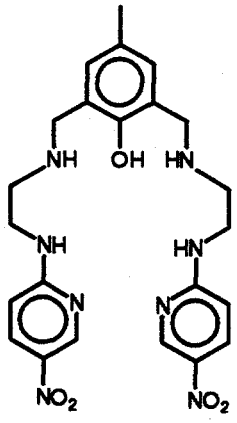

BNPEC

This previously unknown compound was prepared as follows:

Bis(2,6-chloromethyl)-*p*-cresol which had been prepared previously [1.53 g, 7.5 mmol] was allowed to react with 2-(2-aminoethylamino)-5-nitropyridine [Aldrich, 2.733 g, 15 mmol] in the presence of excess triethylamine [Aldrich, 2.4g., 24 mmol] in dry THF at room temperature for 0.5 h. The solution was then heated to boiling with stirring for 3 hours with occasional replenishment of evaporated solvent. The sample was concentrated to ca. 50 ml and allowed to cool to room temperature. White needles of triethylammonium chloride had formed [1.72g], which were filtered

off. The remaining solution was taken to dryness on a rotary evaporator at 60°C and the red oil redissolved into a minimum of acetone. A yellow emulsion formed upon addition of a large excess of distilled water. The aqueous phase was basified with several drops of 1 N NaOH and extracted 4 times with chloroform. The chloroform layer was separated and taken to dryness to give a yellow-red solid which was collected by scraping the flask. No yield was calculated.

Laser desorption mass spectroscopy negative ion spectrum showed a major peak at 495 m/e corresponding to L^- as well as peaks at 565 and 635 corresponding to $L^-.2HCl\ -2H^+$ and $L^-.4HCl\ -4H^+$ for the crude oil prior to treatment with base and extraction. TLC on reverse phase (C18) silica with methanol eluant showed three components to be present. A repeat of the synthesis without the use of triethylamine resulted in a tan rubbery mass after a small amount of methanol was added to the mixed reagents in THF and a yellow THF solution. After workup of each fraction(*i.e.*, the rubbery mass and the THF solution) separately as before by rotary evaporation, redissolution into acetone, precipitation with water, basification, extraction with chloroform, and rotary evaporation to dryness, a yellow solid was isolated that showed 2 components by TLC, one of which had an r_f identical to that of the amine starting material. C,H,N analysis, NMR, and mass spectra of this sample are pending as of this writing.

11) SYNTHESIS OF $[Co_2(BNPEC)(\mu\text{–}O_2CCH_3)(O_2)](O_2CCH_3)(PF_6).xH_2O$

This compound was prepared by applying the published methodology of Suzuki [Chem. Let. (Jap.) (1981), 1745] to prepare cobalt complexes with other binucleating ligands:

The crude BNPEC ligand (0.87g, 1.87 mmol) was dissolved into 10 ml of deaerated acetone in an open beaker and saturated with argon. $Co(CH_3COO)_2 \cdot 4H_2O$ (0.932g, 3.74 mmol) was dissolved into wet methanol (35 ml) and deaerated with Ar bubbling for 8 min. The solutions were mixed under Ar at room temperature followed by addition of $NaPF_6$ (0.314g, 1.87 mmol) also dissolved into deaerated methanol. The resulting dark brown solution was heated and stirred in air to reduce volume to about 10 ml. After cooling in a refrigerator overnight, a brown precipitate was collected by vacuum filtration onto a 2 ml medium porosity sintered glass funnel, washed with ethanol, and vacuum dried at 87°C/ 6 torr/ 1 hr. 0.217 g of solid were collected.

LIGHT ALKANE OXIDATION EXPERIMENTS OVER SUPPORTED FE (II) COMPLEXES

Previous work in this program identified the possibility of a catalytic cycle in which a light alkane could be hydroxylated to the corresponding alcohol *via* a single iron atom catalyst and a hydroperoxide, rather than a diiron μ-peroxo intermediate:

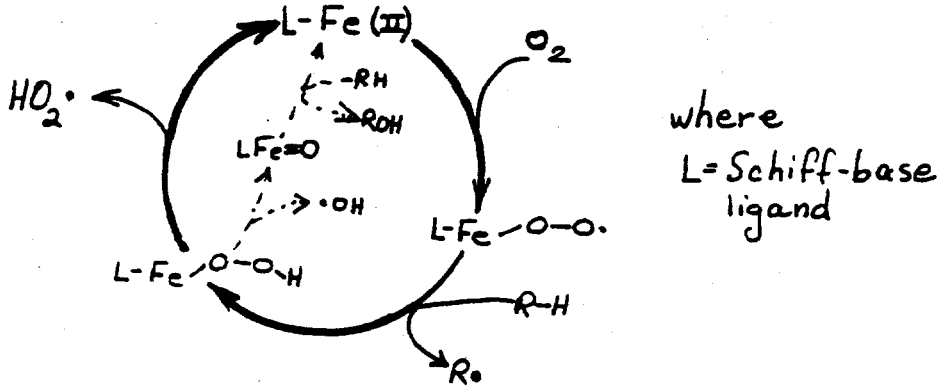

Iron superoxide intermediates are generally regarded as inert towards hydrogen abstraction at or near room temperature. But at the temperatures of interest, 100-300°C, we thought that the superoxide intermediate might form, react with alkanes, and return to Fe(II) if formation of μ-oxo dimer were prevented. The rate-limiting step of the cycle might well be the binding of oxygen, however. Thus, to facilitate the cycle above, we reasoned that the catalyst would contain certain features: needed were a well dispersed iron (II) complex emplaced onto a surface such that irons were far enough apart to preclude the formation of oxo-bridged dimers and which featured electron donating--rather than electron withdrawing---substituents on the ligand to promote oxygen binding by iron (II). We prepared a number of Schiff base complexes of iron appended with either electron donating or electron withdrawing groups and deposited these on several types of hydrophobic surfaces by simple anaerobic impregnation techniques for a first pass examination of catalysis. Although the complexes were mononuclear iron (II) to begin with, we have not characterized the supported materials as of this writing; they may have oxidized to dimers or be poorly dispersed. Most samples were quite dilute in iron concentration.

On the assumption that, once dried, the solids featured isolated mononuclear Fe(II) species, these catalyst candidates then were examined in both pulse and continuous alkane oxidation experiments at high pressure. The pulse experiments were designed to study the stepwise oxygenation of each surface-bound complex and subsequent reaction of the resultant peroxo intermediate with ethane. After an initial dosing at a prescribed temperature with oxygen, the surfaces were pulsed with ethane at high pressure and exposed to a temperature ramp to desorb products. The reactor effluent was continuously monitored in our CDS reactor, as described in earlier reports. The continuous oxidation experiments were conducted using a feed composed of 4.5 vol. % ethane, 18 vol. % oxygen, 18 vol. % water, and the balance nitrogen. Products were analyzed on-line after each period of 1 1/2 hours on stream by GC-MS, multidimensional GC, and continuously by a second MS system which sampled the full, unseparated effluent composition.

Complexes formulated as Fe(II)(X-saloph)(py) where X= $(Me)_2(OCH_3)_4$- or Cl_6 - were examined on S-115 silicalite extrudates, silica gel, or charcoal supports. On either silica gel or S-115 supports, neither complex showed any reactivity in pulse experiments at 80 to 160° without prior hydrogen reduction. Acetone and CO_2 were detected as eluants over the methylmethoxysaloph complex supported on S-115 (by impregnation from THF solution) after the catalyst had been exposed to a hydrogen stream at 30° for 0.5 hr then dosed with oxygen and ethane as before. Some oxygen was absorbed by the treated complex, but since we don't yet have an iron analysis of the catalyst, we cannot calculate stoichiometry. A possible interpretation of this result is that the complex existed as a μ-oxo-dimer or other inert Fe(III) species on the surface rather than as a mononuclear Fe(II) complex. Hydrogen treatment afforded a reduction to a compound which could bind oxygen to form a peroxo intermediate. It is not clear, however, what the mechanism leading to acetone is.

In continuous oxidation experiments at 160-200° and 500 psig, small amounts of ethanol and acetone were detected in the effluent after 1 1/2 hours on-stream over the Cl_6 -saloph complex on S-115. Acetone had been used as a preparative solvent to impregnate the solids with the complexes, and control experiments over a fresh loading of catalyst but without ethane in the feed still showed traces of acetone effluent, apparently left over from the catalyst preparative procedure; no ethanol was observed, nor had any been used in the impregnation procedure. However, the latter acetone component was totally gone after 100 minutes on-stream, whereas, the acetone which appeared in the experiments described earlier which included ethane in the feed evolved in much greater quantities and was not analyzed until 1 1/2 hours on-stream. Although quantitative comparison is not possible with a high degree of precision in these particular experiments, it does appear that additional acetone had been produced from ethane in the original experiment beyond that which contaminated the sample.

In continuous oxidation experiments over the methylmethoxysaloph complex on charcoal at 160°, 450 psig, acetic acid and other producrts were observed, but no ethanol. We are continuing to conduct control experiments, but if reproducible, this result represents a spectacular mild oxidation of ethane! Charcoal is a support which is likely to help in keeping the iron reduced to Fe(II), and a consistent interpretation of the results of oxidation experiments over Fe(II) Schiff base complexes is that the mononuclear Fe(II) species are active catalysts, whereas, the Fe(III)-O-Fe(III) complexes are not. More sophisticated dispersion and anchoring methods which would yield isolated Fe(II) sites would probably improve both activity and life of such catalysts for the heterogeneous catalysis of the low temperature vapor phase selective oxidation of light alkanes by molecular oxygen.

File: C:\CHEMPC\DATA\9296[illegible]
Operator: [illegible]
Date Acquired: 26 Sep 94 11:35 am
Method File: [illegible]
Sample Name: 929621-1 160C, 450psig; loop A
[illegible] (OCH3)4-SALOPH][Py]/Charcoal
ALS vial: 1

1½ hrs on stream

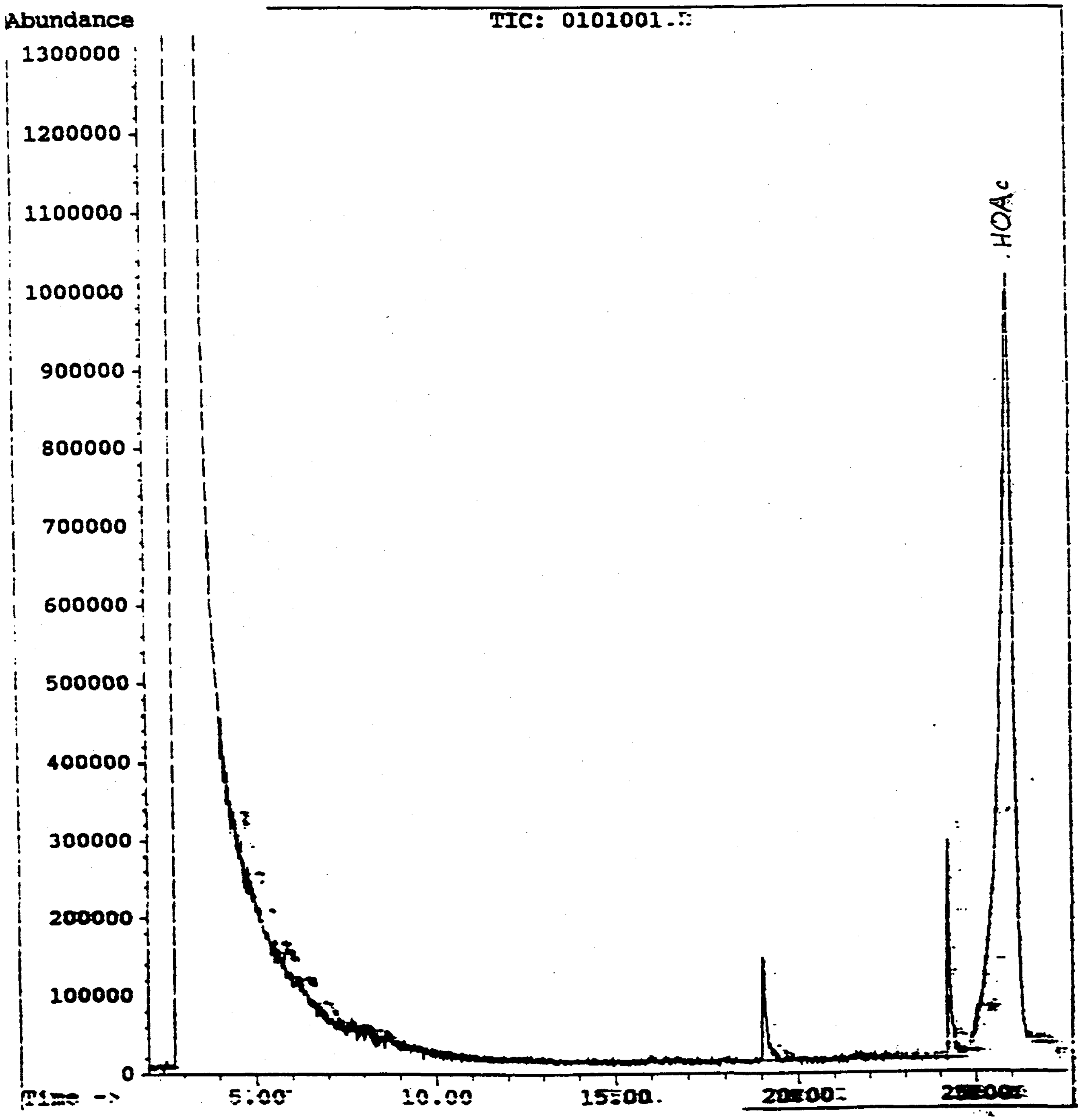

7.0 CONCLUSION

This report details the research performed on Phase VI of the extended Cooperative Agreement. This Phase, entitled C_1-C_3 Research, provides the research support which accompanies the C_4 Proof-of-Concept Phase (Phase V) as the two major activities of the Cooperative Agreement during calendar 1994. It is the objective of this phase to understand the nature of the catalysts and catalytic activity of perhaloporphyrin complexes uncovered during Phases I-III in order that superior catalytic materials can be made and tested which meet commercial criteria for the oxidation of the C_1-C_3 light alkane gases found in natural gas and other available hydrocarbon streams.

During Phase VI, we have examined the physical and electronic structures of the very active perhaloporphyrin catalysts which we have developed, and have gained an understanding of the properties which make them active. This has led us to design and synthesize materials which are cheaper, more active, more robust and, in general superior for carrying out practical catalysis. Our early generation perhaloporphyrin catalysts, while exhibiting unprecedented catalytic activity, were far too expensive for use in converting natural gas or its C_1-C_4 components. The reason for this is that the perfluorophenyl substituents that occupied the meso positions caused these complexes to be very costly to synthesize. During Phase VI we have found new routes to metalloporphyrins having meso-perfluoroalkyl substituenty that are much less costly. Molecular modelling and electrochemical measurements indicate that these meso-substituents should provide a ligand system which makes the metal center even more active than in our early generation catalysts. Initial screening studies confirm this.

During Phase VI we have concluded that, although they are good candidates for C_3 and C_4 oxidations, perhaloporphyrin complexes will probably not be active enough to catalyze oxidation of methane or ethane at low temperatures and not robust enough to be effective at elevated temperatures. Our first generation heterogeneous catalyst, iron sodalite, though robust, will not meet the commercial rate and selectivity requirements. During Phase VI we have designed heterogeneous catalysts aimed at incorporating the best aspects of our early generation heterogeneous catalysts while adding important functions designed to impart greater selectivity and rate. A number of new compositions have been successfully synthesized. In addition, a new highly automated and well controlled oxidation facility methane oxidation laboratory was used to perform the methane oxidation studies in Phase VI of the extended Agreement.